Ceramide Synthase in Transcriptional Regulation and Lipid Sensing

Dissertation

zur Erlangung des

Doktorgrades (Dr. rer. nat.)

der

Mathematisch-Naturwissenschaftlichen Fakultät

der

Rheinischen Friedrich-Wilhelms-Universität Bonn

vorgelegt von

Mariangela Sociale

aus Neapel

Bonn 2018

Angefertigt mit Genehmigung der Mathematisch-Naturwissenschaftlichen Fakultät der Rheinischen Friedrich-Wilhelms-Universität Bonn

1. Gutachter: P.D. Dr. Reinhard Bauer

2. Gutachter: Prof. Dr. Gaia Tavosanis

Tag der Promotion: 12. April 2019

Erscheinungsjahr: 2019

Erklärung

Teile dieser Arbeit wurden bereits im folgender Publikation veröffentlich:

Ceramide Synthase Schlank Is a Transcriptional Regulator Adapting Gene Expression to Energy Requirements. M Sociale, AL Wulf, B Breiden, K Klee, M Thielisch, F Eckardt, J Sellin, MH Bülow, S Löbbert, N Weinstock, A Voelzmann, J Schultze, K Sandhoff, R Bauer. ***Cell Reports 2018*** Jan 23;22(4):967-978. doi: 10.1016/j.celrep.2017.12.090. Epub 2018 Jan 28

DATUM, ORT…….

UNTERSCHRIFT……

Zusammenfassung

Ceramid-Synthasen (CerS) sind hochkonservierte Transmembranproteine, die für die Sphingolipid-Biosynthese notwendig sind. CerSs tragen eine TLC (Tram-Lag1-CLN8)-Domäne, die ein konserviertes Lag1p-Motiv enthält, das für die Ceramidsynthese erforderlich ist. Viele der CerS-Enzyme enthalten auch eine Homöodomäne. Obwohl Homöodomain-Proteine bekanntermaßen die Transkription über die DNA-Bindung regulieren, ist die Homöodomain-Funktion von CerSs nicht genau untersucht und frühere Studien bezweifelten sogar, dass sie als Transkriptionsfaktor fungieren könnte.

In jüngster Zeit konnte gezeigt werden, dass das Drosophila-Homolog namens "Schlank" nicht nur in der Sphingolipidbiosynthese, sondern auch in der Regulation von Körperfett involviert ist. Die Regulierung des Körperfettanteils ist zudem unabhängig von der CerS-Aktivität. Neben der Lokalisierung am Endoplasmatischen Retikulum, wie auch die Säuger CerS, ist Schlank auch an der inneren Kernmembran (INM) lokalisiert. Zwei nukleare Lokalisierungsstandorte (NLS1, NLS2) sind für die nukleare Lokalisierung des Proteins notwendig.

Um die Homöodomänenfunktion von der katalytischen zu unterscheiden, wurden in vivo Homöodomänen-Fliegenmodelle generiert und analysiert. Die Mutation am NLS2-Standort wirkte sich stark auf die Lipolyse und Entwicklung aus und demonstrierte eine wesentliche Funktion der Schlank-Heimatdomäne bei der Regulierung des Körperfettstoffwechsels und des Wachstums.

Diese Arbeit zeigt, dass Schlank die Promotor-Regionen von Lipasen (z.B. Lip3) über die Homöodomäne bindet und die Transkription direkt reguliert. Mutationen des NLS2-Standortes führten zum Verlust der DNA-Bindung und deregulierten Genexpression. Dieser Mechanismus scheint im Säuger CerS2 konserviert zu sein.

Darüber hinaus passt Schlank die Transkriptionsregulation an den Energiestatus an. Werden die Fliegen gehungert nimmt die nukleare Lokalisation und damit die Bindung an die DNA ab. Auf der anderen Seite reagiert Schlank auf sich ändernde Fettsäurespiegel (essentielle Moleküle in der Sphingolipidbiosynthese), erhöht die nukleare Lokalisation und reguliert die Genexpression.

Diese Studie demonstriert eine Doppelfunktion von CerS Schlank als Enzym und Transkriptionsregulator, indem sie den Lipidspiegel misst und die Informationen auf die Ebene der Genexpression transformiert. Diese Funktion ist erforderlich, um die Lipid-Homöostase zu regulieren und aufrechtzuerhalten.

Abstract

Ceramide synthases (CerS) are highly conserved transmembrane proteins necessary for sphingolipid biosynthesis. CerSs carry a TLC (Tram-Lag1-CLN8) domain, containing a conserved Lag1p motif required for ceramide synthesis. Many of the CerS enzymes also contain a homeodomain. Although homeodomain proteins are known to regulate transcription via DNA binding, the homeodomain function of CerSs is frequently not investigated and previous studies doubted that it could act as a transcription factor.

Recently, it has been shown that the *Drosophila* homologous of CerS called "Schlank", is not only involved in sphingolipid biosynthesis but also in the regulation of body fat. Moreover, the regulation of body fat is independent of CerS activity.

Besides localizing at the endoplasmic reticulum, as each mammalian CerSs, Schlank also localizes at the inner nuclear membrane (INM). Two nuclear localization sites (NLS1, NLS2) are necessary for the nuclear localization of the protein.

In order to distinguish the homeodomain function from the catalytic one, *in vivo* homeodomain animal models were generated and analyzed. The mutation in the NLS2 site severely affected lipolysis and development, demonstrating an essential function of the Schlank homeodomain in the regulation of body fat metabolism and growth.

This work shows that Schlank binds the promoter regions of lipases (e.g., *lip3*) via the homeodomain and directly regulates transcription. Mutations of the NLS2 site led to loss of DNA binding and deregulated gene expression. This mechanism seems to be conserved in mammalian CerS2.

Furthermore, Schlank adjusts transcriptional regulation according to the energy status. Upon starvation, nuclear localization and consequently DNA binding diminish. On the other hand, Schlank responds to changing fatty acid levels (essential molecules in sphingolipid biosynthesis), increasing nuclear localization and regulating gene expression.

This study demonstrates a double function of CerS Schlank as an enzyme and a transcriptional regulator, sensing lipid levels and transducing the information to the level of gene expression. This function is required to adjust and maintain lipid homeostasis.

To Zio Franco, whose eyes could say even more than his words..

Index

List of Figures

List of Figures

1 Introduction

Cellular processes are mediated by the orchestrated action of numerous biomolecules that form complex interaction networks. The cellular interactome, protein-protein, protein–DNA, and protein– metabolite are extraordinarily complex interaction networks (Gavin et al., 2010). Two-thirds of the cellular proteome operates at a membrane surface or within a membrane comprising thousands of different lipid species.

Different types of eukaryotic cells differ for lipids-membrane composition. Cells need to sense the concentration of every single lipid, assimilate those signals and regulate the activity of different enzymes to fit the demands of the membranes. A small fraction of membrane lipids, which levels always need to be adjusted to maintain the fluidity and the subdomain structure of the lipid bilayers are sphingolipid (Futerman and Hannun, 2004). Besides being simple structural lipids, sphingolipids are known to be bioeffector molecules (Hannun and Obeid 2008). Bioactive sphingolipids such as Ceramide, sphingosine-1-phosphate, sphingosine and complex sphingolipids such as glucosylceramide, function as signaling molecules. They are involved in several biological processes including apoptosis, cell proliferation, cell migration and inflammation (Reynolds et al., 2004; Fox et al., 2006). Altered sphingolipid regulation, metabolism, or storage is linked to several human diseases. The most common and multifactorial are for instance metabolic disorders (diabetes and insulin resistance), cancer pathogenesis (incidence and progression) (Schiffmann et al., 2009), and Alzheimer's disease (Farooqui et al., 2010; van Echten- Deckert & Walter, 2011). Some lower incident or hereditary diseases are, for instance, Nieman-Pick disease (Schweitzer et al., 2009), and Gaucher disease (Fuller et al., 2010).

1.1 Sphingolipid biosynthesis

The chemical reactions and the enzymes involved in sphingolipid biosynthesis are well known, and are highly conserved during the evolution (Figure 1.1). Ceramide is the molecular precursor for all complex sphingolipids, and it is synthesized at the cytosolic face of the endoplasmatic reticulum (ER). Ceramides consist of a long-chain sphingoid base to which a CoA-activated fatty acid residue of different chain length is attached via an amide bond. In the *de no*vo synthesis pathway, dihydrosphingosine is N-acylated to

dihydroceramide by Ceramide Synthase (CerS) (Kolesnick et al., 2000). Under physiological conditions the so formed ceramides, are readily consumed; transported to the Golgi with a vesicular or non-vesicular (by CERT, ceramide transfer protein) related mechanism and converted to complex sphingolipids. From the salvage pathway (breakdown of complex sphingolipids), glycosphingolipids and sphingomyelin are degraded by several lysosomal enzymes (glycosidase, acid- and neutral-sphingomyelinase and acid ceramidase) to sphingosine (that can be then reacylated to ceramide), ceramide and phosphorylcholine (Marchesine and Hannun, 2004; Kitatani et al., 2008). Vice versa under stress conditions, ceramide can accumulate leading to apoptosis (Obeid et al., 1993). All of these mechanisms place CerSs at the center of the sphingolipid metabolism.

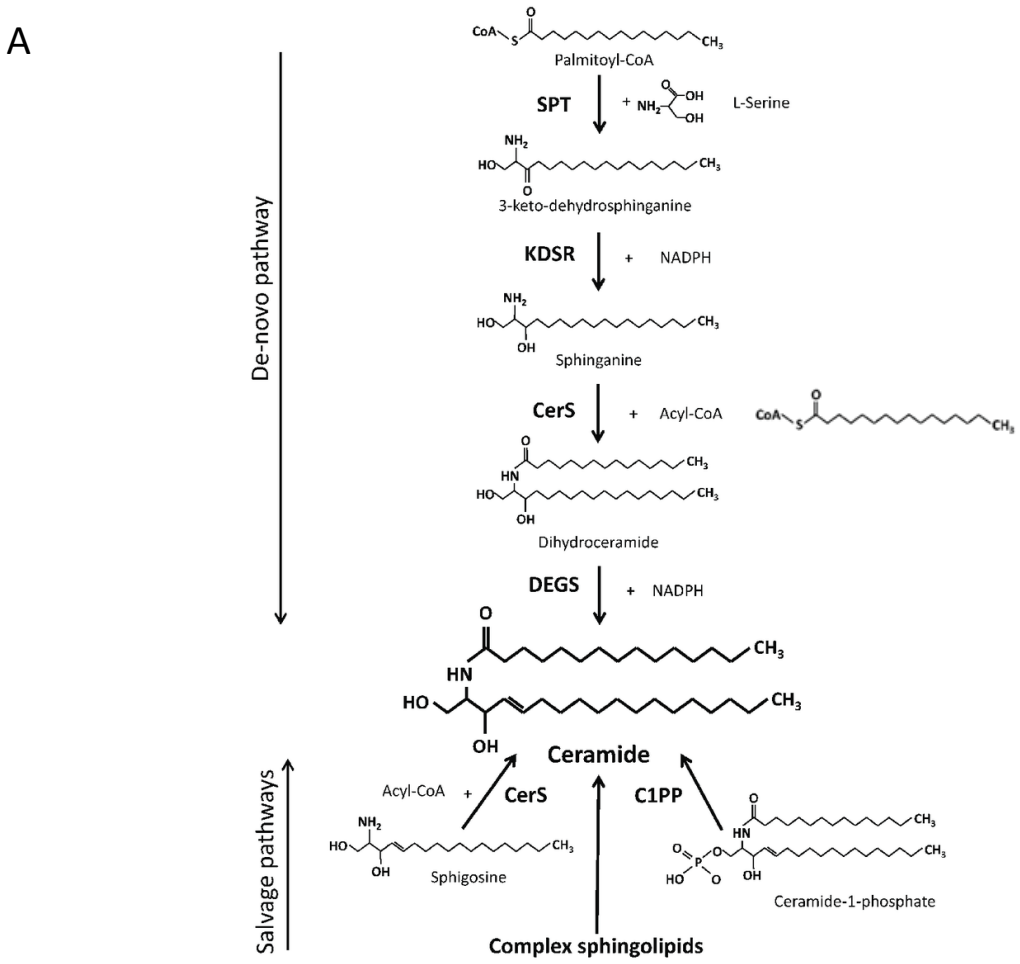

Figure 1.1. Schematic of sphingolipid biosynthetic and salvage pathways. SPT—serine palmitoyltransferase, KDSR—3-keto-dihydrosphinganine reductase, CerS—ceramide synthase (various isoforms in mammals), DEGS—dihydroceramide desaturase (various isoforms), C1PP—ceramide-1-phosphate phosphatase, Acyl-CoA—fatty acyl coenzyme A, NADPH—nicotinamide adenine dinucleotide phosphate, reduced. Image modified from Zabielski et al., 2017.

1.2 Ceramide Synthase functional domains

CerSs are multispanning transmembrane proteins, and although the exact number of transmembrane domains (TM) and their topology has not been resolved experimentally, based on TM prediction tools the going assumption is based on an odd number (5 to 7) of TM (Tidhar R. et al., 2018). CerSs are a family of highly conserved enzymes, expressed in all eukaryotes (Voelzmann and Bauer, 2010).

The first CerS gene was found in a study in Saccharomyces Cerevisiae. It was initially described as longevity assurance gene (LAG1) because its deletion promoted longevity in yeast (Mello et al., 1994). Subsequently, different LAG1 homologs were identified as CerS genes. In mammals, ceramide is synthesized by a family of six CerS (CerS1 to CerS6) that structurally share a distinct 200 amino acid domain, the Tram-Lag-CLN8 (TLC) domain, described as a lipid-sensing domain. Within the TLC domain lies, the Lag1p motif, a conserved stretch of 52 amino acids indispensable and responsible for the enzymatic activity of the protein. Two consecutive and conserved histidine (H) residues are likely to be involved either in the catalysis or substrate binding (Spassieva et al., 2006). Each CerS has a preference for a selected range of acyl-CoA groups, regulating a subset of ceramide species. For instance, CerS2 uses C22-C24-acyl-CoAs, whereas CerS5 and -6 use C16-CoA (Laviad et al., 2008; Riebelling et al., 2003 and Mizutani et al., 2005). Very recent experiments with chimeric proteins show that eleven residues determine the acyl chain specificity of CerS. Those residues are located in a loop between the last two transmembrane domains, with a shorter loop necessary for very-long-chain acyl-CoAs (due to a more open conformation of the protein) (Tidhar et al., 2018).

All of the mammalian CerSs except CerS1, display, in addition, a homeodomain (or Homeobox (Hox)-like domain, Hox-domain). The Hox-domain is generally known to mediate DNA and RNA interactions in a variety of proteins and organisms (Dubnau and Struhl, 1996). For CerS, it was shown that the major portion of the Hox domain (residues 1 to 34) is generally variable. Conservation is higher in the distal portion of the Hox-domain sequence enriched in positively charged amino acids. It is believed that the last stretch of amino acids within the homeodomain and flanking the TLC domain is necessary for the stability and enzymatic activity of the protein (Mesika et al., 2007; Levy & Futerman, 2010). Thus, it had been concluded that the homeodomain in CerS is unlikely to function as a genuine transcription factor (TF) (Levy and Futerman, 2010) and it more likely had a role in modulating CerS activity without playing a role in acyl chain specificity (Mesika et al.,

2007). However, in a 1-hybrid system, the isolated CerS homeodomain was shown to be able to bind DNA, suggesting that it did not lose its DNA-binding capacity (Noyes et al. 2008). It is nevertheless classified in several studies as CERS homeobox gene class (Holland et al., 2007, Bürglin & Affolter, 2016). Schematic of protein structure in Figure 1.2 (Sociale et al., 2018).

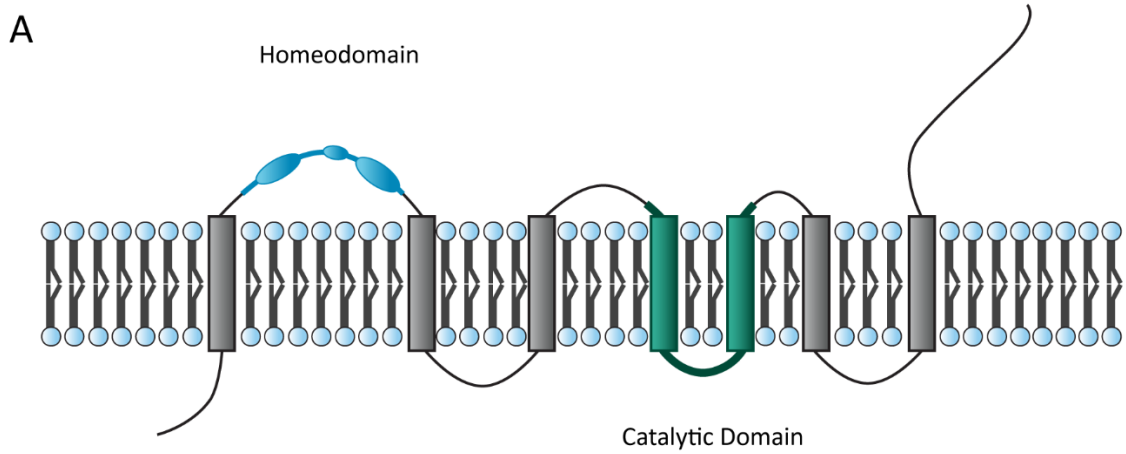

Figure 1.2. Putative Schlank protein topology. A) Gray boxes indicate TM domains, blue marks the homeodomain and its helices, and in green the lag1p motif (catalytic domain).

Even though CerSs and alteration of ceramide levels have been extensively studied in the last years, regulatory mechanisms are still lacking. Altogether, the specific function of the homeodomain in CerS has largely been neglected, and information on whether the homeodomain has a function in transcriptional regulation is missing.

1.3 Ceramide Synthase subcellular localization and regulation

CerSs are mainly localized to the ER (van Meer & Lisman, 2002), and very recently their localization at the inner nuclear membrane (INM) has been proved in both *Drosophila* and *Danio Rerio* (Voelzmann et al., 2016 and Mendelson et al., 2017). Unpublished data on the *Drosophila* CerS, using scanning-N-glycosylation mutagenesis (based on the evidence that only ER-faced regions are glycosylated) point to an N-terminus facing the ER-lumen and the C-terminus facing the cytosol, resulting in an uneven number of TMDs (7), with the homeodomain facing the cytosol (Anna-Lena Wulf, PhD thesis).

In mammals, CerSs are differentially expressed in different tissues, with overlapping expression patterns for more than one CerS (Levy and Futerman, 2011). However, the

sphingolipid acyl-chain composition does not always correlate with CerS expression (Mullen et al., 2011). CerS can be phosphorylated, glycosylated, and it was shown that CerS could form both homo- and heterodimers (Sridevi et al., 2009, Mizutani et al., 2006 and Laviad et al., 2012). CerS knockdown (KD) in cell culture experiments causes changes (mostly upregulation) in non-targeted CerSs (Hannun and L. M. Obeid, 2011). Similarly, *in vivo*, with an inactive CerS2 (CerS2 H/A mice), expression levels of CerS5 and CerS6 were increased. These findings, presume a compensatory mechanism to keep overall ceramide levels constant or to avoid toxic accumulation of substrates (Bickert et al., 2018).

CerS like-homeodomains are classified together with HNF (hepatocyte nuclear factor), TALE (transcription activator-like effectors), and ZF (zinc finger) due to the similarity in expression pattern according to gene expression data analysis of embryonic development in mouse (Dunwell and Holland 2016). Recently, genome-wide association studies identified a missense coding single-nucleotide polymorphism (SNP) (E115A) within the homeobox of the CerS2 gene. This SNP might be associated with indicators of insulin resistance or impaired glucose tolerance (Raichur et al., 2014). A subsequent publication showed that transcriptional activation of acid ceramidase (ASAH1) in mammals is not mediated by ceramide itself and did not depend on CerS6 catalytic activity. Moreover, every CerS (2-6) but CerS1 (lacking the homeodomain) was able to affect the regulation of ASAH1 (Tirodkar et al., 2015), suggesting a functional role for CerS homeodomain.

1.4 *Drosophila* Ceramide Synthase Schlank

Contrary to mammals, in *Drosophila,* only one gene is encoding for one CerS. This gene is named *Schlank* ("*slim*" in German), after the observation that different mutant alleles for Schlank affected fat storage causing a slim phenotype. In those mutants, different genes involved in lipid metabolism resulted in deregulated expression, such as *lipase3* (*lip3*) a Triacylglycerol lipase (Bauer et al., 2009). These data provided evidence that Schlank, besides synthetizing ceramide, can regulate lipogenesis and lipolysis during larval growth, suggesting a novel role for CerSs in regulating body fat metabolism. However, not every phenotype of the Schlank mutants could be explained by the loss of ceramide synthesis. Partial rescue of the mutant´s defects was obtained when a catalytically inactive Schlank (carrying a mutation in one of the conserved histidines, position 215) was overexpressed in the genetic background of the mutants. These findings pointed to a possible homeodomain function. Although the possibility that Schlank could act as transcriptional regulator via the

homeodomain is quite tempting, this would suppose a nuclear function and a nuclear Schlank pool.

1.5 Schlank nuclear localization and nuclear function

The nucleus is a highly compartmentalized organelle. The nuclear envelope (NE) consists of an outer nuclear membrane (ONM), in continuous with the ER, and an inner nuclear membrane (INM). The INM can form invaginations able to reach the nucleoplasm, framing in this way a nucleoplasmic reticulum (Malhas et al., 2011). The INM harbors a unique set of membrane proteins, many of which interact with intermediate nuclear filaments and chromatin components and thus play an essential role in nuclear organization and gene expression regulation (Zuleger et al., 2012). The NE covers the nucleus entirely except where nuclear pore complexes (NPCs) are inserted. Transport receptors (Importins α/β) mediate nuclear import interacting with cargo proteins via nuclear localization signals (NLSs) on the cargo.

Very recently, it was shown that endogenous Schlank protein is also localized at the INM, in *Drosophila* Schneider cells (S2) and fat body cells. To prove Schlank nuclear localization, several Schlank constructs fused with a green fluorescence protein (GFP) were overexpressed in S2 cells. Schlank Full length-GFP protein (amino acids (aa) 1-400) was found to localize at the ER and the nucleus. Next, the N-terminal portion of the protein (aa 1-138) that included, according to prediction, the first TM and the homeodomain with a GFP was used in S2 cells experiments. The GFP signal for this Schlank variant was found to accumulate to the nucleus. The strongest nuclear signal was associated with GFP-homeodomain fusion proteins containing the homeodomain only (GFP-Schlank aa73–133) or the complete stretch between the first two potential transmembrane domains (GFP-Schlank aa64–138) including newly found NLS sequences (NLS1, RPKK, aa78–81, and an atypical bipartite-like NLS2, RLDKKK-X19-RLRR, aa97–125) within the Schlank homeodomain. When NLS1 (ΔRPKK) or part of NLS2 (Δaa119–125) was deleted, the GFP homeodomain fusion protein (aa 64-138 ΔNLS) was detected mainly in the cytoplasm and hardly detected in the nucleus. A scheme for homeodomain and NLS sites is shown in Figure 1.3.

Moreover, by RNA interference (RNAi) in clonal analysis in fat body cells, was proved that the two NLSs are recognized by Ketel, the *Drosophila* homolog of Importin-β, and needed for the nuclear import. More importantly, appeared clear that the nuclear function of

Schlank is required for the regulation of fat metabolism and acts independently from the catalytic activity of the protein. This was demonstrated through overexpression of several Schlank variants in rescue experiments of the previously mentioned Schlank allele mutants (P-element mutants). Oppositely to the expression of several Schlank variant (included a deficient catalytic activity variant), the expression of an NLS2 mutant Schlank variant failed to rescue *lip3* overexpression (Voelzmann et al., 2016).

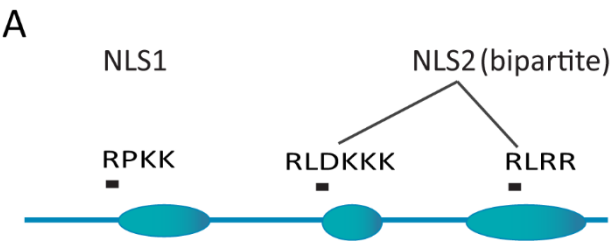

Figure 1.3. Schematic of homeodomain and NLSs. A) Monopartite-like NLS1 (RPKK, aa 78–81) and atypical bipartite-like NLS2 (RLDKKK-X19RLRR, aa 97–125) are depicted above the homeodomain.

1.6 The fate of fat

Under normal feeding conditions, dietary lipids, such as triacylglycerols (TAG), are broken down into free fatty acids (FFA) and monoacylglycerols (MAG) in the intestinal lumen. These digested lipids can then be absorbed by the intestinal cells, where the TAGs are resynthesized and packaged together with cholesterol, cholesterol esters, and carrier proteins to form lipoprotein particles. These lipids can be either utilized by cells or deposited as lipid droplets (LD) in storage tissues, as the fat body organ in Drosophila or the adipose and liver in mammals. The larval fat body, for instance, serves as a dynamic source for maintaining energy homeostasis and as a reservoir for stored lipids during the prolonged period of non-feeding (caused by nutrient deprivation or during metamorphosis) (Sieber and Thummel, 2009). At times of demand, fatty acids (FA) are released from cellular LDs by the action of TAG hydrolases or lipases, shifting the animal metabolism to lipolysis.

Unesterified fatty acids or FFAs are biomolecules that serve multiple functions. FA represent constituents of essentially all lipid classes, regulate gene expression by acting directly or indirectly as ligands/cofactors for nuclear receptors, affect protein function by post-translational acylation of target peptides, and, above all, serve as the most energy-dense substrate in the body for the production of ATP via β-oxidation. However, excessive cellular concentrations of FFAs are toxic to cells and tissues. Because of their amphipathic nature, FFAs act as detergents, damage cell and organelle membranes, and perturb the cellular acid-

base homeostasis. To avoid toxicity, FFAs are re-esterified with glycerol, and the resulting TAG are then deposited in LDs in every cell of the body. Accordingly, TAG stores function as buffer for incoming lipids to prevent lipotoxic concentrations of FFAs (Lusis and Pajukanta, 2008). Thus, these mechanisms need to be tightly controlled and orchestrated to maintain lipid homeostasis and growth.

Simultaneously, a small fraction of FA is used by the sphingolipid biosynthetic pathway for the production of ceramide and complex sphingolipids. In the context of ceramide synthesis, FAs and specifically medium chain fatty acids (MCFA) are needed in two steps of the pathway (Figure 1.1). The initial step of the reaction is the condensation of serine with palmytoil-CoA (C14) operated by Serine palmitoyltransferase (Spt) to form sphinganine. CerS then catalyze the N-acylation between the sphinganine backbone and fatty acyl-CoA of different chain length (C-n). In *Drosophila* mainly C14 activated fatty acids are linked to sphinganine for the production of ceramide (Bauer et al., 2009). Ceramide imbalance in tissues has been implicated in the impairment of many metabolic processes.

1.7 Ceramide lipotoxicity

Ceramide lipotoxicity has been shown to affect almost every cell or tissue type examined so far, causing a wide range of effects in a cell-type- specific and context-dependent manner. In fact, alteration of ceramides have been involved in both insulin tolerance and insulin resistance (Shimabukuro et al., 1998; Shulman et al., 2014), obesity associated with low-level of inflammation (Goldberg et al., 2015; Youm et al., 2011), protection or induction of steatohepatitis (Turpin et al., 2014; Xia et al., 2015; Raichur et al., 2014), atherosclerosis (Glaros et al., 2008), and cardiomyopathy (Walls et al., 2018; Goldeberg et al., 2012; Russo et al., 2012).

Numerous lipidomic and inflammasome analysis of plasma sera detected a correlation between plasma ceramides alteration and most of the pathologies described above. The fact that ceramides are biosynthetic intermediates that do not exist in a steady-state concentration and composition represents a challenge in interpreting this profiling. Although most of the metabolic disorders are associated with increased food uptake, little is known about how ceramides fluctuate in response to feeding or other environmental factors.

An understanding of the mechanisms on how ceramides are regulated and how ceramides regulate physiological and pathological events in specific cells may provide new targets for therapeutic intervention.

1.8 Aim of the thesis

Despite the abundance of publications on CerSs, the exact mechanisms of how ceramide synthesis is regulated and on how CerS activity is modulated is to date still far beyond clear. Most of the publications only deal with the effect on altered ceramide levels on physiological and pathophysiological processes not investigating the regulatory mechanisms. Although it became clear during the last years that not only the enzymatic activity plays essential roles in cellular processes but rather the protein itself, the possible homeodomain function is still ignored.

By using the first established *in vivo* animal models for the homeodomain (Anna-Lena Wulf, Ph.D. thesis), this thesis aimed to identify the homeodomain function *in vivo* and its role in regulating fat metabolism.

2 Results

2.1 Schlank *in vivo* models to investigate domain-specific function

To study the homeodomain function *in vivo*, homologous recombination and phage φC31 integrase based genomic engineering approach was used (Anna-Lena Wulf, Ph.D. Thesis). The Schlank gene (exon 2 to exon 6) was replaced by homologous recombination with attP sites generating a *Schlank*^{KO}

(KO) line. Next, target constructs containing the deleted genomic *Schlank* DNA were reintegrated. The reintegrated DNA without (WT) and with a point mutation either in the NLS1 site, or NLS2 site, or E118A of the homeodomain or in the catalytic domain (H215D) were reintegrated into the native Schlank locus in the *Schlank*^{KO} founder line (Figure 2.1) (Sociale et al., 2018). Reintegration of the target constructs restored the target locus, qRT-PCR (quantitative Real-Time Polymerase Chain Reaction) analyses revealed that the transcript levels of *Schlank* and of genes within or close to its genomic locus were similar in *Schlank* knock-in (KI) wild-type (*KIWT*), *Schlank*^{KINLS2} (*KINLS2*), *Schlank*^{KINLS1} (*KINLS1*), *Schlank*^{KIH215D} (*KIH215D*), *Schlank*^{KIE118A} (*KIE118A*), and w1118 control animals (Sociale et al., 2018, Appendix Figure A5.1, A). This confirmed the expression of reintegrated genomic DNA.

The mutation in *KINLS1* affects the monopartite-like NLS1 site (RPKK, 80-81), located at the beginning of the first helix with the homeodomain, where two positively charged amino acids are exchanged with two non-charged amino acids (RPKK to RPMM). The mutation in *KINLS2* affects the portion of the bipartite-like NLS2 (RLRR, 122-124) site residing in the third helix of the homeodomain. In this case, two positively charged amino acids are substituted with two negatively charged ones (RLRR to ALAR). Those two mutations were chosen because they altered Schlank nuclear localization in cell culture experiments. The mutation E118A in the *KIE118A* mutant is the Drosophila homologous of a SNP (E115A) found in human CerS2, associated with diabetes and insulin resistance. This mutation was not tested for localization in cell culture experiments. The mutation H215D in *KIH215D* mutants abolishes the catalytic activity of the protein.

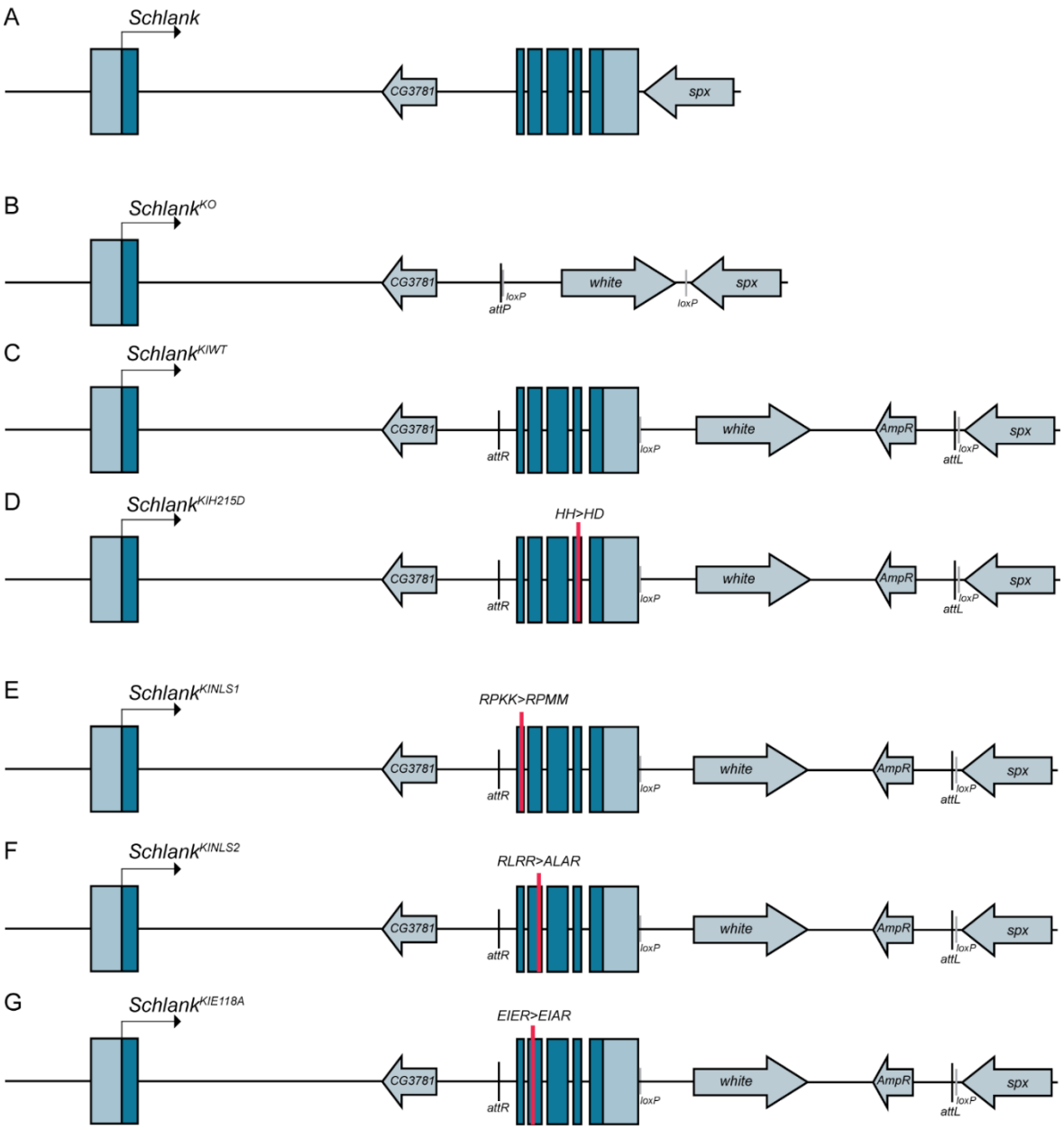

Figure 2.1. Schematic representation of genomic engineering. **A)** Schlank gene is formed by 6 exons that are regulated by splicing. The area targeted for homologous recombination corresponds to part of the first intron and the following gene spx. The first exon and intron are not targeted because of the presence of CG3781 gene coding for a protein with ubiquitin protease activity. **B)** Schlank locus after targeting, exons 2-6 replaced by attP site (*KO*). **C)** Diagram showing the reintegration of the deleted WT gDNA to generate *KIWT* or **D)** with a mutation in the coding region of the catalytic domain from histidine (H) into Aspartic Acid (D) in position 215 (HH>HD) that impairs the enzymatic activity. **E-F-G)** Diagram showing the reintegration of the deleted gDNA with mutations within the homeodomain coding region, in the NLS1 coding site for two to methionines (M) instead of two lysines (K) RPKK>RPMM to generate *KINLS1*. For the NLS2 coding site of two arginines (R) into alanine (RLRR>ALAR) to generate *KINLS2* and for the homologous of a mammalian SNP for the coding region of the amino acid in position 118 for a alanine (A) instead of a glutamic acid (E) to generate *KIE118A* (modified from Sociale et al., 2018).

2.2 Phenotypical characterization of homeodomain mutants

To investigate and understand the homeodomain function, an in-depth analysis of different Schlank KI alleles (Figure 2.1, A; G) was carried out taking advantage of the first established *in vivo* homeodomain models. A scheme of where the different mutations within the Schlank protein are localized is presented in Figure 2.2, A.

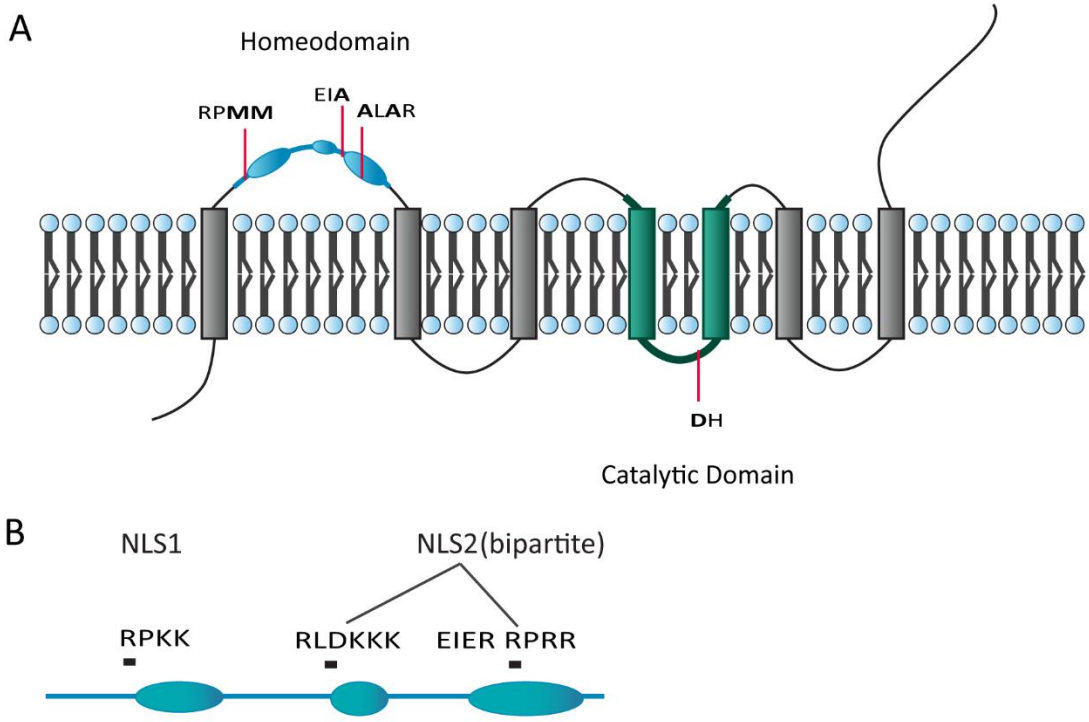

Figure 2.2. Schematic of the mutations within Schlank. **A**) The red bars indicate where the different mutations are directed. Bold letters within amino acids (aa) sequence highlight the mutations. **B**) Schematic of Homeodomain monopartite-like NLS1 (RPKK, aa 78–81) and atypical bipartite-like NLS2 (RLDKKK-X19RLRR, aa 97-102 and 122–125) are depicted above the homeodomain. The position where the E>A SNP is located is also depicted (EIER, aa 116-119).

The above-mentioned fly lines were analyzed for survival and development, body fat content and Schlank nuclear localization. Since *KIWT* flies were not distinguishable from the commonly used W^{1118} or Oregon R- control fly regarding survival, development, fitness, gene expression (See Appendix, Figure A5.1, A) and any other analysed parameters, the data of these additional controls (W^{1118} and *Oregon R-*) have been omitted from this thesis. Therefore, the *KIWT* was used as a control in all of the experiments described here, because of the similarity in genetic background.

2.2.1 Phenotypical analysis of Schlank mutants

The phenotypical analysis of *KO* and *KIH215D* mutants, showed an early larval lethality, proving once more CerS as center player in biological processes. Meanwhile, the homeodomain mutants show different degrees of developmental delay and survival rate. *KINLS1* larvae and adults are not distinguishable from *KIWT* control flies (Figure 2.3, A, B), *KIE118A* show a few hours delay in reaching the pupariation stage. Generally, pupariation occurs on day 5 (120 h) after egg laying (AEL), when larvae are kept at 25°C. In the case of *KIE118A*, the pupation of 76% of the selected larvae occurred around 130 h AEL (Figure 2.3, A). The hatched *KIE118A* adults showed a lifespan similar to *KIWT* and *KINLS1*, but they happened to die earlier on average (Figure 2.3, B). In contrast, the developmental delay and the survival rate for *KINLS2* mutants were more dramatic. Notably, at day 5 AEL, *KINLS2* mutants were still entering the second instar larval stage (L2), only around 20% of the counted larvae reached the pupation stage which occurred for most of them around day 11. The few flies who managed to hatch as adult flies (~10%) showed several defects in motoric dysfunction, analyzed by climbing assays (Christoph Schwarzkopf, Master Thesis). The developmental delay of *KINLS2* is not surprising considering the slimness phenotype of these larvae. It is well known that to undergo pupation *Drosophila* larvae need to reach a critical mass or weight (Edgar, 2006, Davidowitz et al., 2003, Nijhout, 2003). After 9 days (d) of larvae stage the *KINLS2* larvae reach *KIWT* in length, but they appeared thinner (Figure 2.3, C; Sociale et al., 2018), resembling partially the phenotype of the previously published Schlank P-element mutants (*Schlank*^{G0061}, *Schlank*^{G0349}) (Bauer et al., 2009).

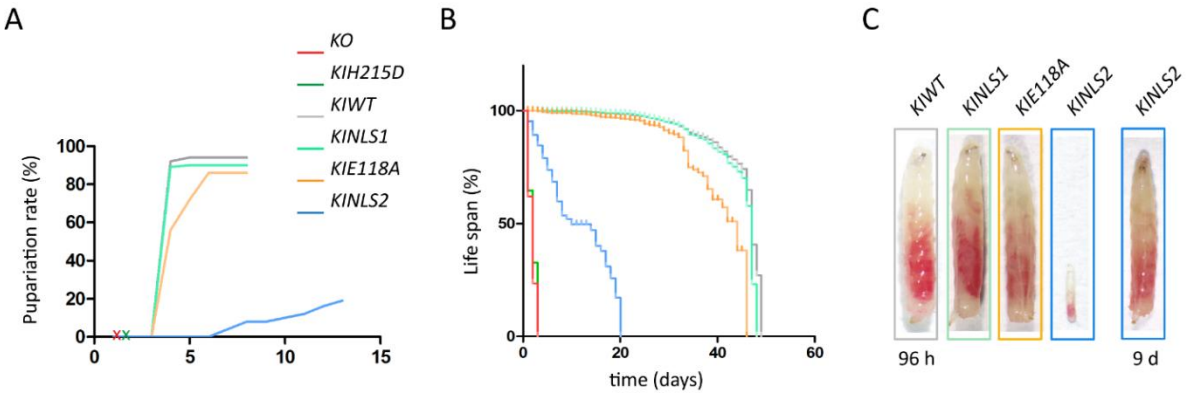

Figure 2.3. Life Span analysis of *Schlank* KI alleles. A) Pupariation rate. The green and red "X" are referring to *KO* and *KIH215D* that do not pupariate, grey and turquoise refer to *KIWT* and *KINLS1* respectively, that pupariate as WT flies, orange referrers to *KIE118A* showing a reduced puparation rate and a slight developmental delay. The blue line represents *KINLS2* mutants; that show a severe developmental delay and a

reduced survival rate at around day nine some of the larvae reach the third instar larval stage (L3) and start to pupariate, mostly the survived larvae reach pupariation around 13 d AEL. **B)** Life span analysis; *KO*, and *KIH215D* die during the first 48h AEL (red and green) as L1. A reduced percentage of *KINLS2* (blue) hatch as a small sized adult, showing motoric dysfunction and mostly die within the first ten days of life as adults, *KIE118A* (orange) also show a small reduction of life span when compared to *KIWT* and *KINLS1* (grey and turquoise). **C)** Monitoring of food intake by feeding red-colored yeast and phenotypical analysis of mutant larvae. *KINLS2* show developmental delay and a slimness phenotype when morphologically reaching the L3 stage (e.g., 9 d) (analysis of anterior and posterior spiracles, See Materials and Methods, 4.2.1).

2.2.2 Analysis of body fat homeostasis

To exclude that the difference in body fat was merely due to a difference in food uptake, the larvae were fed with red-colored yeast (Figure 2.3, C), showing non-altered food uptake. As mentioned above, TAGs are the primary form of stored lipid in the fat body organ in Drosophila, and TAG metabolism leads to the production of FFAs. To verify whether an impairment of TAG metabolism would be responsible for the slim phenotype of the mutant, analysis of fat body cell size, TAG and FFA content were carried out.

No differences were observed for fat body cell size (quantification in Figure 2.4, A) and in the relative amount of TAG and FFA for *KINLS1* and *KIE118A* (Figure 2.4, B, C). In contrast, *KINLS2* mutants showed an easily noticeable difference in cell size, with *KINLS2* cells more than 50% smaller than *KIWT*. Representative image for *KIWT* and *KINLS2* are shown in the Appendix Figure A5.2, A. Interestingly, when using the FLP/FRT system to perform clonal analysis in fat body cells, the overexpression of a full-length wild-type Schlank variant in the background of *KINLS2* significantly increased cells size while overexpression of $Schlank^{RNAi}$ managed to reduce cells size even more. The direct conclusion of these findings is that Schlank can regulate size in a cell-autonomous way. This might be dependent on the homeodomain function since the overexpression of $Schlank^{NLS2}$ (NLS2-HA) did not influence cell size (Benjamin Franz Syllwasschy, Bachelor Thesis). Moreover, the analysis of body fat content confirmed a reduction in TAG levels and an increase in FFA levels for *KINLS2* mutants (Figure 2.4, B, C).

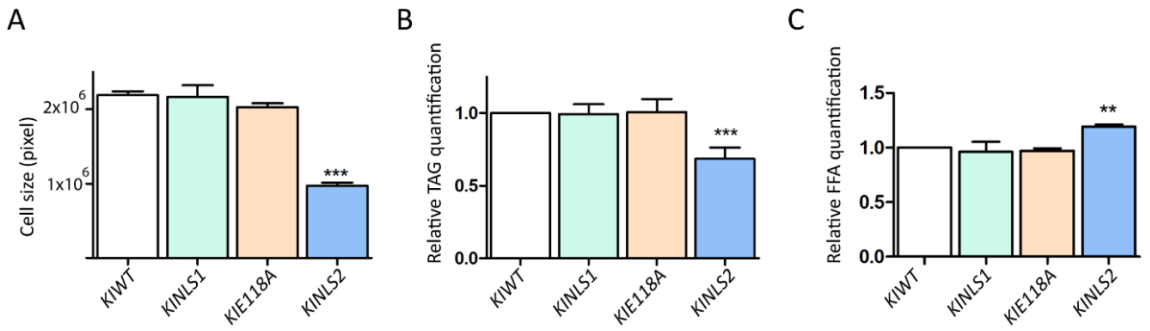

Figure 2.4. Analysis of cell size and body fat. A) Reduced cell size in *KINLS2*. Representative image for *KIWT* and *KINLS2* are shown in the Appendix Figure A5.2, A. **B**) Relative TAG quantification normalized to dry weight show a reduction in the TAG for *KINLS2* mutants in accordance with the phenotype. C) Relative FFA normalized to protein concentration showed an increase in FFA for KINLS2 mutant. Error bars indicate SEM, **$p < 0.01$, and ***$p < 0.001$.

Stored TAG are broken down by lipases in glycerol and FFA, these can then be utilized to gain energy through mitochondrial β-oxidation. For this reason, the transcription level of genes involved in lipid metabolism and particularly in lipolysis was examined.

In the past years, several lipases have been studied in the context of lipid homeostasis and linked to body fat regulation in *Drosophila*. The lipases *CG6295* (Palanker et al., 2009), *CG6277* and *CG8093* (Nirala et al., 2012), *brummer* (bmm) (Grönke et al., 2005) were chosen because associated with reduced TAG levels. Despite being a gastric lipase, *magro* was tested because it is linked with reduced body fat (Sieber and Thummel, 2009). *Lipase3* (*lip3*) was also examined because strongly upregulated in *Schlank*^{G0061} mutants. Moreover, in these mutants *lip3* could be repressed upon overexpression of a *Schlank* WT variant (Bauer et al., 2009).

In agreement with the observed TAG reduction and increased FFA, qRT-PCRs revealed an increase of *lip3*; *CG6295*; *CG6277*; *CG8093* and *magro* transcripts in *KINLS2* larvae, but not in *KIE118A* and *KINLS1* (Figure 2.5, A, B). The lipase *bmm*, not deregulated in *KINLS2* mutants, together with *lip3* are responsive to starvation (Zinke et al., 2002; Grönke et al., 2007) and have been used in combination with other components of the insulin signaling pathway (ILS) as starvation markers. The Insulin signalling starts with the secretion from the brain of *Drosophila* insulin like peptides (DILPs) that as extracellular ligands, bind to the Insulin Receptor (InR), initiating a phosphorylation cascade and through Akt (serine/threonine-specific protein kinase (PKB)) inhibit the transcriptional activity of Foxo (the main effector TF of ILS).

In a food-deprived situation, Foxo remains constitutively active and regulates the translational regulator *4E-BP* (eukaryotic initiation factor 4E binding protein, *thor* in

Drosophila) and *InR* itself, providing a feedback mechanism and regulating different genes including *bmm*. To exclude any impairment of the ILS, starvation response genes such as *InR, thor, bmm* and several others were tested in *KINLS2* mutants. Genes involved in ILS were not transcriptionally upregulated in *KINLS2* larvae (Figure 2.5, C). However, their expression could be induced upon starvation (Figure 2.5, E), indicating a normal starvation response.

Moreover, the expression of factors involved in lipid homeostasis as *SREBP* (sterol regulatory element binding protein) and *DHR96* (*Drosophila* hormone receptor 96) responsive to Cholesterol, and *FAS* (fatty acid synthase) was also analyzed by qRT-PCR. Although *SREBP* and *DHR96* were not affected in transcriptional regulation, the expression of *FAS* was moderately increased (Figure 2.5, F).

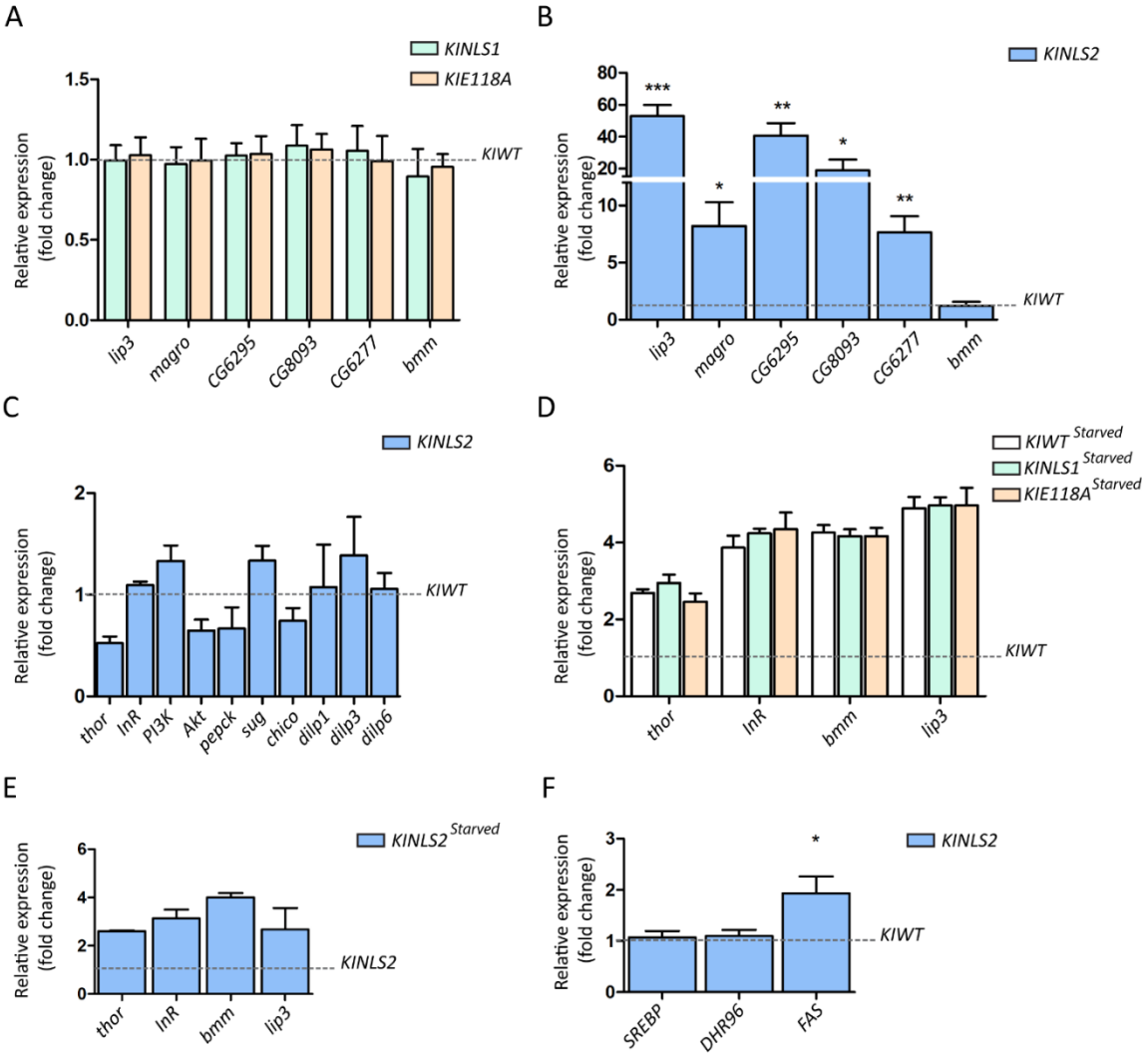

Figure 2.5. Analysis of gene involved in TAG metabolism and ILS. A) Lipases expression in *KINLS1* and *KIE118A* normalized to *KIWT* gene expression. **B)** Lipases expression in *KINLS2* normalized to *KIWT* gene expression, any of the lipases tested resulted chronically upregulated. **C)** Genes involved in ILS in *KINLS2* are

normally expressed, normalized to *KIWT* gene expression. **D)** Analysis of starvation response for genes involved in ILS for *KIWT*, *KINLS1*, *KIE118A* and *KINLS2* **E)** show an unaltered response to starvation normalized to *KIWT* gene expression for starved *KINLS1*, *KIE118A* and *KIWT*, normalized to *KINLS2* for starved *KINLS2* (**E**). **F)** Relative expression of genes involved in lipid homeostasis show normal expression levels for *SREBP* and *DHR96*, but an upregulation in *FAS* for *KINLS2* normalized to *KIWT* gene expression. Transcript levels were quantified using qRT-PCR (normalized to *rp-49*). Error bars indicate SEM. *p < 0.05, **p < 0.01, and ***p < 0.001.

Fatty acid biosynthesis and breakdown occur by different pathways, are catalyzed by different sets of enzymes, and take place in different compartments of the cell. When a cell or organism has more than enough metabolic fuel to meet its energy needs, *FAS* is overexpressed to convert the excess of fuel in FAs, and subsequently they are converted into TAGs. For these reasons, the *de novo* rate of TAG and FA was also measured. Accordingly, *de novo* TAG synthesis was reduced, while in contrast FA synthesis was slightly increased, supposing an alteration of FA catabolic and metabolic processes in *KINLS2* (Figure 2.6).

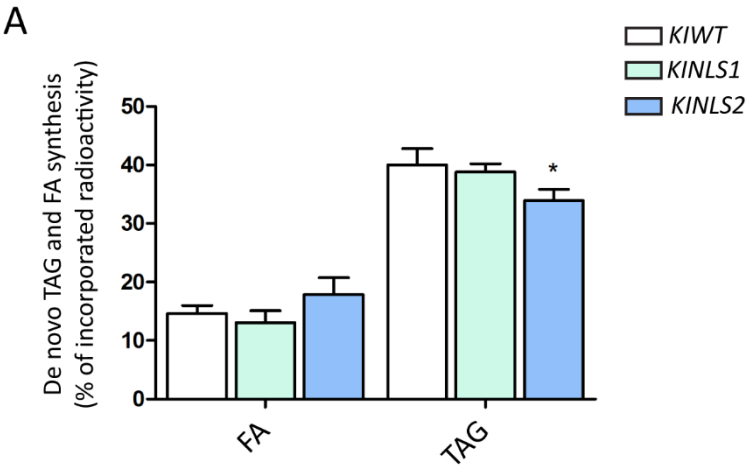

Figure 2.6. Analysis of lipogenesis. Metabolic labeling experiment in larvae using [1-14C]-acetic acid to determine TAG and FA generation. Equal amounts of radioactivity were applied to TLC plates, and percentage of the incorporated label was quantified. Biosynthesis of TAG is reduced in *KINLS2* mutants whereas generation of FA is increased. No change is observable for *KINLS1*. This data are not yet available for *KIE118A.* Error bars indicate SEM. *p < 0.05, **p < 0.01, and ***p < 0.001.

These pathways are regulated at the level of gene expression although the detailed mechanism by which these genes are regulated is not yet clear. However, if FA synthesis and TAG breakdown were proceeding simultaneously, like in the case of *KINLS2* mutants, the two processes would constitute a futile cycle, simply causing a waste of energy. This is confirmed in *KINLS2* by low ATP levels and hyperphosphorylation of AMPK, a well-known cellular energy sensor (Azim M. Sarker, Master Thesis).

2.2.3 *De novo* Ceramide Synthase activity

To rule out the impact of the enzymatic function of the protein on any of the observed phenotypes, a *de novo* ceramide synthase assay was performed. First instar larvae were selected and kept on standard food until 48h AEL. After this time, radioactive acetate mixed with inactivated yeast was fed for 18h. Subsequently, lipids were extracted and TLC (Thin Layer Chromatography) was performed (Dr. Bernadette Breiden). Unexpectedly, the *de novo* ceramide synthesis rate was reduced for *KINLS1* but resulted unchanged for the *KINLS2* mutants (Figure 2.7, A). Meaning that the phenotypes of *KINLS2* mutants were exclusively linked to the Schlank homeodomain and strengthening its function in relation to body fat homeostasis.

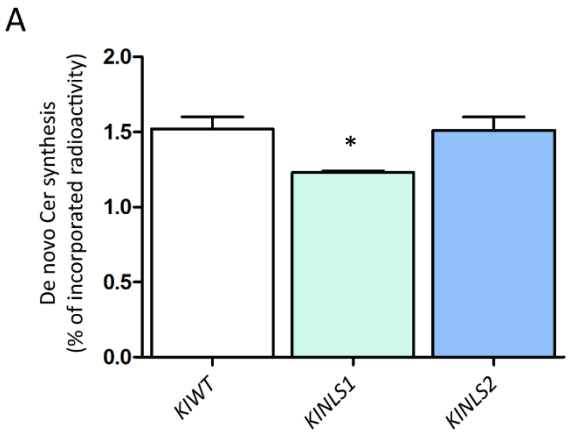

Figure 2.7. Analysis of *de novo* CerS. A). Metabolic labeling experiment in larvae using [1-14C]-acetic acid to determine *de novo* ceramide generation. Equal amounts of radioactivity were applied to TLC plates, and percentage of the incorporated label was quantified. Biosynthesis of ceramide in *KINLS2* mutants showed no difference in comparison with *KIWT* controls, while *KINLS1* shows reduced *de novo* ceramide synthesis. This data are not yet available for *KIE118A.* Error bars indicate SEM. *p<0.05.

2.3 Schlank nuclear function and transcriptional regulation

Each of the mutant fly lines was tested for impairment of nuclear localization in fat body cells of L3 larvae (Figure 2.8, A). Previously it was shown that the NLS2 and NLS1 sites are necessary for nuclear localization in cell culture experiments and that mutation of the NLS2 site resulted in the loss of Schlank nuclear function in lipid homeostasis in P elements mutants (Voelzmann et al., 2016). For *KINLS1* and *KIE118A* mutants, no difference in nuclear localization was observed. Considering the severity of *KINLS2* phenotypes, a complete ER retain for Schlank carrying the NLS2 mutation was expected. Instead, Schlank nuclear localization was not dramatically reduced (~15%) for *KINLS2*, in comparison with *KIWT* (Sociale et al., 2018). This reduction does not seem sufficient to explain all the severe phenotypes of *KINLS2* mutants. Representative image for *KIWT* and *KINLS2* are shown in the Appendix Figure A5.2, B

A

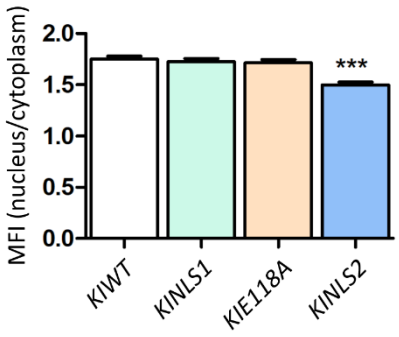

Figure 2.8. Analysis of Schlank nuclear localization. A) Relative mean fluorescence intensities (MFIs) of nucleus/cytoplasm, determined in fat body cells of *KINLS2* and *KIWT* (L3) larvae using α-Schlank antibody recognizing the C-Terminal of the protein (α-Schlank CT). Cells were stained for Lamin Dm0 to mark the nuclear membrane, Spectrin to mark cell membrane and DAPI. Representative image for *KIWT* and *KINLS2* are shown in the Appendix Figure A5.2, B. Error bars indicate SEM, *** p<0.001.

2.3.1 Extensive framework of deregulated gene expression

Following the data pointing to deregulated transcriptional response (Figure 2.5 B, E, F), genome-wide transcriptome data of the fat body of *KINLS2* and *KIWT* L3 larvae using quantitative RNA-sequencing (RNA-seq) were generated and followed by bioinformatics analysis (in collaboration with AG Schultze).

An unbiased principle component analysis based on all 10,760 present genes and hierarchical clustering on the 1,000 most variable genes revealed significant transcriptional changes between *KIWT* and *KINLS2* mutants. Using a one-way ANOVA-model, differentially expressed genes between the two conditions were determined, and the fold changes against the p-values were plotted in a volcano plot (Figure 2.9, A). 664 genes were significantly up- or downregulated with a fold change of ≥3 and a p-value of 0.05. The majority of genes was upregulated in *KINLS2* (503 genes). The topology of variable genes between *KIWT* and *KINLS2* mutants is visualized by mapping the fold change among the two conditions onto the nodes of the network, representing the genes. Highlighting the 664 significantly up- and downregulated genes revealed two distinct clusters of co-expressed genes (Figure 2.9, B).

Furthermore, the 10 genes with the highest and lowest fold changes were used to identify their nearest neighbours in the co-expression network and gene ontology enrichment analyses on the two resulting gene sets were performed. A significant enrichment for genes downregulated in *KINLS2* and their neighbours was not detected, but a list of significantly enriched GO-terms was determined for the gene set based on the genes upregulated due to the NLS2 mutation (Figure 2.9, C). Interestingly, all significantly enriched GO-terms describe metabolic processes and show a striking overrepresentation of terms associated with lipid metabolism, matching the phenotype observed for the mutant animals and underlining

the relevance of Schlank in this regard. Taken together, the RNA-seq analysis revealed a substantial impact of the NLS2 mutation on transcription.

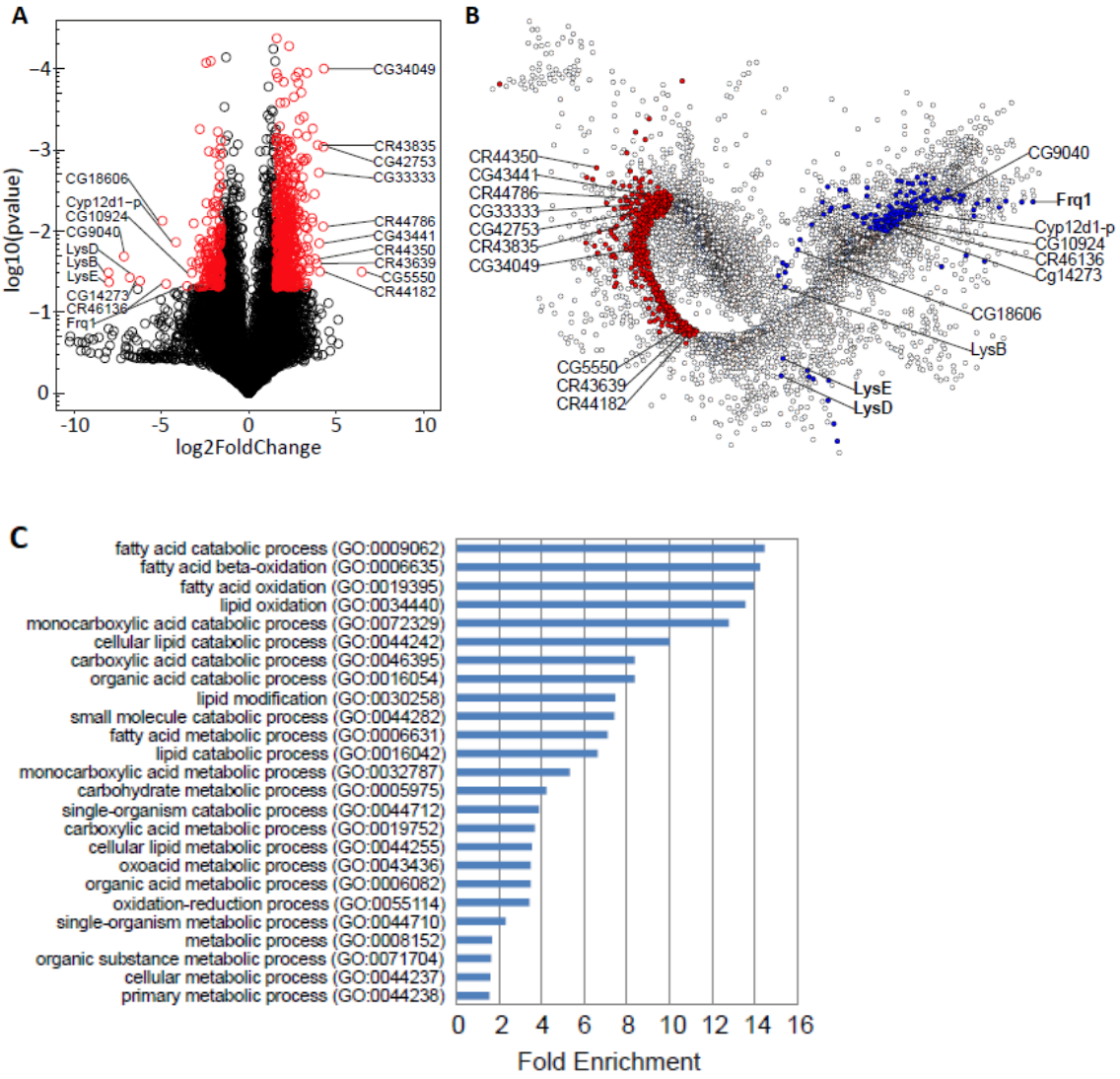

Figure 2.9. Altered gene expression in *KINLS2* mutants. A) Volcano plot of all present genes. Genes significantly up- or downregulated (fold change |FC| > 3; p-value < 0.05) in *KIWT* over *KINLS2* mutants are marked in red. Sorted by fold change the gene symbols of the most up and downregulated genes were added to the plot. **B)** Using the same dataset, a coexpression network was calculated. Genes significantly upregulated in *KINLS2* mutants were marked in red, while downregulated genes were coloured in blue. Gene symbols of the most regulated genes were added to the plot. **C)** The 20 most up- and down-regulated genes together with their nearest neighbours taken from the co-expression network (Figure 2.9; **B**) were used to perform a gene ontology enrichment analysis. Significantly enriched GO terms for genes upregulated in *KINLS2* are listed according to their fold enrichment.

2.3.2 DNA binding mediates transcriptional regulation

It is possible to hypothesize from qRT-PCRs, RNA-seq data, and from the mild reduction in nuclear localization in *KINLS2* mutants that a functional Schlank homeodomain is needed to regulate transcription. Although previous publications questioned that CerS homeodomain might act as a transcriptional regulator, the modelling of the Schlank homeodomain revealed that the folding corresponds to the standard DNA binding architecture of homeodomain like transcription factor as the well-known Drosophila Ubx (André Voelzmann, Ph.D. Thesis; Sociale et al., 2018). Moreover, scanning promoter regions of *lip3* and *magro* for Schlank binding site (described by Noyes et al., 2008; JASPAR database) showed several binding sites for the putative Schlank consensus (Sociale et al., 2018) (Figure 2.10, A, B).

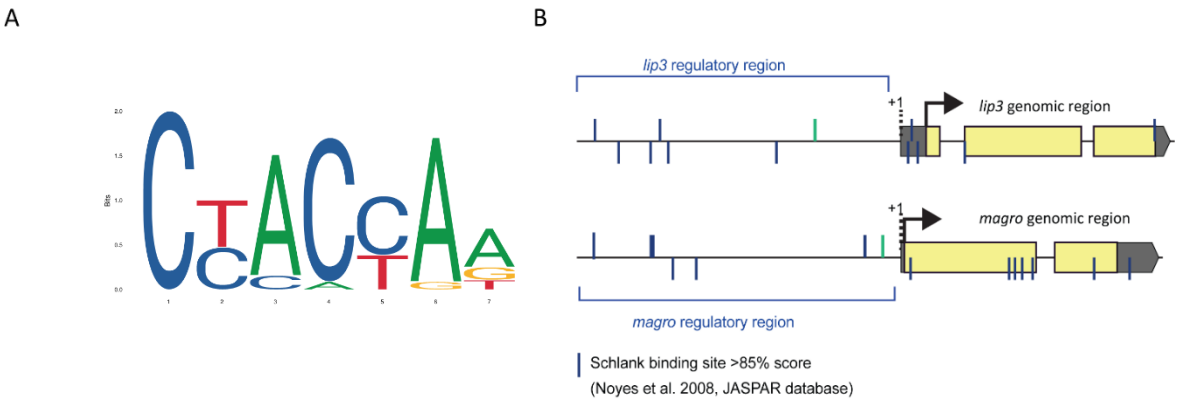

Figure 2.10. Schlank binding consensus. A) Schlank consensus obtained by JASPAR database based on position frequency matrices (PFMs) and TF flexible models (TFFMs) of TFs across multiple species from six taxonomic groups. **B)** Scanning of *lip3* and *magro* gene locus for Schlank binding consensus. The bars indicate different Schlank binding consensus within the lipases regulatory regions but also within the gene locus. The green bars identify the sites amplified in the experiments described below (ChIP).

To verify whether Schlank might be able to bind DNA, Chromatin Immunoprecipitation (ChIP) assay was established. For the simplicity of the system, S2 cells were used to perform every ChIPs.

Firstly, ChIP was performed with two different Schlank specific antibodies on endogenous Schlank; the fist one recognises the beginning of the homeodomain (α-Hox), while the second one recognises the C-Terminal part of the protein (α-CT). Pull down with an α-Histone H3 was chosen as a positive control (Histone proteins are bound almost everywhere in the genome) and as a negative control for the immunoprecipitation (IP), an α-

IgG antibody was used. Every ChIP always included an Input sample representative of the whole DNA extract.

Linker-mediated PCR was considered to be the first and more immediate way for the visualization of the IP results. Linkers were ligated to the whole pull down and used for amplification by PCR. Subsequently, the pull-down was amplified with *lip3* or *magro* specific primers (randomly chosen site among the different ones found by JASPAR scanning tool with a matrix score higher than 90%; green bars in Figure 2.10, B). Afterward, the PCR samples were run on an agarose gel. It is possible to notice in Figure 2.11, A, that, among all of the unspecific bands, a band of the right size (~100 bp) appeared in every sample except the for IgG sample, where no band was present. Afterward, the same set of primers was used for qRT-PCR. Primers for negative controls were also included, amplifying regions of *sprouty* (*sty*) (commonly used as negative control for ChIP in *Drosophila*, Xu et al., 2012). The expression fold for each amplified gene in the IP was normalized on its IgG expression fold. In Figure 2.11 B, it is possible to appreciate that there is an enrichment of *lip3* and *magro* promoter for the pull down of Schlank α-CT and Schlank α-Hox in comparison with the negative control *sty*. No enrichment for *lip3* and *magro* regulatory regions is present in the Input and H3 samples, meaning that they were selectively pulled down by Schlank specific antibodies. These results prove not only that Schlank homeodomain could bind DNA, but also that the whole transmembrane protein is involved in the regulation at the DNA.

Next, the impact of the different mutations on DNA binding was analysed. To this end, different Schlank mutant variants fused with a hemagglutinin tag (HA-tag) were overexpressed in S2 cells (p*UAS*T-Schlank-HA vectors were cotransfected with pAc-GAL4 vector), *UAS-Schlank*^{WTHA} (WT-HA), *UAS-Schlank*$^{NLS2\text{-}HA}$ (NLS2-HA), *UAS-Schlank*$^{NLS1\text{-}HA}$ (NLS1-HA) (Bauer et al., 2009; Voelzmann et al., 2016), and the newly generated *UAS-Schlank*$^{E118A\text{-}HA}$ (E118A-HA) and *UAS-Schlank*$^{H215D\text{-}HA}$ (H215D-HA), also to rule out any impact from the catalytic domain on DNA binding. Confirming the results of the ChIP experiments on the endogenous Schlank, an enrichment in regulatory regions of *lip3* and *magro* was observed when precipitating the WT-HA. No difference was observed regarding the DNA binding capabilities of NLS1-HA, E118A-HA, and H215D-HA proving that the homeodomain function is also independent of the enzymatic activity of the protein (Figure 2.11, C). In contrast, NLS2-HA failed to precipitate regulatory regions of *lip3* and *magro* since no enrichment was observed in comparison to the negative control *sty* (Figure 2.11, D). Furthermore, in-depth bioinformatics studies revealed that the NLS2 mutations are

overlapping with the putative DNA-binding region in the third helix of the homeodomain, and particularly that the mutated Arginine in position 122 is described as a critical residue for sequence-specific DNA-binding of Hox-domains (Bürglin and Affolter, 2016).

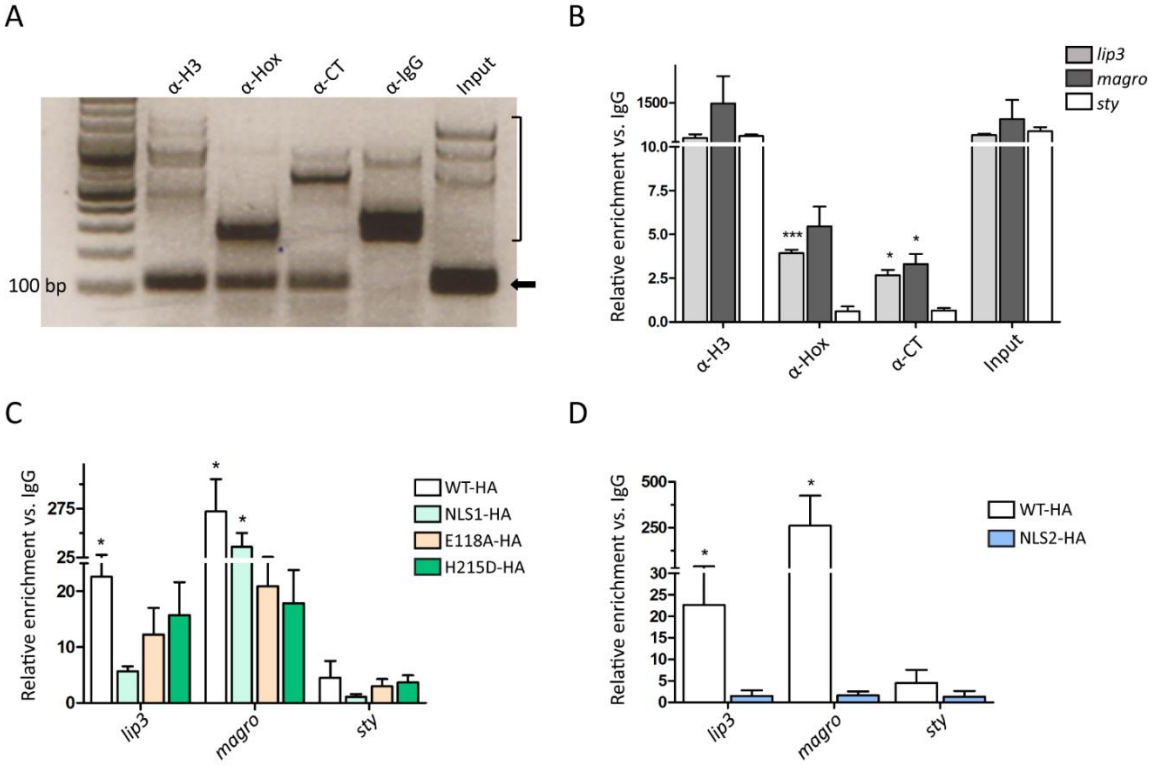

Figure 2.11. Schlank binds *lip3* and *magro* promoter regions. A) Analysis of Schlank pull down (ChIP) material from S2 cell extract by linker-mediated-PCR, using α-Hox, α-CT, α-IgG, and α-H3 antibodies as negative and positive controls, respectively. The Input sample is representative of the initial amount of DNA. The square bracket highlights unspecific bands while the arrow indicates the expected, specific 120bp band (representative amplification for *magro* promoter region). **B)** Quantification by qRT-PCR of ChIP; promoter regions assayed were those of *lip3*, *magro*, and *sty* (negative control). Expression was normalized to the relative expression of the IgG sample (n = 3). **C)** Quantification by qRT-PCR of ChIP material from S2 cell extract transfected with HA-WT, E118A-HA, NLS1-HA and H215D-HA (n = 3) using α-HA antibody. The mutations do not affect DNA binding since *lip3* and *magro* regulatory regions result enriched in comparison with sty. **D)** NLS2-HA IP does not pull down selectively and in an enriched fraction *lip3* and *magro* regulatory regions in comparison with sty (n = 4). The Positive control used is WT-HA. Error bars indicate SEM, * $p<0.05$.

2.3.3 Schlank DNA binding is necessary to repress *lip3 in vitro* and *in vivo*

To gain more information about the transcriptional regulation and to further prove Schlank DNA binding properties, luciferase reporter assay was performed. A *lip3* upstream regulatory region (1.7 kb) was cloned into a firefly-luciferase reporter assay plasmid (Dominic Peters, Bachelor thesis). S2 cells were cotransfected with the *lip3*-firefly, the Schlank variant of interest and with a Renilla luciferase control reporter. The system was tested by overexpression of WT-HA, $Schlank^{RNAi}$, and an unrelated TF *UAS-AP-2* (AP-2). As general control, an *UAS-nuclearGFP* (neGFP) was used. As shown in Figure 2.12 A, the overexpression of the unrelated TF AP-2 did not change *lip3* reporter activity. In contrast, HA-WT strongly repressed *lip3* reporter activity while an increase in luciferase activity was observed when $Schlank^{RNAi}$ was overexpressed. These results confirm the hypothesis postulated in previous publications (Bauer et al., 2009; Voelzmann et al., 2016) that Schlank is needed for the repression of *lip3*. This regulatory mechanism would be in accordance with several publications on Hox protein showing that they act as repressors, particularly during development (Gabelein et al., 2004; Agelopoulos et al., 2012).

Next, the impact of the different mutations (NLS1-HA, E118A-HA, H215D-HA, and NLS2-HA) on *lip3* reporter activity was evaluated. In accordance with ChIP results the overexpression of either NLS1-HA, E118A-HA, H215D-HA where the DNA-binding capability is not affected (Figure 2.11, C), could repress *lip3* luciferase activity (Figure 2.12, B). However, when NLS2-HA, mutation that abolishes DNA binding (Figure 2.11, D) was overexpressed, the suppression of *lip3* reporter activity was lost (Figure 2.12, B). In conclusion, these data provide evidence that the DNA binding mediated via the NLS2 site within the homeodomain is required for transcriptional regulation (Figure 2.12, B). Moreover, these experiments suggest that the NLS2 mutation has a dominant negative effect on transcriptional regulation.

The NLS2 site is conserved in all the mammalian CerSs (mCerSs) except CerS3, which nevertheless still contains the two arginines that are mutated in the NLS2 mutants (Voelzmann et al., 2016). Alignment for NLS2 site is shown in Appendix Figure A5.7, A.

Therefore, a mammalian homeodomain-containing CerS was tested for the ability in regulating *lip3* expression. CerS2 was chosen because it was already proven to be able to rescue Schlank P-element mutants (Bauer et al., 2009). Thus, HA-CerS2 and newly generated CerS2-NLS2-HA carrying a mutation in the NLS2 (**RR**R**R** to **A**R**A**R) and CerS2-H215D-HA carrying a mutation in H215D, were generated and tested in the luciferase reporter system (Figure 2.12, C). The expression of both WT-HA and H215D-HA CerS2

variants resulted in a repression of the *lip3* reporter activity, while CerS2-NLS2-HA failed to repress lip3 luciferase activity (Figure 2.12, C) comparably to Schlank variants (Figure 2.12, B). Thus, these data show that the mammalian CerS2 could also regulate transcription and that the NLS2 site would be indeed conserved and required for this function.

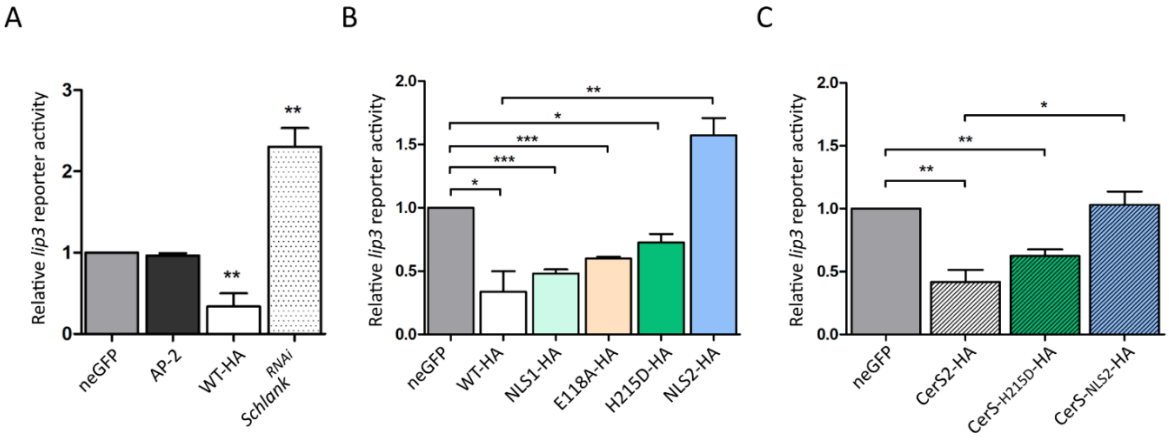

Figure 2.12. Schlank represses *lip3* transcription. A) A 1.7 kb *lip3* enhancer was introduced into a luciferase reporter plasmid containing an actin basal promoter and firefly luciferase (*lip3* reporter). Relative luciferase induction upon expression of neGFP, unrelated TF AP-2, WT-HA, and *Schlank*^{RNAi} is indicated, normalized to Renilla luciferase control transfection (n= 3). **B)** Relative luciferase induction upon expression of either WT-HA, NLS1-HA, E118A-HA, or H215D-HA, suppresses luciferase activity, while expression of NLS2-HA increases *lip3* reporter activity (n = 3). **C)** Relative luciferase induction upon expression of either HA-CerS2, CerS2-H215D-HA, or CerS2-NLS2-HA (n = 3), the mutations in mCerS2 behave as Schlank on lip3 reporter activity. Error bars indicate SEM, *** p<0.001, ** p<0.01,* p<0.05.

To confirm these results, obtained in cell culture experiments, also *in vivo*, the Gal4/UAS system was used. Several UAS Schlank variants fly lines were crossed in the background of *KINLS2* mutant. The expression was driven from the first hours of larval development until the L3 stage using a specific fat body driver (cgGAl4, Pastor-Pareja et al., 2011). The samples were frozen and processed for qRT-PCR analysis of *lip3*. *Lip3* transcription was strongly repressed upon expression of WT-HA (*UAS-Schlank-HA*, CT-HA tag) or HA-WT (*UAS-HA-Schlank*, NT-HA tag), and H215D-myc (*UAS-SchlankH215D-myc*, CT-myc tag). On the contrary, confirming the *in vitro* experiments, HA-NLS2 (*UAS-HA-SchlankNLS2*) did not repress *lip3* expression (Figure 2.13, A).

CerS2 variants were also tested *in vivo*. HA-CerS2, CerS2-H215D-HA, and CerS2-NLS2-HA variants were expressed in the fat body of *KINLS2* mutants. Transcription of *lip3*

was repressed upon expression of HA-CerS2 or CerS2-H215D-HA in *KINLS2* mutants while CerS2-NLS2-HA did not repress *lip3* expression (Figure 2.13, B).

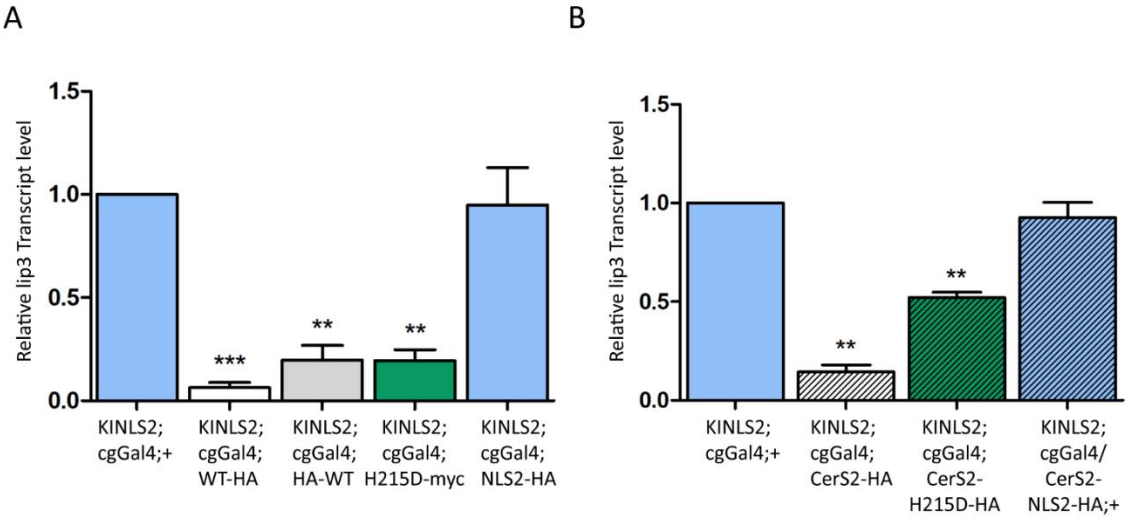

Figure 2.13. *Lip3* transcriptional regulation *in vivo*. A) Transcript levels of *Iip3* in L3 *KINLS2* mutant larvae upon expression of HA-WT or WT-HA, H215D-myc, or of a Schlank NLS2 variant (NLS2-HA) under control of the cgGal4 driver line. **B)** Transcript levels of *lip3* in *KINLS2* mutant larvae upon expression of CerS2-HA, CerS2-H215D-HA or CerS2-NLS2-HA using the cgGal4 driver line. *KINLS2* larvae carrying the cgGal4 driver line but not expressing Schlank variants were used as a control. Transcript levels were determined using qRT-PCR (n = 3) and normalized on *rp-49* expression. Error bars indicate SEM, *** $p<0.05$, ** $p<0.01$, *$p<0.001$.

These data provide substantial evidence that Schlank controls lipid metabolism by regulating transcription via the homeodomain and that the catalytic activity is not required for this function. Furthermore, this function seems to be conserved in the mammalian CerS2.

2.4 The physiological role of Schlank in the regulation of lipases

2.4.1 Schlank DNA binding and nuclear localization depend on nutrient availability

The previous data prove that Schlank can regulate transcription via DNA binding. However, how and when the regulation takes place in physiological conditions remains an open question. As mentioned earlier, *lip3* is generally upregulated in starvation (Zinke et al., 2002) and it has been used for several years as a starvation marker. To understand whether the transcriptional regulation of Schlank on *lip3* would be starvation-dependent, DNA binding during starvation was tested. To eventually determine DNA binding in starvation, S2 cells were firstly transfected with HA-WT Schlank variant. After 48h incubation with complete nutrient-rich medium to allow the cells to express the constructs efficiently, S2 cells were starved for 6h in serum-free media (FBS, fetal bovine serum) and subsequently processed for ChIP. As showed above, HA-ChIP from fed S2 cells resulted in enriched regulatory regions of *lip3* and *magro*.

In contrast, in the HA-ChIP from starved S2 cells, the investigated regulatory regions were no longer enriched (Figure 2.14, A). The same experimental set up was also used for luciferase reporter assay. Confirming what was observed by ChIPs, HA-WT was no longer able to suppress the luciferase activity when S2 cells were starved, similar to the results obtained when the NLS2 mutant variant was used for the reporter assay (Figure 2.14, B and Figure 2.12, B, modified from Sociale et al., 2018).

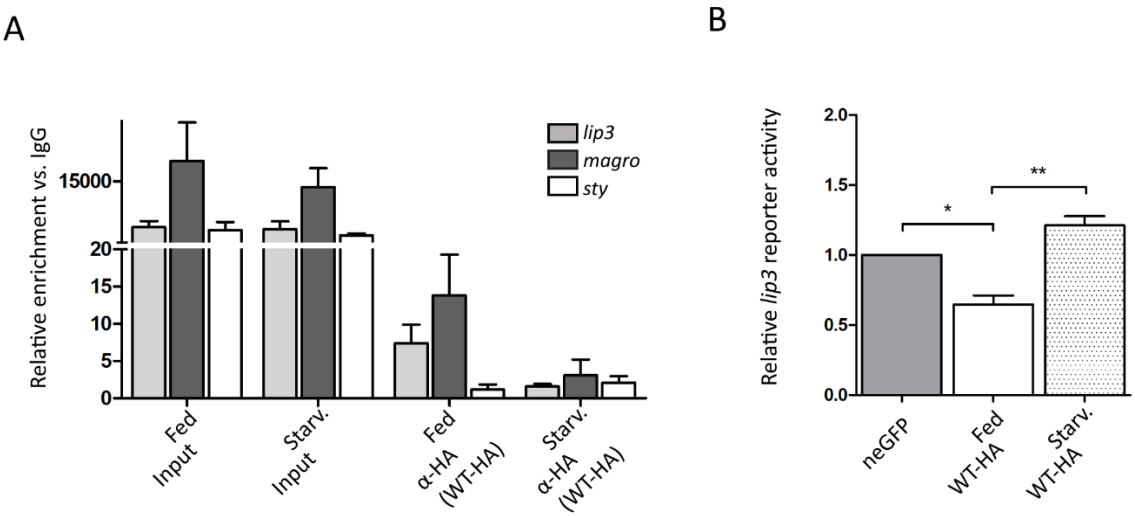

Figure 2.14. Schlank DNA binding in starvation. A) Quantification by qRT-PCR of ChIP material from S2 cell extract transfected with HA-WT, which then were fed or starved for 6h, using a-HA antibody (n = 3). **B)** Relative luciferase induction upon expression of either HA-WT in fed and starved S2 cells (n = 3). Error bars indicate SEM. ** $p<0.01$, *$p<0.05$.

In the likely case that Schlank would act as a suppressor of *lip3* and *magro* during feeding conditions, it would need to leave the enhancer regions of these two genes to allow the activation of gene expression by other factors, for instance under starvation. Thus, it was tested whether Schlank would change localization during starvation. After expression of *HA-WT*, Schlank nuclear localization and specifically the ratio nucleus versus cytoplasmic Schlank was measured in S2 cells after 3, 6, and 12h of starvation. The quantification revealed a reduced Schlank nuclear localization upon starvation. To rule out that this observed strong effect was due to an artefact deriving from the expression of a tagged protein, the same experiment was conducted in non-transfected S2 cells and the localization of endogenous Schlank was determined. Also in this case, a significant reduction in nuclear localization was observed upon serum starvation (Figure 2.15, A, B, C, Sociale et al., 2018).

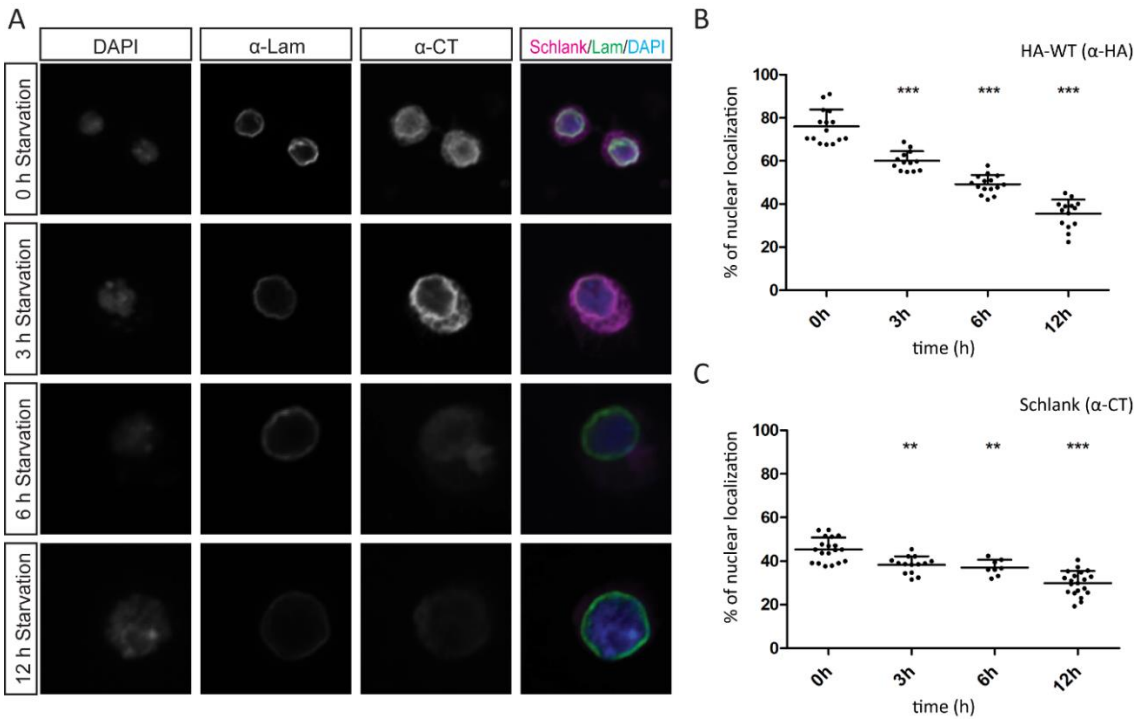

Figure 2.15. Schlank nuclear localization upon serum depletion (starvation). A) Representative images of S2 upon serum deprivation stained with α-lam (green) and Schlank (magenta) and DAPI. **B)** Nuclear localization of HA-WT determined in S2 cells, **C)** and of endogenous Schlank nuclear localization upon starvation at different time points using α-HA and α-CT respectively. The ratio of colocalized Schlank and DAPI versus cytoplasmic Schlank was quantified and plotted as percentage of nuclear Schlank. Error bars indicate SEM. ***p<0.001, ** p<0.01, *p<0.05

In this context, nuclear localization was also evaluated during *in vivo* larval starvation in fat body cells, confirming that nuclear Schlank diminished upon starvation. (Sociale et al., 2018, Appendix Figure 5.4, A).

2.4.2 Lipid sensing and transcriptional regulation

Metabolic regulation and physiological feedback systems are central to all aspects of postembryonic life in every organism, and at the cellular level, they need to adjust gene expression quickly.

In the context of ceramide synthesis MCFA are needed in two steps of the pathway (Figure 1.1, A). Schlank links to sphinganine mainly C14-CoA-activated fatty acids for the production of ceramide (Bauer et al., 2009).

Moreover, FBS (depleted in our starvation assay for S2 cells), besides containing nutrients and factors needed for the survival and cell propagation, is rich in lipid and fatty acids. Different sera contain distinct compositions of FAs (Lagarde et al., 1984). In established cell lines, different sera cause an alteration in FAs composition. Since serum deprivation associates with reduced Schlank nuclear localization, FAs of different chain length were tested in S2 cells to verify whether they would affect Schlank localization during serum starvation. FA-conjugated with bovine serum albumin (BSA), (either C12-BSA, or C14-BSA, or C16-BSA) were added to the medium. BSA alone was used as vehicle control.

The experiments were performed on transfected HA-WT and endogenous Schlank. In both cases, with a minor but significant percentage for endogenous Schlank, supplementing FAs in a serum deprivation status shifted Schlank localization from the ER toward the INM supposing that Schlank might directly or indirectly sense the lipids and nutrient composition and shuttle between INM and ER (Figure 2.16, A, B, C).

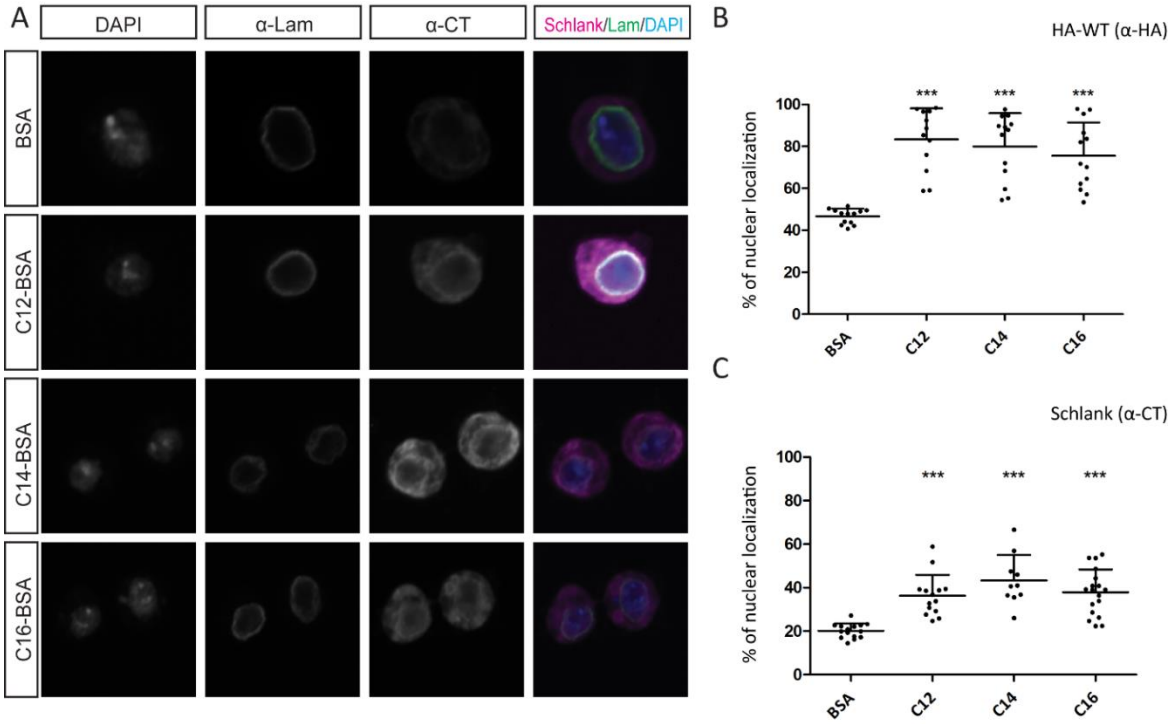

Figure 2.16. Schlank nuclear localization upon FA administration. A) Representative images of S2 cells upon administration of several C-chain FA (C12, C14, C16), stained with α-lam (green) and Schlank (magenta) and DAPI (blue) upon serum deprivation (BSA control). **B**) Nuclear localization of HA-WT determined in S2 cells, **C**) and of endogenous Schlank nuclear localization upon FA administration at different time points using α-HA and α-CT respectively. The ratio of colocalized Schlank and DAPI versus cytoplasmic Schlank was quantified and plotted as percentage of nuclear Schlank. Error bars indicate SEM. ***p<0.001.

2.4.3 Fatty acid availability and adapted transcriptional response

The nuclear localization experiments upon changing nutrient conditions have highlighted the fact that Schlank responds to FA and shifts subcellular localization.

To assess whether the shift to nuclear localization upon FA feeding correlates directly with the transcriptional response operated by Schlank, an *ex vivo* assay was established in this thesis. Since *lip3* is expressed mostly in the larval fat body while *magro* is a gastric lipase, fat body and gut were chosen for this assay. Fat body and gut of *KIWT* were exposed in a sugar-free Ringer´s solution, an isotonic solution that resembles the body fluids of the animal. Sugar (glucose or trehalose) was not used in the solution to mimic starvation and allow, in first instance, an upregulation of *lip3* expression. To test the responsiveness to FA, different chain length FA-conjugated with BSA, (either C12-BSA, or C14-BSA, or C16-BSA) were added to the solution. BSA alone was used as vehicle control.

On condition that FA are responsible for the signal to downregulate lipases, it should be possible to observe a downregulation of *lip3* in comparison with BSA control.

Indeed, there is a repression of *lip3* and *magro* in *KIWT* fat body and gut when C12, C14, and C16 are supplemented with the solution (Figure 2.17, A). To rule out a possible and unspecific effect on transcriptional regulation caused by a gain of energy through increased β-oxidation upon fatty acid treatment, β-oxidation was blocked with an inhibitor of carnitine palmitoyltransferase (cpt1), commonly called Etomoxir keeping the same experimental setup. The treatment with the inhibitor did not affect the results (Figure 2.17, B, Sociale et al., 2018) meaning that Schlank is responsible for adapting transcriptional regulation according to fatty acid status.

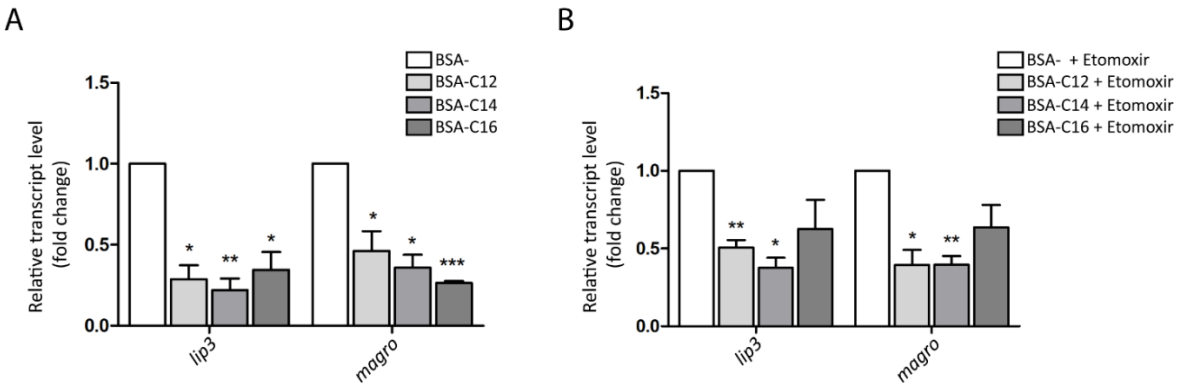

Figure 2.17. *Ex vivo* assay of dissected fat bodies and gut from *KIWT*. A) qRT-PCR on *KIWT* fat body/gut after 6h incubation with saturated fatty acids of different chain length (C12, C14, and C16) coupled to BSA. BSA only was used as a control. **B)** Same experimental setup with the addition of 200 µM of Etomoxir, used to block β-oxidation. Expression level normalized on *rp-49.* Error bars indicate SEM (n=3). ***p<0.001, ** p<0.01, *p<0.05

Furthermore, to prove that this transcriptional response upon FAs administration is indeed operated by Schlank through DNA binding the same set of *ex vivo* experiments were performed for *KINLS2* mutants. Because *KINLS2* mutants are no longer able to regulate transcription, no changes in *lip3* and *magro* expression was expected when FAs are supplemented. Indeed in samples obtained from *KINLS2* animals, *ex vivo* fatty acid treatment did not lead to a suppression of *lip3* and *magro* (Figure 2.18, A, B).

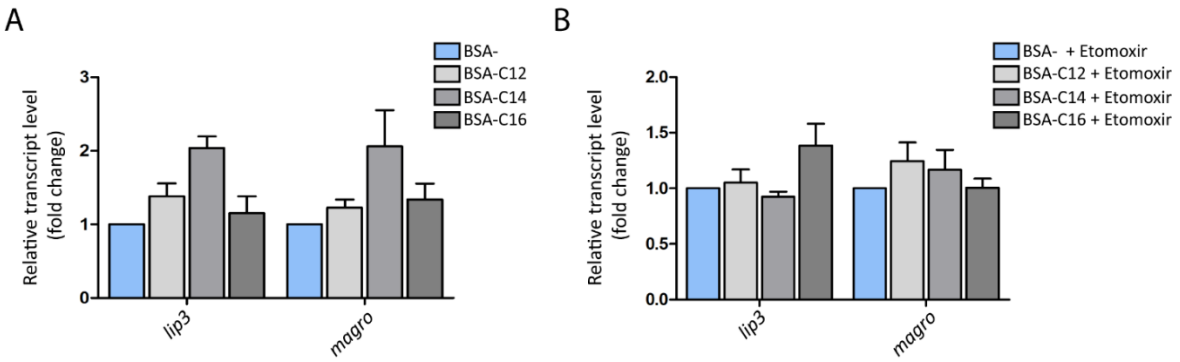

Figure 2.18. *Ex vivo* assay of dissected fat bodies and gut from *KINLS2*. A) qRT-PCR on *KINLS2* fat body/gut after 6h incubation with saturated fatty acids of different chain length (C12, C14, and C16) coupled to BSA. BSA only was used as a control. **B)** Same experimental setup with the addition of Etomoxir used to block β-oxidation. Expression level normalized on *rp-49*. Error bars indicate SEM (n=3).

2.4.4 Fatty acid availability and *in vivo* transcriptional response

In previous studies, it was shown that supplementing lipid-rich foods during larvae feeding, can increase organismal fat content in *Drosophila* mutants associated with different metabolic phenotypes (Ruiz-Sanz et al., 2001). For example, a partial dietary rescue of the previously published *Schlank*^{G0061} mutant was obtained by supplementing soy lipids. In fact, a higher number of larvae survived to adulthood (Bauer et al., 2009). To test whether the administration of FA-rich food would also rescue the *KINLS2* mutants, different oil-supplemented-diets were administered to the mutants. L1 larvae were fed with soy oil, olive oil, coconut oil, and cacao butter added to the yeast. Even though it was not possible to observe a rescue in development, L3 larvae were processed to measure *lip3* gene expression. None of the supplemented oil rescued the *lip3* phenotype of *KINLS2* mutants (Sinah Löbbert, Bachelor Thesis).

In the hypomorphic *Schlank*^{G0061} animals the DNA binding site is not affected and theoretically could still mediate a transcriptional response, which is agreement with the observed rescue upon dietary supplementation (Bauer et al., 2009). The fact that supplemented oils did not rescue the *lip3* phenotype of *KINLS2* mutants supports the idea that adaption of transcriptional regulation according to fatty acids status requires Schlank DNA binding.

2.4.5 The role of the catalytic motif in lipid sensing and signal transduction

The task of maintaining lipid homeostasis is achieved by proteins combining the ability of TFs and the sensing of the energy status either alone or in combination with other factors (Varga et al., 2011). TFs as SREBP (Rawson 2003), a membrane-bound TF, and PPAR (Peroxisome proliferator-activated receptors)(Varga et al., 2011), a member of the nuclear receptor hormone superfamily, regulate gene expression in response to changing lipid content. Schlank, as per the above-mentioned factors, possesses a lipid binding domain (TLC; Lag1p) that needs to recognize and bind sphinganine (or sphingosine from the salvage pathway) and FA-CoA to catalyze the reaction of N-acylation.

Therefore, the catalytic motif of the enzyme would represent a good candidate for the FAs sensing, transducing the signal for shifting nuclear localization to the homeodomain. To test this hypothesis, the *ex vivo* fatty acid treatment was performed while inhibiting the catalytic activity of the protein.

Fumonisin B1 is a commonly used inhibitor for ceramide synthase activity, blocking the reaction of N-acylation (Wang et al., 1991). Fumonisin B1 was tested in two different concentration for the *ex vivo* assay (Ikram Arahouan, Bachelor Thesis), particularly 50 µM and 100 µM. Although, on average, a loss in the regulation of the tested lipases could be observed (Figure 2.19, A, B), like the one occurred for *KINLS2* (Figure 2.18, A, B), the data present high variability and low reproducibility. This might be due to the toxicity of the inhibitor in such a delicate experimental setup.

Next, *KIH215D* animals with a mutation abolishing the catalytic activity (Figure 2.1, D) were used to investigate the role of the catalytic domain in lipid sensing.

However, these animals die approximately at 48h as L1 larvae (Figure 2.3, A, B) when, the larval fat body is almost inexistent and *lip3* gene expression is still low (Pistillo et al., 1998). Thus upon removal of the cuticle and most organs, the rest of the animal was used in the *ex vivo* experiments followed by RNA extraction and qRT-PCR analysis. Under these conditions, *lip3* expression was not regulated upon FA administration for either *KIWT* or *KIH215D* samples (Figure 2.19, C, D).

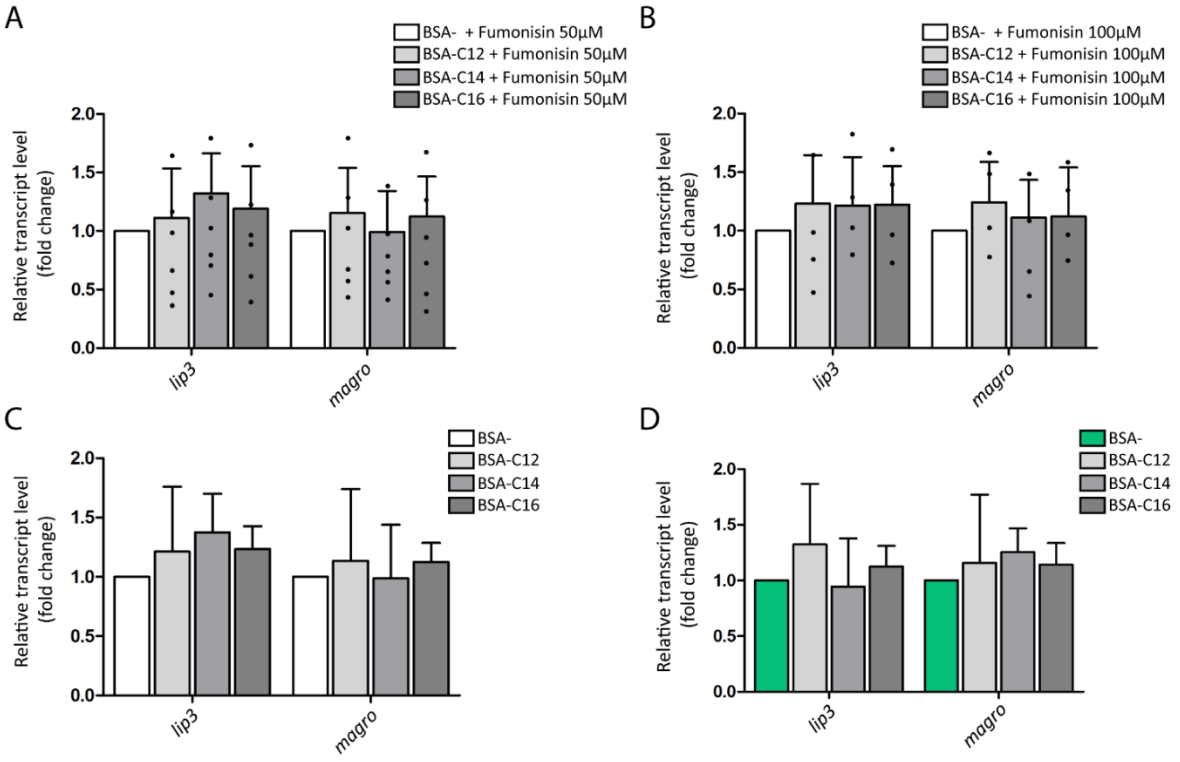

Figure 2.19. ***Ex vivo*** **assay of dissected fat bodies and gut blocking catalytic activity. A)** qRT-PCR on *KIWT* fat body/gut after 6h incubation with saturated fatty acids of different chain length (C12, C14, and C16) coupled to BSA with addition of an inhibitor of Ceramide synthase activity (Fumonisin B) in two different concentration 50µM (n=6) and **B)** 100 µM (n=4). Black dots indicate the value for each of the replicate. BSA only was used as a control. **C)** qRT-PCR on L1 *KIWT* (n=3) or **D)** qRT-PCR on L1 *KIH215D* (n=3). Expression level normalized on *rp-49*. Error bars indicate SEM.

To overcome the problems caused by developmental delay and larval lethality of both *KIH215D* and *KINLS2*, as a side project, a strategy for conditional mutagenesis was established. Schlank WT genomic DNA (gDNA) was cloned either in combination with HA-tagged gDNA carrying the H215D or the NLS2 mutation into a so-called Allele switch vector (described by Baena-Lopez et al., 2013). This vector carries attB sites, as used for the generation of the different KI lines (Figure 2.1, A-G), and two different multiple cloning sites (MCS) spaced out by FRT (Flippase Recombinase Target) sites. The FRT sites can be recognised by Flippase (Flp), allowing and initiating site-directed recombination between two FRT sites. Flp-mediated excision of the FRT cassette, provokes the excision of the Schlank WT and subsequently the expression of the HA-tagged mutant variant at specific times and places (scheme of the genomic locus of the *Allele switch*^{KIH215D} line is shown in Figure 2.20, A, See Appendix Figure A5.5 for recombination scheme). The availability of

numerous tissue-specific Flp-lines, together with the possibility of studying the mutations in time and tissue-specific manner, makes these newly generated lines a tool of great value.

Notably, switching from a WT to an H215D mutation during L2 would allow monitoring *lip3* expression upon FA administration to understand the role of the catalytic domain in lipid sensing.

To this end, the *Allele Switch*^{KIH215D} line was crossed with a CD2 heat shock-sensible Flp. Larvae (44-48h) were then heat shocked for 2h and allowed to develop until L3 (HA expression tested 48h after heat shock, Ikram Arahouan, Bachelor Thesis). Those samples were used for *ex vivo* FAs assay as previously described. The result shows a reduction in *lip3* and *magro* expression after treatment of the, now, *KIH215D* animals upon WT Flp-out (Figure 2.20, B). These preliminary experiments might suggest that Schlank does not require an intact catalytic motif for transcriptional regulation upon fatty acids stimulation.

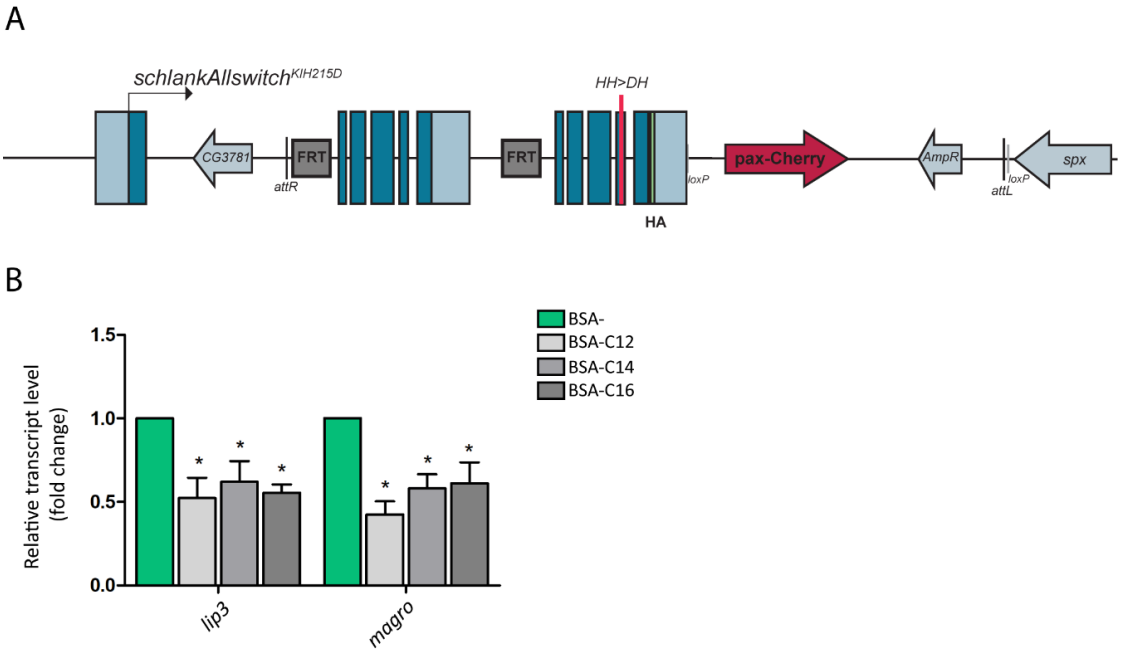

Figure 2.20. ***Allele Switch*^{KIH215D} *and ex vivo assay*. A)** Schematic of Schlank locus after reintegration of *Allele Switch*$^{WT\text{-}KIH215D}$ in magenta is highlighted the mutation in the second *Schlank* allele, in light green is highlighted the HA tag to follow the occurrence of the switch and the red arrow represent the pax- cherry gene expressed in larvae and adult for the genotype selection. **B)** qRT-PCR on switched (48h) *KIH215D* fat body/gut after 6h incubation with saturated fatty acids of different chain length (C12, C14, and C16) coupled to BSA. Expression level normalized on *rp-49*. Error bars indicate SEM (n=3). ***p<0.001, ** p<0.01, *p<0.05.

2.5 Interaction partner and *lip3* regulation

Homeodomain proteins all bind to a very similar set of "AT"-rich DNA-binding sites and can activate some target genes and repress others at the same time. This information raises the basic question of how the specificity is achieved and how they orchestrate the various transcriptional responses (Mann et al., 2009). Hox DNA-binding specificity is modified through interactions with other DNA-binding proteins for the formation of a heterogeneous protein-TF-cofactor complex (Mann, 1995; Mann and Affolter, 1998; Mann and Chan, 1996). These enable Hox functional specificity *in vivo* at particular target sites. Although *in vivo* study of endogenous Hox target gene regulatory elements has provided insight into the roles of cofactors at specific targets, relatively few target sites have been studied, and there is no clear understanding of the role of cofactors in Hox specificity. Indeed at some regulatory elements, the cofactors appear to be required for specific functional activity, gene activation rather than repression, and not for DNA-binding specificity (Li et al., 2011; Beh et al., 2016).

Interestingly for this thesis, it was noticed that several of the lipases deregulated in *KINLS2* mutants, besides *lip3*, were described in the literature as Foxo indirect target genes. For instance, although being responsive to Foxo overexpression, *magro* regulatory region does not contain conserved consensus binding sites for Foxo (Karpac et al., 2009). Foxo proteins are a group of TFs belonging to the Forkhead family. This family is characterized by a conserved DNA-binding domain, and it is known to be the main downstream effector of the ILS. They are involved in metabolism, stress protection, cellular differentiation, cell-cycle arrest and apoptosis (Greer and Brunet, 2008; Partridge and Brüning, 2008; Salih and Brunet, 2008). Foxo TFs, like Hox proteins, have a similar, if not identical, DNA-binding domain. Direct interaction of Foxo proteins with diverse TF families can mediate the regulation of a plethora of cellular processes independently of Foxo DNA-binding, in a cell type-specific way (van der Vos and Coffer, 2008). Noteworthy, Foxo proteins have been shown to interact with multiple members of the nuclear hormone receptor (NHR) family leading to changes in the transcriptional activity of both proteins.

For those reasons, it was tested whether Foxo could also regulate *lip3* expression. Firstly, *lip3* expression was measured in $Foxo^{\Delta 94}$ mutants (Slack et al., 2011), which are characterized by a slight developmental delay, but survive until adulthood. At around 90h AEL, Foxo mutants were starved for 6h, and *lip3* gene expression was measured by qRT-PCR (Figure 2.21, A). Notably, *lip3* is no longer upregulated upon starvation suggesting that *lip3* might also be a Foxo target. In addition, *Foxo-GFP* (Foxo) overexpression and $Foxo^{RNAi}$

were tested on *lip3* luciferase reporter in S2 cells. Strikingly, Foxo overexpression suppressed *lip3* luciferase activity, and *Foxo*^{RNAi} caused an increase in luciferase activity (Figure 2.21, B) as observed for Schlank overexpression and RNAi (Figure 2.12, A). To assess whether and how Foxo and Schlank might regulate transcription of *lip3* together, different combinations of coexpressed vectors were tested.

The rationale of this experiment follow the assumption that if Schlank and Foxo need each other to modulate *lip3* activity in the absence of one or the other, *lip3* luciferase suppression should not be observed. Schlank was overexpressed together with *Foxo*^{RNAi} and vice versa, and *lip3* activity monitored. In both combinations, it was no longer possible to suppress *lip3* activity (Figure 2.21, C). When Foxo was overexpressed together with Schlank (WT-HA), there was a normal suppression of the luciferase reporter. However, when the NLS2 variant was overexpressed with Foxo, the regulation was abolished (Figure 2.21, D). Thus, Schlank and the DNA binding capacity of Schlank appears to be required to mediate the repressive effect of Foxo on *lip3* regulation in S2 cells and more generally Foxo and Schlank might work together to modulate *lip3* gene expression (Figure 2.21, C, D).

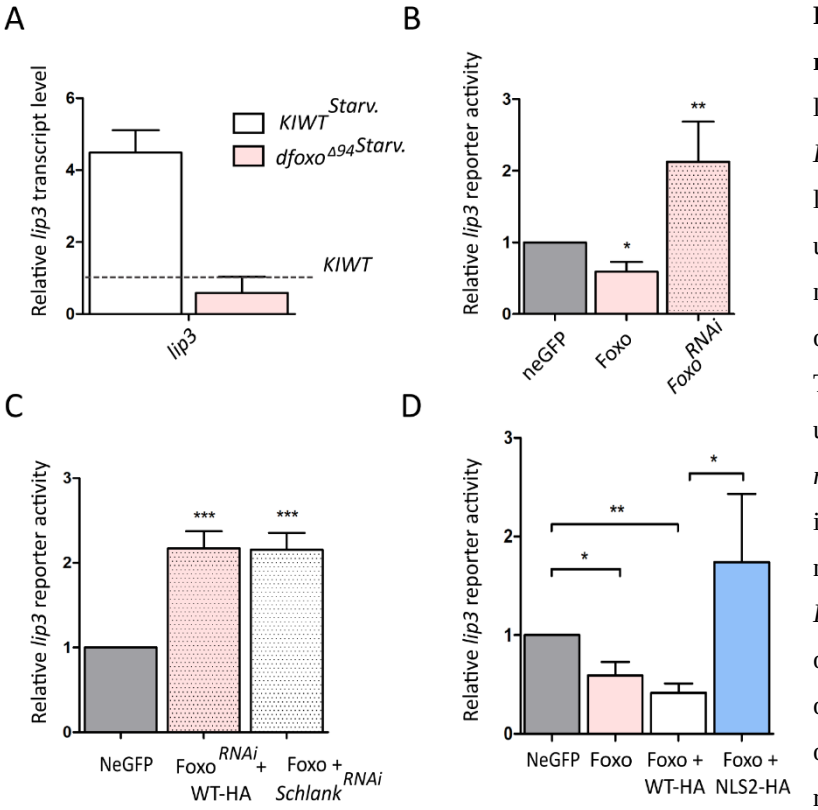

Figure 2.21. Foxo and *lip3* regulation. A) *Lip3* expression levels in starved (L3 90h to 96h) *KIWT* larvae and Foxo mutant larvae that fails to upregulate *lip3* upon starvation. Samples normalized on the *lip3* expression of non-starved *KIWT* (dotted line). Transcript levels of *lip3* quantified using qRT-PCR (normalized to *rp-49*). **B)** Relative luciferase induction upon expression of neGFP, *Foxo-GFP* (Foxo) and *Foxo*^{RNAi}, **C)** KD of Foxo while overexpressing Schlank and KD of Schlank (WT-HA) while overexpressing Foxo abolished repression on *lip3* reporter. **D)** and co-expression of HA-WT or NLS2 with Foxo have opposite effect on *lip3* reporter activity. Error bars indicate SEM (n=3). ***p< 0.001, ** p<0.01, *p<0.05.

To verify whether they might interact directly or indirectly, coimmunoprecipitation (coIP) experiments were carried out. HA-tagged Schlank and GFP-tagged Foxo were transfected and expressed in S2 cells. Using the respective antibody, each of them was separately precipitated from extracts of S2 transfected cells. GFP-Foxo was able to coIP HA-Schlank and vice versa (Figure 2.22, A). To confirm that the NLS2 would affect the DNA binding rather than the stability of the protein and consequently the interaction between Schlank and Foxo, a coIP experiment was performed on extracts containing the coexpressed *Foxo-GFP* and *NLS2-HA* fusion proteins. The interaction was not affected and maintained despite the mutation.

Essential to understanding this possible synergistic interaction between Schlank and Foxo is the evidence that, opposite to Schlank, Foxo is shuttling from the cytoplasm to the nucleus upon starvation, representing a controversy for this interaction. It is also true that the localization of both, Schlank or Foxo is never exclusively ER/Cytoplasmic or INM/Nuclear. To gain more information about the *lip3* regulation by Foxo in starvation more luciferase assays were performed. In starvation, the overexpression of Foxo increased the luciferase activity, while $Foxo^{RNAi}$ no longer increased luciferase activity (2.22, B).

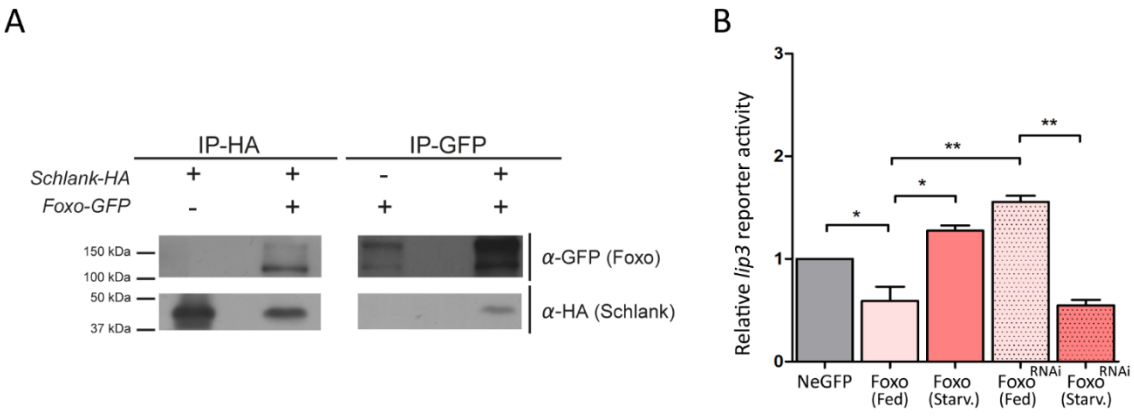

Figure 2.22. Schlank-Foxo interaction and *lip3* regulation upon starvation. **A)** CoIP of HA-tagged Schlank with GFP-tagged Foxo and vice versa. S2 cells were either transfected with expression plasmids for both, HA-tagged Schlank (~47 KD) and GFP-tagged Foxo (~110 KD) or with HA-tagged Schlank or GFP-tagged Foxo only, which were used as negative controls. No unspecific CoIP signal was detected using protein extract of S2 cells. Immunoblot was performed alternatively with α-HA or α-GFP antibodies. **B)** *Foxo* and *lip3* regulation upon starvation. Relative luciferase induction upon expression of *Foxo-GFP* (Foxo) and $Foxo^{RNAi}$ (6h), *lip3* gets enhanced by $Foxo^{RNAi}$ in a fed status (as in Figure 2.21**B**), while the suppression of *Foxo* ($Foxo^{RNAi}$) during starvation does not upregulate *lip3* expression. Foxo is needed during starvation to upregulate *lip3* expression. Reporter activity normalized to Renilla luciferase control transfection (n= 3).Error bars indicate SEM. *p < 0.05, **p<0.01.

These results represent a proof that in starvation, Foxo is needed for the overexpression of *lip3*. Because of the non-exclusivity of the localization and the need of cells to quickly regulate transcription, Schlank and Foxo might always be present in more or less amount on the enhancer of *lip3* depending on the feeding status. During starvation, Schlank nuclear localization diminishes, while Foxo nuclear localization increases and perhaps through the modulation of the complex by cofactors or other TFs, *lip3* expression might be enhanced.

3 Discussion

Regulation of lipid homeostasis and maintenance of stable cellular lipids patterns on individual cell surfaces and within different compartments of the cells requires precise control of lipid biosynthesis, degradation, and intracellular transport. During the past years, more and more pathologies and pathophysiological processes have been associated with disruption of lipid homeostasis. These processes are not only related to energy consumption but numerous signalling events. How eukaryotic cells sense and control their lipid composition remains an open question for several classes of lipids. For those reasons, it is necessary to understand how metabolic enzymes are regulated, identify the dedicate lipid sensors, and track down the regulatory machinery of the signalling cascade.

3.1 CerSs and transcriptional regulation

The findings that the nuclear pool of Schlank at the INM plays a role in the regulation of body fat homeostasis has opened up an unexplored and appealing field of research.

Schlank localizes at ER and the INM. Ketel, the homologous of Importin β in Drosophila, is involved in Schlank nuclear import, recognizing NLSs within the homeodomain. Notably, Schlank was never found floating in the nucleus, but the presence of an inner ring circumscribed by lamin staining is particularly visible in fat body cells (Voelzmann et al., 2016; Sociale et al., 2018, Appendix Figure 5.2, B). The TM-free homeodomain failed to rescue the previously described Schlank P-element mutants (Appendix Figure 5.4, B; Sociale et al., 2018), meaning that the protein needs to be anchored to the membrane to accomplish its nuclear function. Analysis of *in vivo* models carrying different mutations within the homeodomain, generated via homologous recombination (Figure 2.1, A; G), clearly showed that at least one of the mutation correlates with an altered nuclear function (Figure 2.3; 2.4). Essentially, the NLS2 mutation is associated with deregulated transcription of lipase expression, and with a number of deregulated genes involved in several other cellular processes appearing in the RNA sequencing analysis output (Figure 2.5; 2.9).

In the last years, numerous screenings in mammalian CerSs KO models have shown that ceramide imbalance is associated with deregulated gene expression (Pewzner-Jung et al., 2010; Bickert et al., 2018). The novelty about the screening described here resides in the fact that the altered gene expression regulation in the *KINLS2* mutant is not due to a loss of

catalytic activity of the protein (Figure 2.7, A), or to a loss of interaction with other proteins but it is exclusively related to the homeodomain function, as the protein expression and its enzymatic function were unaltered. These findings prompt a more accurate investigation into the nuclear function of Schlank and the possibility that Schlank might regulate transcription via DNA binding.

3.1.1 CerSs as DNA binding proteins: transcription factor or chromatin remodeller?

Some INM and ER connected-ONM proteins interact in the nuclear lumen to take part in chromatin regulation. Proteins that are integral to the INM are generally linked to transcriptional silencing. Meanwhile, proteins whose localization is regulated by nuclear pore complexes or their components have been linked to both transcriptionally inactive and active loci in different organisms (Mekhail et al., 2010).

The NLS2 site is located in the third helix of the homeodomain. This portion of the homeodomain is known to be essential for establishing the first contact with the DNA. Different classes of homeodomains show in general high variability (Noyes et al., 2016). Amino acids considered essential for the function are substituted with others of similar properties, and only a few residues are highly conserved and remain invariant in each class. The NLS2 mutation affects one of these critical residues, an Arginine (R) in position 50 (**R**LRR to **A**LAR), described to be crucial for DNA binding (Bürglin and Affolter, 2015).

By performing ChIP experiments, it was possible to show that Schlank can bind DNA specifically to regulatory regions of genes that were deregulated (*lip3* and *magro*) (Figure 2.11, B) in the *KINLS2* mutant. The NLS2 mutation specifically abolished the DNA binding, while the mutation in the catalytic motif (H215D) and other mutations within the homeodomain (NLS1, E118A) (Figure 2.11, C, D) did not affect the binding. The fact that the NLS1 and E118A mutations within the homeodomain did not alter DNA binding and gene expression, even though ceramide synthesis was affected for *KINLS1* mutants (Figure 2.7, A) was not expected.

Moreover, it was shown by luciferase assay, that the NLS2 site is indeed responsible for the regulation of *lip3* (Figure 2.12 A, B) *in vitro*. This confirms *lip3* as a direct Schlank target gene. Rescue experiments in the background of the *KINLS2* mutant further strengthen the results on *lip3* transcriptional regulation operated by Schlank *in vivo* (Figure 2.13, A).

Besides *lip3*, it would be fair to assume that the altered gene expression of some of the enzymes of the sphingolipid pathway is the result of the loss of the DNA binding (Appendix Figure A5.3, C). However, whether the several deregulated genes appearing in the RNA-seq (Figure 2.9, A, B, C) are indeed Schlank target genes is to date hard to define. It was not possible to prove this during this work, even though different approaches were used.

The first approach used was the scan of the promoter/enhancer regions of genes whose expression resulted deregulated in the RNA-seq for Schlank binding motif. This analysis was not possible due to the observation that the putative and variable Schlank binding consensus is spread all over the genome and not directly associated to promoter/enhancer regions. This generally occurs for most of the other Hox-domain-transcription factors. ChIP-seq of ChIPs samples from S2 cells on endogenous Schlank was performed in a second attempt. Even though the ChIP showed a positive output by qRT-PCR, the sequencing resulted in several genome-spread picks. Poor quality libraries resulted from the sequencing approach used. The reasons behind this are not yet clear and more tests are needed to figure out which parameters have to be changed.

The observation of the "randomly-scattered" Schlank consensus binding sites, however, is actually in agreement with several publications on Hox-domain and chromatin remodelling. Genome-wide occupancy data reveal a wide discrepancy between predicted and observed binding of TFs. The vast majority of consensus motifs found in the genome are not bound by the respective TF (Wang et al., 2012). The presence of a binding motif per se is not sufficient for directing TFs to their target sites in the genome. The interaction TF-DNA *in vivo* is also determined by chromatin landscape, nucleosomes conformation, and from the presence of the DNA binding consensus in the minor or mayor grove of the DNA. While TFs appear to preferentially bind to regions of open and accessible chromatin (Kaplan et al., 2012; Kaplan et al., 2011), pioneer TFs often identified as homeodomain proteins, can interact with several other components and actively open condensed chromatin (Zaret and Mango, 2016). Control of gene expression by homeodomain proteins indeed relies on interaction with chromatin remodelling complexes, specific histone modification, various types of DNA-binding proteins and tissue-specific TFs, non-coding RNAs and cofactors (Bobola et al., 2017). Experimental evidence for these plausible properties for Schlank comes from a yeast 2-Hybrid screening previously performed. The results showed a strong interaction with a Chromatin-Decondensation factor 31 (Df31) (Reinhard Bauer personal communication). To study more in detail these proposed mechanisms for how Schlank exerts its function some ambitious and challenging experiments might be performed in the future.

The newly generated AlleleSwitch$^{KIWT\text{-}KINLS2HA}$ and the AlleleSwitch$^{KIWT\text{-}KIWTHA}$ lines (Appendix Figure A5.5) might be used to establish an *in vivo* ChIP protocol. The benefits of using this set of experiments to solve the previously described problems of the ChIP-seq would be multiple. S2 cells are embryonic derived cells that tend to differentiate after few passages in cell culture and/or different conditions (as shown in Appendix Figure A5.8 for the overexpression of elovl-4, unrelated to this project). The possibility of switching time and tissue specifically (overcoming the problems related with protein overexpression) to the tagged Schlank variant would allow to immunoprecipitate the HA-Schlank in a precise organ or subset of cells, with no need for organ dissection or cell-sorting. Moreover, the possibility to compare the latter with NLS2-HA ChIP would represent a standardized (α-HA IP) "yes or no" set of experiments that would be much easier to analyse for ChIP-seq. It would be exciting, also, to combine these experiments with studies of chromatin accessibility. For instance, ATAC- or FAIRE-seq might be performed. These experiments, together with the previously described HA-ChIP-seq would allow to verify the status of the chromatin when Schlank is bound (HA-WT) or not bound (NLS2-WT).

3.1.2 The function of the NLS2 site in vertebrates

In this thesis, it was also possible to show that mutation of the NLS2 like motif in the murine CerS2 led to a loss of transcriptional control on *lip3* luciferase activity *in vitro* (Figure 2.12, C) independently of the catalytic activity (H215D). Moreover, by rescues experiments was possible to demonstrate this regulation on *lip3* also *in vivo* (Figure 2.13, B), indicating that the NLS2 motif might play a similar role in mammals.

Five out of six CerSs in mammals have a homeodomain, and all except CerS3 have an NLS2 like motif (Appendix Figure 5.7, A). More experiments are needed to prove the effective CerS DNA binding capabilities in a mammalian system. ChIPs and luciferase assays should be established in a mammalian cell line in order to affirm that mammalian CerS is binding DNA. For instance, CerS6 was shown to transcriptionally activate Acid Ceramidase (ASAH1) in different mammalian cell lines (Tirodkar et al., 2015), representing a good target for luciferase experiments. A very recent publication confirmed some of the data of this thesis work in *Danio Rerio* (Mendelson et al., 2017). CerS2b protein is activating its expression, and while the mutation in the equivalent NLS2 site (**RR**RR-**WS**RR) abolished the regulation, the mutation in the catalytic motif did not. This confirms the conserved

function of the NLS2 site in another model organism. This experimental evidence is promising for a transcriptional regulation homeodomain-dependent for mammalian CerS.

3.2 Possible mechanisms of transcriptional regulation via Foxo-interaction

The remodelling activities described for several homeodomain proteins underlie their ability in promoting reprogramming activities, binding on closed chromatin facilitating the binding of secondary factors (of site-specific TFs and co-activators) and assembly of active transcriptional complexes for local gene expression. In fact, it has been suggested that Hox proteins do not activate gene expression themselves, but act as transcriptional 'guarantors' to promote activation of target genes regulated by other TFs (Zheng et al., 2015), adding or altering the specificity of the Hox-protein.

Foxo was chosen as a possible interaction partner for Schlank. This is because some of the lipases found deregulated in *KINLS2* were described in the literature as indirect Foxo targets. Moreover, it has already been shown that the association of Foxo with several other TFs either inhibit or enhance their transcriptional activity (Li et al., 2001, Li et al., 2003, Fan et al., 2007).

In this thesis, it was possible to show by luciferase assay experiments that Foxo can regulate *lip3* when its activity was modulated alone, or in combination with Schlank (Figure 2.21, A; C). Despite the fact that ILS and Foxo activity were not affected in the *KINLS2* mutants (Figure 2.5, C, E), a motif enrichment analysis for Foxo among the 20 mostly up and down-regulated genes from the RNA-seq, resulted in three differentially regulated Foxo target genes (LyseD, LyseE, and Frq1, highlighted in bold in Figure 2.9, B). Supporting and expanding the potential regulatory interaction between Schlank and Foxo.

Interaction of Foxo proteins with diverse TF families or cofactors can lead to altered transcriptional responses through a variety of mechanisms. Foxo-binding elements are found adjoining or overlapping with other TFs, or far away from the enhancer/promoter regions. The examples are numerous where enhancer regions are located far in the genome even on different chromosomes and still are necessary for the transcriptional regulation (Kulaevaa et al., 2012). Foxo might for example bind to its binding motif in a region that is not associated with *lip3* regulatory region, and because of the nuclear positioning of the DNA, still being in close proximity and able to physically interact with Schlank. This could result in an enhanced transcriptional response or repression as for Schlank and *lip3* (Figure 2.12; 2.21). Moreover, the association between Foxo and other proteins can often recruit additional

factors. The recruitment of histone acetylase transferases (HATs) or histone deacetylases (HDACs) to promoters, and the association with diverse TFs can, for example, lead to activation or suppression of transcription. Foxo-TFs association can also result in an altered cofactor distribution to target promoters. When one of the components in a complex is a limiting factor and also binds Foxo, it may result in inhibition of transcription or may even lead to increased proteolytic degradation of Foxo or Foxo-associated TFs.

In most cases, phosphorylation of Foxo leads to a disruption of the complex. Interestingly, Foxo has been shown to interact with several NHR independently of the presence of the NHR ligand, as for instance the PPAR- α and γ, the hepatic nuclear factor-4 (HNF4) in mammals. They are also involved in metabolic processes underlining the importance and the interconnection of lipid metabolism and insulin signalling (van der Vos and Coffer, 2008).

Although the experiments in this thesis have provided evidence for a possible interaction between Schlank and Foxo, and for a possible regulatory mechanism of *lip3* gene expression, the molecular mechanisms and the biological and physiological relevance of this interaction genome-wide are still elusive.

More experiments are needed to better understand the modulation of *lip3* expression. Several coIP experiments should be performed. For instance, coIPs could be performed during starvation to monitor perhaps a reduction or a loss of interaction.

To understand which portion of Schlank is responsible for the interaction it could be possible to overexpress ad coIP the several available, truncated, and mutated Schlank variants (Anna-Lena Wulf, PhD thesis; André Voelzmann, PhD Thesis). In fact, by bioinformatics tools (DisEMBL, Appendix Figure A5.6, A, Linding, et al., 2013) it was possible to identify within the Schlank C-Terminal portion a low complexity region, known from literature to mediate and facilitate protein-protein interactions (Dyson and Wright, 2005; Pancsa and Fuxreiter, 2012).

The interaction between these two key and regulatory proteins *in vivo* also needs to be carried on in the future. The double mutant *KINLS2-FoxoΔ94* resulted in being larval lethal as well as foxo knock down (*UAS-Foxo*^{RNAi}) in the background *KINLS2* mutants (Sinah Löbbert, Bachelor Thesis). New insights might be acquired by playing with the expression of these two factors in clonal analysis. Using the newly generated Schlank-allele switch lines would overcome the lethality of the double mutants and *lip3* activity could be monitored in different tissues and developmental stages.

The importance of this interaction is reflected in a number of previous publications that although not investigating the homeodomain function, established a link between the

activities of CerSs 2, 5, and 6 and the level of C16-Cer with obesity and insulin resistance (Reali et al., 2017; Turpin et al., 2014; Gosejacob et al., 2016). The data described above might represent the first connection between ILS and CerSs.

3.3 Schlank function in fat metabolism regulation and lipid homeostasis

This thesis demonstrates that Schlank binds DNA via the homeodomain and that the NLS2 site is necessary for the binding (Figure 2.11; 2.12). Schlank´s role in adapting transcriptional response depending on the energy status, is reflected by the fact that Schlank DNA binding, as well as nuclear localization, shift during fed and starved status (Figure 2.14; 2.15). Moreover, it was shown that FA are targeting Schlank to the nucleus and they represent the signal to repress *lip3* expression (Figure 2.16; 2.17).

This mechanistic model is consistent with the phenotypes observed in *KINLS2* mutants highlighting that Schlank transcriptional regulation is needed to maintain lipid homeostasis. The mutant phenotypes associated with lack of transcriptional regulation that affects storage of TAG, FA synthesis (Figure 2.4; 2.6), and, generally, lipolytic and lipogenic processes (Figure 2.5, 2.9), beside sphingolipid biosynthesis (Appendix Figure A5.3, A).

This thesis aimed at understanding the role of Schlank nuclear function in regulating fat metabolism. As mentioned in the introductory paragraph describing the fate of fat, the quantity and quality of dietary lipids are known to have an impact on the composition of tissue lipids in *Drosophila* (Jones et al., 1992) and mammals (Aoun et al., 2012, Field et al., 1984). Nevertheless, the composition of intracellular TAG stores also depends on the action of other enzymatic systems and reflects the activities of enzymes responsible for synthesizing, desaturating and elongating FFAs (Papackova and Cahova, 2015).

TAGs stored in the form of cytoplasmic lipid droplets are not only passive energy depots. Their degradation forms pleiotropic bioactive intermediates, which contribute to the regulation of several cellular processes functioning as cofactors for transcription factors or enzymes.

Lipases are the enzymes responsible for intracellular TAG hydrolysis, so they not only ensure energy substrate release but actively regulate energy metabolism of the cell. From the hydrolysis of TAGs originate FFAs. FFAs may be generated *de novo*, imported from the plasma pool or generated by lipoprotein lipases and then transported into the cell. FFAs are not mobilized in direct proportion to their content in TAG but selectively according to their molecular structure. FAs are essential substrates for oxidation and production of cellular

energy as well as precursor molecules for all lipid classes. They act as powerful signalling molecules, which regulate numerous cellular processes associated with lipid metabolism and which ensure precise FFA release and demand. FFAs and their derivatives may regulate intracellular processes at several levels as gene transcription activation, post-transcriptional modification of proteins (for instance acylation) and direct modulation of enzyme activities as co-activators (Raclot et al., 1999). Thus FFAs can become harmful to cells also if present at low concentrations and must be released under tight metabolic control. Depending on their structure, FFAs can initiate diverse signalling independently or dependently of gene transcription modulation. The indirect effects of FFAs derive from many mechanisms. These effects are mostly due to changes in fatty acyl composition of membrane lipids which determine membrane fluidity, lipid raft structures and, as a consequence, signal transduction (Vessby et al., 2002, Jump et al., 2002).

To regulate cellular metabolism transcriptionally, FAs act as agonistic ligands of different nuclear receptors. When activated, these factors bind to the promoter regions of specific genes and selectively affect their transcription. FFA-binding nuclear transcription factors belong to several families, including PPAR, and SREBP. Short chain fatty acids (SFA), for instance, stimulate the expression of genes involved in the SREBP pathway and cholesterol homeostasis (Jackson et al., 2006; Lin et al., 2005, Jump et al., 2005). Poly-unsaturated fatty acids (PUFA), potently suppress genes involved in *de novo* lipogenesis (Xu et al., 1999), FFA desaturation (Worgall et al., 1998) and elongation (Jump et al., 2005) via SREBP.

All of these distinct pools may serve as a source for signalling molecules, which differ concerning to tissue, metabolic stimuli, and lipase-derivation. Whether these FAs directly serve as nuclear receptor ligands, or if they need to undergo an esterification/hydrolysis cycle first is not yet known (Papackova and Cahova, 2015).

Additionally, more than one step of sphingolipid *de novo* biosynthesis depends on the availability of FA-CoA (Figure 1.1, A). In the first rate-limiting step of the pathway, FA-CoA is required to generate the substrate of ceramide, sphinganine and secondly it is required for acylation of the sphinganine to produce ceramide. Thus, the supply of FAs should be expected to play a key role in the determination of the rate of ceramide synthesis and quantity of ceramide generated by the *de novo* synthesis pathway.

Lip3 is responsible for the accumulation of FFAs (Bülow et al., 2017). During starvation Schlank does not bind to DNA, changes subcellular localization (between INM and ER), releasing *lip3* enhancer (Figure 2.14; 2.15) which gets activated. In animals, during starvation conditions FAs are mostly used to gain energy through β-oxidation correlating

with reduced FAs available for ceramide synthesis. During development and particularly during the latest larval stages, ceramides and in general sphingolipids are necessary for proceeding to pupariation. Under this condition, by increasing the ER localization, Schlank could be waiting to be triggered by a signal, and ready to welcome sphinganine and FA-CoA for the production of ceramides.

Furthermore, it was not only possible to show that in a FA-overloaded condition, Schlank is shuttling from the ER to the nucleus but also that FAs are the signal for the repression of lipases during starvation (nuclear localization and *ex vivo* experiments, Figures 2.15, 2.16, 2.17, 2.18). Regrettably, for the methods used in thesis, it was not possible to univocally prove that Schlank senses the lipid status of the cell directly or, more specifically, that the binding of the FAs to the catalytic domain triggers the shift in localization and lipases repression (Figure 2.19).

The *ex vivo* experiments of samples of the *AllSwitch*^{KIH215DHA} line (Figure 2.20, B) are only preliminary data. The perfect genetic control (*AllSwitch*^{KIWTHA}) that would allow the switch from a WT to a WT-HA Schlank variant is missing in this experimental setup. Due to difficulties in cloning two identical and perfectly matching sequences in the same construct (WT; WTHA), this fly line has not yet been generated.

The percentage of cells "switching" from WT to H215D was not tested previously to performing this experiment. For this reason, these experiments need to be repeated, and in parallel, the Flp efficiency needs to be monitored by antibody stainings.

Moreover, further experiments are needed to prove the non-involvement of the catalytic domain in lipid sensing and signal transduction. In a recent publication, it was shown that the acyl chain specificity of CerSs is connected to a stretch of amino acids residing between the last two transmembrane domains (6th and 7th) (Tidhar et al., 2018).

Although it is not known, how the protein is folded, which shape the enzymatic pocket assumes, and where exactly sphingosine and FA-CoA are binding, it is possible that with the experiments described here (Figure 2.19; 2.20), the side of the catalytic pocket deputised to the binding of sphinganine has been blocked. Fumonisin B1 has a high structural similarity to sphinganine, supposing that it binds to the same portion of the protein that the latter would be binding. Furthermore, the HH motif (important for catalytic activity and mutated in *KIH215D*, Figure 2.1, D; 2.2, A) is located within the Lag1p motif, between the 4th and the 5th transmembrane domain, again not overlapping with the area described for acyl chain specificity between the 6th and 7th transmembrane domain (scheme for FA and sphingosine binding, Figure 3.1, A). In summary, it is highly probable that FA are still binding to the

protein after inhibition with Fumonisin and despite the mutation in the HH conserved domain.

It is known that FAs can act as cofactors. Suppose that the binding of FAs would be indeed the signal that Schlank needs to shuttle to the nucleus to regulate transcription, this would still be possible in the above described experimental setup.

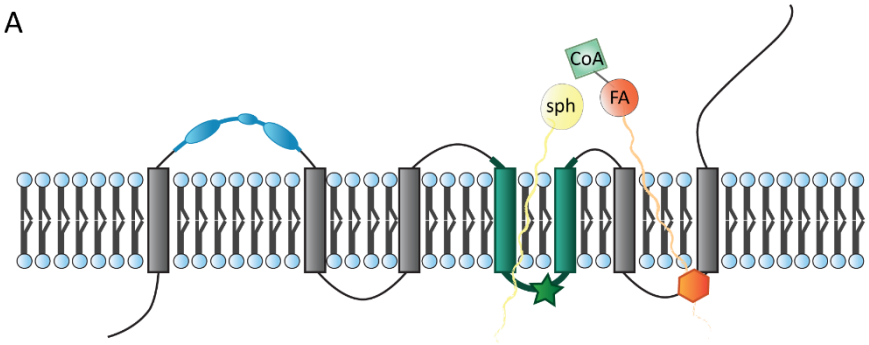

Figure 3.1. Scheme for FA and Sphinganine binding to Schlank. Schematic of Schlank protein and where FA and Sphinganine might bind. The green star indicates the mutation in HD, while the orange polygon indicates the position of the aa responsible for acyl-chain specificity. In yellow is indicated sphinganine, in orange the FA activated with CoA (green square).

In a possible mechanistic scenario, the over-binding of FA to the catalytic domain in the absence of sphinganine might act as a signal for nuclear translocation communicating that there are enough FAs available to be utilized as energy supply and for ceramide synthesis. Moreover, the binding of the FA as a ligand could also act as a cofactor inducing conformational changes leading to dimerization or recruitment of corepressor complexes.

Interestingly, it was recently published that Ceramide synthase 2b mediates genomic sensing and regulation of sphingosine levels during Zebrafish embryogenesis. Mutations in the NLS2 site (**RR**RR-**WS**RR) of the Zebrafish CerS2b, similar to the NLS2 mutations described here, abolished the ability to respond to changing sphingosine (Mendelson et al., 2017). In this work, CerS2b would shuttle to the nucleus and upregulate its own expression upon sphingosine treatment.

The possibility that Schlank as CerS2b might be able to sense sphingosine levels is quite intriguing, and it would be easy to prove with the different methods established in this thesis. *Ex vivo* experiments might be performed with the addition of sphingosine or by blocking sphingosine generation. Moreover, it would also be possible to block the sphingolipid biosynthetic pathway at different levels upstream of Schlank. By blocking the first step of the pathway with an inhibitor of Spt and by blocking the synthesis of sphinganine, it would be possible to verify whether sphinganine is needed to convey the message for regulating transcription, or to better understand at which level of the pathway FAs are acting.

Alternatively, other proteins might sense FAs availability initiating a signal cascade, which then would cause the shuttling of Schlank. It is known that for instance that NLSs are usually revealed or masked by phosphorylation. Bioinformatics analysis for prediction of phosphorylation sites on Schlank resulted in the highest score for a Threonine (T) adjacent to the first part of the bipartite NLS2 site (Appendix Figure A5.6, B, B´). Studies of this T by mutagenesis, cell culture experiments and fly line generation might be carried out, to verify whether this amino acid is phosphorylated and if it is necessary for nuclear localization.

In Summary, this work helped to unravel how Schlank regulates TAG, FA and lipase expression showing that the transcriptional regulation, exerted by DNA binding through the homeodomain, is dependent on the availability of FAs.

Moreover, based on this work and particularly on the findings that Schlank shuttles to the nucleus and regulates transcription in the presence of FA, it was possible to demonstrate that in a model of peroxisomal biogenesis disorders (PDBs), Schlank is mislocalized. This causes an upregulation of *lip3* and FFA-induced lipotoxicity. Moreover, MCFA (C12, and C14) administered via feeding of Coconut Oil, could rescue and stabilize most of the pathologic phenotypes by targeting Schlank to the nucleus, thus downregulating *lip3* expression (Sellin et al., 2018). PBDs are rare genetic diseases caused by mutations in one of the approximately 16 peroxin (PEX) genes, which are involved in the assembly and maintenance of peroxisomes. Patients with PBDs of the Zellweger syndrome spectrum have severe pathologic symptoms and usually, die during their first five years of life. Thus, the shuttle mechanism of Schlank upon FA described here has profound pathophysiological relevance.

3.4 CerSs and pathophysiological processes

Numerous studies with mouse KO models linked CerSs (2, 5, 6) function with lipid metabolism, obesity, diabetes and insulin resistance (Pewzner-Jung et al., 2010, Park et al., 2013, Park et al., 2014, Raichur et al., 2014). For some of the mammalians KO, particularly for CerS2, it was possible to observe different phenotypes with different grades of severity even in heterozygosis. Meanwhile, CerS5 and Cers6 KO mice did not reveal a phenotype under normal conditions but instead, upon high-fat diet, these mice were protected from diet-induced obesity (Turpin et al., 2014; Gosejacob et al., 2016). As *KINLS1* and *KIE118A* mutants did not show an obvious phenotype (Figure 2.3; 2.4; 2.5), like CerS5 and CerS6, it might be interesting to challenge these homeodomain mutants with different diets. *KIE118A* is a model to study the SNP found by The Meta-Analyses of Glucose and Insulin-related

traits Consortium (MAGIC), associated with altered parameters for metabolic dysfunction and markers of diabetic kidney disease. It is not yet known whether the catalytic activity in *KIE118A* mutants is affected. However, *KINLS1* mutants have a reduced catalytic activity (Figure 2.7, A), and, even though, transcriptional regulation of tested genes under normal conditions is not altered in these mutants. High sugar and lipid-rich food might be administered to these mutants. These experiments, together with luciferase assays in different culture media, might give more information about the importance of the mutations. The pathologies of the mammalian KOs were mostly attributed to ceramide imbalance and alteration in chain length specificity functions. Also in *Drosophila*, ceramide metabolism and accumulation were suggested as causal factors in the development of lipotoxic cardiomyopathy (Walls et al., 2018).

Interestingly, a recent publication from the CHARGE Consortium found an association between high levels of odd-numbered chain saturated fatty acids (OCSFA) C:23 and 9 SNPs on CerS4 coding regions. This was done by analysing the circulating OCSFA in 11,494 European individuals (De Oliveira Otto et al., 2018). Another genome-wide association study has found 8 SNPs for Cers4 associated with high levels of VLCFA (Very Long Chain Fatty Acid)(Lemaitre et al., 2015).

All of the above mentioned mammalian CerSs have a conserved putative NLS2 site (Appendix Figure 5.7, A). As the NLS2 site was shown to be functional in CerS2 in this work (Figure 2.12, 2.13), it will be interesting for future studies in mammals to elucidate whether the homeodomain might contribute to the development of obesity-associated insulin resistance, and whether also in mammals the interaction with Foxo might play a role in mediating transcriptional response.

In economically well-developed countries, excessive consumption of food and over-eating has led to a significant portion of the society suffering from metabolic dysfunctions such as obesity, lipodystrophy syndromes or insulin resistance. These diseases are often associated with a chronic dysregulation of the balance between lipolysis and lipogenesis. In response to changing dietary conditions the expression of genes involved in lipid metabolism needs to be adapted in order to maintain metabolic homeostasis. However, exact molecular mechanisms in these adaptive responses that coordinate genomic response to altered metabolic conditions to promote the lipid storage or lipid mobilization still remain largely elusive. The identification of a new mechanism for the CerS family member Schlank as a central regulator in adaptive response that coordinate genomic response to altered metabolic

conditions, represents an important step in unravelling the molecular network underlying lipid-based metabolic disorders.

Moreover, Schlank function in sensing FA and transducing the signal to the level of gene expression could have clinical implications in ceramide associated pathologies. As it was shown for peroxisomal loss associated diseases (Sellin et al., 2018), many other sphingolipidoses or pathologies of the central nervous system such as multiple sclerosis, epilepsy, Alzheimer's or Parkinson's disease, associated with altered CerS expression or altered CerS localization (Wegner et al., 2016; Hannun and Obeid, 2018) might be improved by a change in uptake of dietary lipids. This could represent a non-invasive and life-changing way of intervention in severe and debilitating diseases.

4 Materials and Methods

4.1 Constructs and fly lines

4.1.1 Vectors

p*UAS-GFP*-schlank-aa64–138 (Voelzmannet al., 2016), the complete stretch between the first two potential transmembrane domains containing the homeodomain including all NLS sequences, was used to produce pP*{UAS-schlank-Hox}* transgenic flies. *foxo*^{RNAi} and *schlank*^{RNAi} constructs were obtained from Vienna *Drosophila* Resource Center (VDRC ID respectively dna 4348 and dna 15550.

4.1.2 Cloning and fly lines generation

The fly lines *Schlank*^{RIVFRTWTHA}, *Schlank*^{RIVFRTNLS2HA}, *Schlank*$^{All.SwitchH215DHA}$ *and Schlank*$^{All.SwitchNLS2HA}$ were generated by homologous recombination and φ mediated integration. pP{*UAS CerS2NLS2HA*}, pP{*UAS CerS2H215DHA*}, pP{*UAS h_elovl4HA*} were generated by P-element transformation into *w*^{1118} flies (BestGene Inc., Chino Hills, CA, USA).

Name Vector	**Description Vector**	**Description Fragment**	**Sites Restr.**	**Description procedure**	**Fly Line**
Allele switch KIWT	RIV FRT MCS1 FRT MCS3 pax-cherry	Schlank-	NheI; XhoI	Cutted from pGE attB KIWT	N
pUASTCerS2-NLS2	pUAST	CerS2 cDNA- mutated in NLS2 site ARAR->ALAL from IDT; HA Tagged Ct	EcoRI; XhoI	IDT Synthesis Synthetic cDNA (mouse)	Y
pUAST CerS2-HD215	pUAST	CerS2 cDNA- mutated in H215D from IDT; HA Tagged Ct	EcoRI; XhoI	IDT Synthesis Synthetic cDNA (mouse)	Y
pUAST_elovl4HA	pUAST	elovl4 HA From IDT HA tagged Ct	XhoI; XbaI	IDT Synthesis Synthetic cDNA (human)	Y
	pUAST	Schlank cDNA- mutated in H215D from	EcoRI; XhoI	IDT Synthesis Synthetic cDNA (mouse)	N

pUAST_Schlank-H215D HA		IDT; HA Tagged Ct			
pUAST_Schlank_E118A	pUAST	Schlank cDNA- mutated in E118A from IDT ; HA Tagged Ct	EcoRI ; XhoI	IDT Synthesis Synthetic cDNA	N
miniwhite_SchlankHA	RIV FRT	Schlank-Drosophila melanogaster, CT HA tag	NotI, AscI	pGE attB KIWT ALK, PCR	Y
miniwhite_Schlank-NLS2-HA	RIV FRT	mutagenesis in NLS2 site; CT HA tag	NotI, AscI	Mutated fragment cutted from pGE attB KINLS2 (Mlu1,NdeI), inserted in mini white Schlank HA	Y
AlleleSwitch *KIWT-H215DHA*	AlleleSwitch KIWT;pTV-cherry	mutagenesis in H215D site, CT HA tag	PacI, AgeI	PCR, pGE attB H215D	Y
AlleleSwitch *KIWT-NLS2HA*	AlleleSwitch KIWT;pTV-cherry	mutagenesis in NLS2 site; CT HA tag	PacI, AgeI	PCR, miniwhite_Schlank_ NLS2-HA	Y
AlleleSwitch *KIWT-KIWTHA*	AlleleSwitch KIWT;pTV-cherry	Insertion of KIWTHA	PacI, AgeI	PCR, miniwhite_SchlankH A	N

4.1.3 Fly Stocks

Flies were kept on standard fly food in plastic vials. Unless differently stated they were stored at 18°C or 25°C. The following fly stocks were obtained from the Bloomington Stock Centre: w^{1118}; P{*cg-GAL4.A*}2 (# 7011) and w^{1118}; foxo$^{\Delta 94}$/TM6B, Tb1 (#42220), Df(1)dx81, w*/Dp(1;Y)dx+1/C(1)M5 (#5281). pP*{UAS-schlank NTHA}*, pP*{UAS-schlank CTHA}*, pP*{UAS-CerS2}* (Bauer, et al., 2009), pP*{UAS-GFP}*, and pP*{UAS-schlank^{NLS2}}* (Voelzmann et al., 2016) and p*UAS-GFP*-schlank-aa64–138 (Voelzmann et al., 2016).

4.2 Life span analysis

4.2.1 Larvae selection

For any experiment, only male larvae were taken. Females of homozygous stocks were crossed to *FM7a, P{Dfd-GMR-nvYFP}* carrying males. Eggs were collected for 4 h on apple juice agar plates and larvae were sorted for the absence of the dfd-nvYFP marker and transferred to a new plate.

For all experiments with mutant larvae showing developmental delay, if not stated otherwise, morphological criteria were used to ensure that wild type and mutant animals of the same developmental stage were selected (wandering third instar larvae (L3), a stage when feeding has ceased (Ainsley et al., 2008). In particular, $schlank^{KINLS2}$ larvae were staged as developmentally comparable with 96h w^{1118} or $schlank^{KIWT}$ when their anterior spiracles were open but had not yet protruded from the cuticle and when posterior spiracles turned to dark orange. Mutant larvae not showing any developmental delay were staged according to hours from AEL.

4.2.2 Survival assay

Eggs were collected for 4h and after 24h first instar larvae were selected by the absence of the fluorescence marker. 25 larvae were counted and monitored throughout larval, pupae and adult stages. The experiments were performed in triplicate.

4.2.3 Starvation and oil feeding experiments

Eggs were collected for 4h and after 24h first instar larvae were selected by the absence of the fluorescence marker. For starvation, at 90h AEL (or morphological criteria for mutant larvae), 10 larvae were washed in PBS to remove any residual yeast on the cuticle surface. Then larvae were transferred to a new apple-juice agar plate with fresh yeast for the experimental control and in parallel on a PBS-agar plate (1%). To avoid larval escape as well as low oxygen levels (when plates are wrapped with paper) a cage for eggs laying was placed over the plates. Starvation was conducted for 6h at 25°C. After the starvation time larvae were washed in PBS and frozen in TRizol. For lipid rescues, larvae were fed with supplementary oils in vivo. Twenty-five larvae were put on an apple juice agar plate with yeast with the addition of either 5% coconut oil or olive oil, or cacao butter, or broccoli oil. This experiment was performed in triplicate for each oil used. When the larvae reached the L3 stage (by morphological criteria), they were washed and frozen in TRizol.

4.3 Gal4/ UAS system

The Gal4/UAS system is a binary system that allows the ectopic expression of transgenes (Brand and Perrimon, 1993). The Gal4 gene is encoding for the yeast transcription activator protein Gal4 which recognizes and binds to the UAS enhancer (Upstream Activation Sequence). The Gal4 is usually expressed under the control of tissue/time specific enhancer.

4.3.1 Rescue experiments

For rescue experiments, male flies with different *schlank* or *CerS2* variants, combined with *FM7a,* P*{Dfd-GMR-nvYFP}1,* were crossed with *schlank*^{KINLS2} */ FM7a,* P*{Dfd-GMR-nvYFP}1* P{*cg-GAL4.A*}2 females, that drives the expression of Gal4 in the fat body organ. Hemizygous GFP negative males carried the reintegrated mutant *schlank*^{KINLS2} allele. Schlank variants and fly lines used in this thesis for rescue experiment are listed above.

4.4 Flp-FRT system

The FLP/FRT system is a site-directed recombination system. The recombination enzyme Flippase (Flp) recognizes and targets specific DNA regions, flipase recognition target (FRT) sites. Initially identified in Saccharomyces cerevisiae, the yeast FLP-enzyme and its FRT recombination targets are used in *Drosophila* (Golic and Lindquist, 1989) to mediate mitotic recombination *in vivo* during development in a controlled manner (Theodosiou and Xu, 1998). The induction of the recombination events is usually performed by expressing the FLP under the control of the heat-shock (hs) promoter allowing the high expression of FLP at specific developmental time windows.

For expression of the H215D-HA from the *Alleleswitch* $^{KIWT\text{-}H215DHA}$ line a heat shock CD2 Flp was used (*hs*FLP y_1 w*; *act5c* promoter FRT CD2stop FRT GAL4, UAS-GFP / TM6B, Tb_1). Being the Gal4 under control of the actin promoter, the expression of the Flippase is ubiquitous.

AllSwitch$^{KIWT\text{-}KIH215DHA}$*;+;+* were crossed with hsFLP y1 w*; +/+; act5c promoter FRT CD2stop FRT GAL4, UAS-GFP/TM6B, Tb1 and selected for Cherry fluorescence; and absence of Tubby (conferred from TM6B, balancer). At 48h AEL larvae were heat shocked for 2 hours at 29°C, (the line confers expression in the fat body organ already at 25°C), after 48h selected for GFP fluorescence and processed for experiments.

4.5 Metabolic labelling of larval lipids

The metabolic labeling of lipids was carried out by Dr. Bernadette Breiden. TAG, FA, and Ceramide synthase activity was determined by measuring *de novo* TAG, FA and ceramide generation after 18h labeling of larvae with [1-14C]-acetic acid. For metabolic labeling, larvae were fed with inactivated yeast paste containing [1-14C]-acetic acid (61Ci/mol) as a C1-precursor for lipids. Larvae were homogenized, lyophilized and weighed. Lipids were extracted in chloroform/methanol/water (2:5:1 v/v/v). Same amounts of radioactivity of the desalted lipid extract were applied to each line on the TLC plates. Unpolar lipids (fatty acid, triacylglycerol) were separated with n-hexane/diethylether/glacial acetic acid (70:30:1, v/v/v) and ceramides with chloroform/methanol/glacial acetic acid (190:9:1, v/v/v). Radioactive bands were visualized with a Typhoon FLA 7000 (GE, Germany) and quantification was performed with the image analysis software ImageQuantTL (GE, Germany). Lipids were identified using commercially available reference standards (ceramide (C18:1/C18:0) (Sigma, Germany), phytoceramide (Cosmoferm, Delft, Netherlands), trioleoylglycerol (Sigma, Germany), and stearic acid (Fluka))

4.6 Triacylglycerols (TAG)

The TAG content was quantified by a coupled colorimetric assay. Circa 10 L3 of different genotypes were homogenized in 100µl of PBS using the Precellys 24 (3x 15 sec, 5000 Upm) and frozen in liquid nitrogen. The lyophilization was performed overnight by Dr. Bernadette Breiden. The dry weight was determined by weighting the samples after lyophilization and the values were used to normalize TAG amount. Samples were resuspended in 400µl of PBST and after centrifugation of 13,000 rpm for 3 min (4°C) the supernatant was transferred to new Eppendorf tubes and heated for 10 min at 70°C. Two 1.5ml Eppendorf tubes were used per each sample with 20µl of the samples in parallel two tubes with the glycerol standards (1,0 mg/ml, 0,5 mg/ml, 0,25 mg/ml, and 0,125 mg/ml) and PBST (blank) were also prepared. To measure free glycerol, one of the tubes was treated with 20µl of PBST, while the other one was treated with 20µl of triglyceride reagent (containing lipases to break down the TAG). Next, the probes were incubated for 45 min at 37°C. Afterwards the samples were centrifuged at 13,000 rpm for 3 min and 30µl of the supernatant of each sample was transferred to a 96 well plate. In the next step, 100µl of free glycerol reagent was added to each well and mixed. The plate was sealed with parafilm and then centrifuged to remove

condensed water and air bubbles. Subsequently, the plate was incubated for 5 min at 37°C. The absorbance was then measured at 540nm using the TECAN plate reader. The TAG assay was performed in triplicates for each of the genotypes and always included *KIWT* control.

4.7 Free Fatty acid assay (FFA)

FFA or Non-esterified fatty acids (NEFA) were measured by an adaptation of the copper-soap method (Tinnikov et al., 1999). In brief, three 3rd instar larvae were weighed and homogenized in 20µl of 1M phosphate buffer per mg tissue. 25µl of the supernatant were transferred to 500µl of Chloroform/Heptane 4:3, and lipids were extracted by shaking the vial for 5 min. Unspecific background provoked by phospholipids was circumvented by addition of 23 mg of activated silicic acid. 300µl of the chloroform phase were transferred to 250µl of Cu-TEA (copper-triethanolamine). After shaking and centrifuging, 150µl of the organic phase were transferred to fresh tubes. Liquid was evaporated in a 60 °C heat block, and lipids were dissolved in 100µl of 100% ethanol. Copper was detected by complexation with a mixture of dicarbazone - dicarbazide, and the color intensity was measured in a 96 well plate at 550 nm in a TECAN platereader (Bülow et al., 2017; Sellin et al., 2018).

4.8 *Ex vivo* culture

Ex vivo organ culture was established. After being washed in PBS, third instar larvae were carefully opened and incubated in ice cold Glucose-free Ringer's solution supplemented with different BSA-conjugated fatty acids (C12, C14, and C16) to a final concentration of 200µM for 6h at 4°C (several temperature and conditions were tried with the mentioned resulting the best for tissues morphology). BSA was used as control treatment. For different experimental condition, Etomoxir or Fumonisin B1 were added in parallel to a final concentration of 200µM and 50µM or 100µM for the latter (Xu et al., 2012). Following incubation, the open larvae were then washed and fat bodies and gut were quickly dissected in ice cold Ringer´s solution; and subsequently frozen in in 200µl of TRIzol in liquid nitrogen.

4.9 Immunohistochemistry

Larvae were inverse-prepped in ice-cold PBS, fixed for 60 minutes in 4% methanol-free formaldehyde at room temperature. After several washes in Phosphate-buffered saline with 0.2-0.3% Triton X 100 (PBT) and incubation for 30 minutes in blocking solution (5% donkey serum in PBT), primary antibodies were incubated over night at 4°C. Samples were then washed and incubated in blocking solution as previously described. Secondary antibodies were added for 1.5h at room temperature followed by several washing steps.

4.9.1 Quantification of nuclear versus cytoplasmic Schlank in fat body cells

Cells were imaged for Lamin Dm0 (Inner nuclear membrane; INM), DAPI, Schlank or Spectrin (Cell membrane; CM) and Schlank. The nuclear area was defined as DAPI / Lamin Dm0 stained region. The cytoplasmic area was defined as Spectrin area minus nuclear area. Mean fluorescent intensity (MFI) ratio of Schlank fluorescence of nuclear versus cytoplasmic area per cell was determined. Quantification was done using ImageJ software. Statistical difference in the distribution of the ratios was tested via Mann-Whitney U test.

4.9.2 Size Determination of fat body cells

Cells were imaged for Lamin Dm0 (INM), Schlank, and Spectrin CM), the cell area was defined by Spectrin and outlined by “Hand” tool. Cells at a comparable confocal plane were compared using lamin staining. Cell area was determined using ImageJ software. Statistical difference in the distribution of the ratios was tested via Mann-Whitney U test.

4.10 RNA extraction and quantitative Real Time PCR (qRT-PCR)

Isolation of total RNA was performed in TRizol (Invitrogen). cDNA was transcribed using Qiagen QuantiTect Kit. Realtime PCR was performed in a reaction mix containing cDNA template, primer pairs and iQ SYBR Green Supermix (BIO-RAD). The experiments were performed in an iQ5 Real-Time PCR Detection System from BIO-RAD. Ribosomal protein L32 (*rp-49*) was used as reference gene. For qRT primers see table below. All template reactions were done in parallel and repeated with independently isolated RNA samples from different larval or cell collections.

4.10.1 RNA isolation for RNA-seq

For RNA isolation, fat body cells (from ~30 animals per sample) were isolated and subsequently lysed in TRIzol (Invitrogen) and total RNA was extracted. The quality of the RNA was assessed by measuring the ratio of absorbance at 260nm and 280nm using a Nanodrop 2000 Spectrometer (Thermo Scientific) as well as by visualization of the integrity of the 28S and 18S bands via a RNA analysis ScreenTape assay on a 2200 TapeStation instrument (Agilent).

4.10.2 qRT-PCR primers

Name Primer	**Primer Sequences (F-R)**
Lip 3	5´-TGAGTACGGCAGCTACTTCCCT-3´ 5´-TCAACTTGCGGACATCGCT-3´
Magro	5´-GCACCCACCCACTTGTACTC-3´ 5´-GATCGTTGACCAGCTCCTTC-3´
CG6295	5´-GGAGGACCAGCCGTGGATA-3´ 5´-ATCTCTGGCTCGCACTTCAAC-3´
CG8093	5´-AGTACGATGTGGAGGGCATC-3´ 5´-ATACCTAAGGCGATCCACGT-3´
CG6277	5´-TGGCATTCTTTGCTCTGG-3´ 5´-ACTCGGAAGTGCCATCCT-3´
Bmm	5´-ACGCACAGCAGCGACATGTAT-3´ 5´-CTTTTCGCTTTGCTACGAGCC-3´
Thor	5´-CATGCAGCAACTGCCAAATC-3´ 5´-CCGAGAGAACAAACAAGGTGG-3´
InR	5´-AACAGTGGCGGATTCGGTT-3´ 5´-TACTCGGAGCATTGGAGGCAT-3´
SREBP	5´-CGCAGTTTGTCGCCTGATG-3´ 5´CAGACTCCTGTCCAAGAGCTGTT-3´
DHR96	5´-CAAAGAGAGCATATTTAGGATACCAAG-3´ 5´-CACAGAACCCAC GCTTCCAAG-3´
Ceramidase-RA	5´-CCAAGTCCGCCGTACATGAAT-3´ 5´-TGCGACTTCACGTAGCCAAAG-3´
Ceramidase-RB	5´-GTCGGCAGTCTTCTTTTCGTG-3´ 5´-CACAGGAAACTTACGGCCAGA-3´
Ceramide kinase	5´-GTTGCCTGGACCTGATTCTC-3´ 5´-GGCAAATTGCGAATATCACC-3´

Serinepalmitoyl transferase	5´-ACCCTCTACGAACTGAACAC-3´ 5´-CGGCACAAAGGCAAAGGA-3´
Sphingomyelin-synthase-related (SMSr)	5´-TTCAGGGATGCGAGTGTG-3´ 5´-ACGAATGTGGAAGAGCGAAT-3´
Glucosylceramidase	5´-CACGTGCTCTGTTGGTTCC-3´ 5´-CCAGCCAACGACGAACTC-3´
Fatty Acid Synthase	5´-CCCCAGGAGGTGAACTCTATCA-3´ 5´-GACTTGACCGATCCGATCAAC-3´
Rp-49	5´-TCCTACCAGCTTCAAGATGAC-3´ 5´-CACGTTGTGCACCAGGAACT-3´

4.11 Cell Culture and transfection

Drosophila Schneider cells (S2) were grown in Schneider's Medium supplemented with 10% heat inactivated fetal bovine serum and 1% penicillin/streptomycin (Sigma, St Louis, USA). Transfection was performed approx. 12h after plating of S2 cells using Effectene (Qiagen) according to the manufacturer's instruction. Starvation and FA Treatment were done in Serum Free Optimem with or without BSA-FA for the indicated time. To allow any ectopic expression efficiently, S2 cells were harvested 48h after transfection with the corresponding plasmids.

4.11.1 Luciferase Assays

Luciferase assays was performed using the Dual-Luciferase® System (Promega). After 48h from transfection in a 24-well plate, the media was removed and S2 cells were resuspended in100µl of 1X Passive Lysis Buffer (PLB), and left in shaking for 15 minutes at room temperature. The whole lysates (included cell debris) were transferred in tubes on ice and a centrifuge at 10000g at 4°C was performed for 1 minute. After, the supernatant was readily transferred in a fresh tube (on ice) and the debris discarded. The samples were stored at -20°C up to 1 months. For the luciferase assay, 25µl of lysate were transferred to a micro-96 well white plate (costar® 3693 EIA/RIA plate, 96 well half area). Luciferase activity measurements were done using a MicroLumat*Plus* LB 96V luminometer (Berthold Technology). Immediately before the measurements, 25µl (Scaled down from the 100µl described from the manufacturer) of the first component Luciferase assay reagent (LAR; Substrate for Firefly luciferase) was added to each well. The measurement was set for 3 sec for each well. Subsequently 25µl of the Stop&Glo (Substrate for Renilla luciferase) were added to each well and measurements were repeated. Value of Firefly <500 were not taken

into account for the quantification because comparable to the measurement for LAR alone. Each experiment was repeated three times and is the average of the reading of three different transfected wells.

4.11.2 Antibody Staining

For immunohistochemical staining were used: anti-Schlank-CT from guinea pig or sheep (α−Schlank) 1:50 (see Voelzmann, Bauer, 2011), anti-HA (α−HA, rat, 1:100; clone 3F10; Roche); anti-Spectrin (α−Spectrin; mouse, 1:40) Developmental Studies, Hybridoma Bank (DSHB) and mouse anti-Lamin Dm0 (DSHB) 1:100. Tissue or cell were mounted with DAPI Fluoromount-G (SouthernBiotech).

4.11.3 Quantification of nuclear Schlank in S2 cells

Cells were imaged for Schlank (α-Schlank-CT, endogenus) or HA (α-HA; expression of *UAS-schlank NTHA* (*HA-WT*)) and DAPI fluorescence. The nuclear area was defined as DAPI and Cytoplasm as total Schlank signal minus nuclear area. Mean fluorescent intensity (MFI) ratio of Schlank / DAPI of nuclear versus cytoplasmic area per cell was determined and quantified using the Image J "Intensity Ratio Nuclei Cytoplasm Tool" (Volker Baecker, 2012) and plotted as MFI (nucleus / cytoplasm). Each of the measurement is shown in the dot plot. Statistical difference in the distribution of localization were tested via one-way anova with Bonferroni post-test.

4.12 Chromatin Immunoprecipitation (ChIP)

S2 Cells were crosslinked with formaldehyde (1% final concentration). The reaction was stopped by the addition of glycine (0.125 M for 5 min at room temperature). Cell pellets were lysed in L1 buffer (2 mM EDTA, 50 mM Tris–HCl (pH 8.1), 0.1% Nonidet P-40, 10% glycerol and protease and phosphatase inhibitors) for 20 min at 4°C in rotation. The lysates were homogenized and then centrifuged at 5000 rpm for 5 min at 4°C. Nuclear pellets were resuspended in L2 buffer (5 mM EDTA, 50 mM Tris–HCl (pH 8.0), 1% SDS (completed with protease and phosphatase inhibitors) and kept on ice for 10 min. Nuclear lysates were sonicated to obtain chromatin fragments of an average length of 200 to 700 bp and centrifuged at 10,000 rpm for 10 min at 4 °C. The sonicated supernatant fractions were diluted 5-fold with dilution buffer (5 mM EDTA, 50 mM Tris–HCl (pH 8.0), NP40 0.5%, NaCl 200 mM and protease and phosphatase inhibitors). For each condition 20025µl of

diluted chromatin were incubated with a 50 % Protein A+ 50% Protein G Sepharose (Immunoprecipitation starter kit, Amersham Biosciences, Piscataway, NJ) saturated with salmon sperm for 1h at 4°C on a rotating platform. The precleared chromatin samples were centrifuged at 14,000 rpm for 5 min and incubated with the respective antibodies overnight with gentle rotation at 4°C. Immunoprecipitated samples were recovered by incubation with saturated Protein A and G Sepharose on a rotating platform for 2 h at 4°C. Before the samples were washed, the supernatant of the no-antibody control was taken as input sample. Each sample was washed with 1ml of Low Salt buffer (0.1% SDS, Triton-X-100, 2 mM EDTA, 20 mM Tris-HCl pH=8.1, 150 mM NaCl); high Salt buffer (0.1% SDS, Triton-X-100, 2 mM EDTA, 20 mM Tris-HCl pH=8.1, 500 mM NaCl); LiCl Buffer (0.25 M LiCl, 1% NP40, 1% deoxycholate, 1 mM EDTA, 10 mM Tris-HCl pH=8,1) and TE Buffer (10 mM Tris-HCl, 1 mM EDTA pH=8). Samples were eluted with elution buffer two times 150µl (1% SDS, 0.1 M $NaHCO_3$) and then treated with RNaseA for 10 minutes at room temperature. The protein-DNA crosslinking was reversed at 67°C overnight. $NaHCO_3$ in each sample was neutralized by Tris-HCl (pH 6-7.5). Samples were treated with Proteinase K for 2h at 56°C. Phenol/Chloroform was used for DNA extraction. 1ul of immunoprecipitated DNA was used for analysis by qRT-PCR.

4.12.1 Linker-mediated PCR

The following linkers were used:

5´P-AGAAGCTTGAATTCGAGCAGTCAG (24 mer- 5´phosphorylated)

5´-CTGCTCGAATTCAAGCTTCT (20 mer).

10µM of each primer were let annealed in a PCR cycle, (95°C for 5 min; 70°C for 5 min, 55°C for 5 min) and stored at -20°C.1µl of 1µM of annealed linkers were ligated with 1µl of T4 DNA Ligase (NEB) and DNA Ligase buffer to 7µl of immunoprecipitated material overnight (ON) at 16°C. Subsequently a PCR was run using 10µl of ligation mix; with 1µl of 20-mer linkers (100 µM) in a final volume of 100µl for the reaction (55°C for 2 min, 72°C for 5 min, 94°C for 5 min, [94°C for 1 min, 55°C for 1 min, 72°C for 1 min] x 20 cycle; 72°C for 5 minutes, 4°). The PCR reaction was repeated by using 10µl of PCR instead of 10µl ligation as template. The PCR was then run on 1.5% Agarose Gel.

4.12.2 Primers for qRT-PCR ChIP

Name Primer	Primer Sequences (F-R)
Lip 3_prom	5‘-CACGAGGTGGTCACCAGTGACA-3‘---5‘-CTCAGCATGCCGTGCATGAGGA-3‘
Magro_prom	5´-ATTTTTAAACTAAACCTCAA-3´--5´-ATCTGCTGGTCGAAACCCTG-3´
sprouty	5´-AATCGGCGAGGATGAGTG-3´---5´-GACGGCAGGTGCAAGACAG-3´
miR 278	5´-CGGGTCGGTGGGACTTTC-3´---5´-GACGGCAGGTGCAAGACAG-3´

4.13 Immunoprecipitation and Immunoblotting

Immunoprecipitation and immunoblotting were done as described earlier (Bauer et al., 2006). Briefly, S2 cells or larvae were homogenized in RIPA buffer (150mM NaCl, 1% IGEPAL CA-630, 0.5% Sodium Deoxycholate, 0.1% SDS, 50mM Tris (pH 8.0), supplemented with protease inhibitors (Complete^{TM}; Roche, Indianapolis, USA), and centrifuged at 10,000rpm for 10 min at 4^{o}C. The supernatant was used for determination of protein content, immunoblotting and/or immunoprecipitation. Whole cell S2 lysates (50µg of protein) were separated by 15% SDS-PAGE and transferred to a PVDF-membrane (Immobilon P transfer-membrane; Millipore). The immunoblot membrane was blocked with non-fat dry milk in TBS plus 0.05% Tween (TBST) and then incubated with either anti-HA (rat, 1:500; clone 3F10; Roche), anti-GFP (mouse, 1:500, Santa Cruz), anti-schlank (guinea pig, 1:400), α-actin (rabbit IB: 1:1000 Sigma) antibodies. After washing, bound antibodies were visualized with peroxidase–conjugated donkey anti-rabbit, donkey anti-mouse or donkey anti-rat IgG (1:15000) using the ECL system (Pierce™ ECL Western Blotting Substrate, TermoFisher Scientific).

Co-immunoprecipitation was performed using the immunoprecipitation starter pack (Amersham Biosciences, Piscataway, NJ). To avoid the nonspecific binding of proteins to A/G-Sepharose, preclearing of the cell-lysates was performed for three hours at 4°C in the presence of protein A/G-Sepharose. The cleared supernatant was incubated overnight with α-HA or α-GFP antibodies in a final volume of 500µl. 50µl protein A/G- Sepharose was added to each mixture and incubated for 3h at 4^{o}C. The beads were washed three with 1ml RIPA-buffer and two times with 1ml PBS. resuspended in SDS-Page sample buffer, and

boiled for 3 min. Samples were run on a 12% SDS-gel, transferred to a PVDF-membrane (Immobilon P transfer-membrane; Millipore) and the blot processed as described above.

4.14 RNA-Sequence analysis

4.14.1 Generation of cDNA libraries

Total RNA was converted into libraries of double stranded cDNA molecules as a template for high throughput sequencing following the manufacturer's recommendations using the Illumina TruSeq RNA Sample Preparation Kit v2. Shortly, mRNA was purified from 100ng of total RNA using poly-T oligo-attached magnetic beads. Fragmentation was carried out using divalent cations under elevated temperature in Illumina proprietary fragmentation buffer. First strand cDNA was synthesized using random oligonucleotides and SuperScript II (Invitrogen). Second strand cDNA synthesis was subsequently performed using DNA Polymerase I and RNase H. Remaining overhangs were converted into blunt ends via exonuclease/polymerase activities and enzymes were removed. After adenylation of 3′ ends of DNA fragments, Illumina indexed PE adapter oligonucleotides were ligated. DNA fragments with ligated adapter molecules were selectively enriched using Illumina PCR primer PE1.0 and PE2.0 in a 15 cycle PCR reaction. Size-selection and purification of cDNA fragments with preferentially 200-300 bp in length was performed using SPRIBeads (Beckman-Coulter). The size-distribution of cDNA libraries was measured using the high sensitivity D1000 assay on a 2200 TapeStation instrument (Agilent). cDNA libraries were quantified using KAPA Library Quantification Kits (Kapa Biosystems). After cluster generation on a cBot, a 75 bp single-end run was performed on an Illumina HiSeq1500.

4.14.2 Preprocessing RNA-seq

After base calling and de-multiplexing using CASAVA version 1.82, the 75 bp single-end reads were aligned to the Drosophila Melanogaster reference genome dm6 from UCSC by HISAT2 version 2.0.5 using the default parameters. After mapping of the reads to the genome, we imported the data into Partek Genomics Suite V6.6 (PGS) to quantify the number of reads mapped to each gene annotated in the RefSeq dm6 annotation downloaded in October 2016. The raw read counts were used as input to DESeq2 for calculation of normalized signal for each transcript using the default parameters. After DESeq2 normalization, the normalized read counts were imported back into PGS and floored by setting all read counts to at least a read count of 1. Subsequent to flooring, all transcripts having a maximum over all groups means lower than 10 were removed. After dismissing the

low expressed transcripts the data comprised of 10.760 present genes. RNA-seq data can be accessed under GSE98800.

4.14.3 Statistical and descriptive bioinformatics of transcriptome data

A one-way analysis of variance (ANOVA) model was performed to calculate the 1.000 most variable and the differentially expressed (DE) genes between all groups. DE genes (664 genes) were defined by a fold change (FC) > 3 or < -3 and a p-value < 0.05. To visualize the structure within the data, we performed Principle Component Analysis (PCA) on all genes and hierarchical clustering (HC) on the 1.000 most variable genes with default settings in PGS based on the p-value of the expression values of all samples across all conditions.

To define differences and similarities in transcript expression among the groups, we performed co-expression network analysis based on Pearson's correlation coefficients (correlation r-cutoff 0.98) by using BioLayout Express3D (Theocharidis A *et al.*). The set of all present genes was used as the input for the network analysis. We visualized the network analysis using Cytoscape and colored the nodes within the network, representing the genes, according to their FC among the two conditions.

To assess the functionality of the genes with the highest and lowest fold changes and their nearest neighbors in the co-expression network, we performed a gene ontology enrichment analysis using the PANTHER classification system (Mi H *et al.*). GO-terms were considered significantly enriched with a Bonferroni corrected p-value < 0.05.

4.15 Image acquisition and processing

Images were taken with a Zeiss LSM710 confocal microscope and analysed with ImageJ (National Institute of Health, USA Schneider, Rasband, Eliceiri 2012). Where needed, brightness or contrast was adjusted for the whole image in Adobe Photoshop. For comparative stainings, images were not post-processed. Image panels were assembled in Adobe Illustrator software

4.16 Statistical analysis

Significance was tested using a 2-tailed heteroscedastic Student's t-test (Microsoft Excel) with at least 3 independent biological replicates (n), with Mann-Whitney U test or with one-way ANOVA where indicated (GraphPad Prism).*p<0.05, **p<0.01, ***p<0.001.

5 Appendix

5.1 Schlank locus gene expression verification

After reintegration Schlank and other genes in close proximity were analysed for mRNA levels by qRT-PCR, beside a reduction in *Schlank* expression for *Schlank*^{KO} no differences were observed in expression for any of the other genes and genotypes.

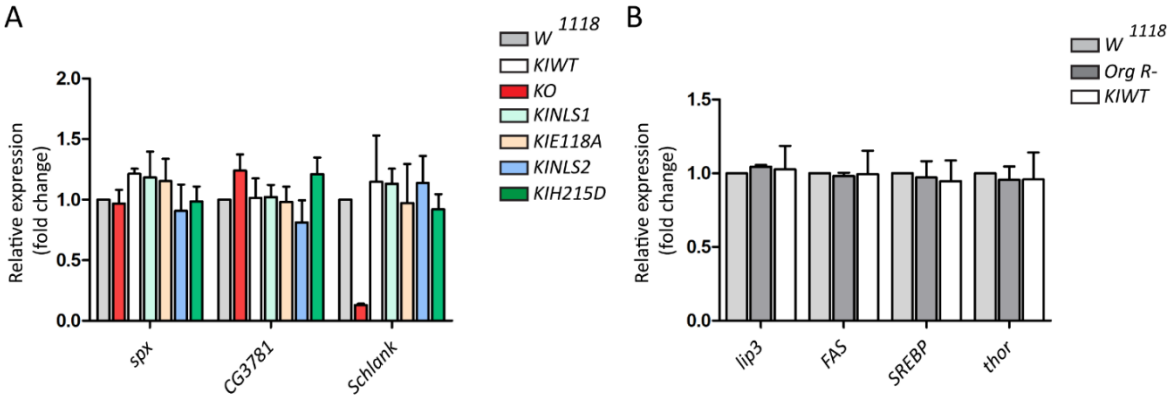

Figure A5.1. Reintegration analysis: quantification of mRNA levels by qRT–PCR. **A**) Strongly reduced *Schlank* mRNA expression in *Schlank*^{KO} mutants in comparison with w^{1118}, *KIWT, KIE118A, KINLS1, KINLS2* and *KIH215D* animals. Residual quantities of Schlank are due to Schlank maternal and zygotic supply (Bauer et al., 2009). Transcripts levels of *Schlank* or of *CG3781* and *spx* laying within or at the 3' region of the *Schlank* gene locus, respectively, resulted similar in *KIWT, KIE118A, KINLS1, KINLS2, KIH215D* and *w*^{1118} confirming the expression of reintegrated gDNA. **B**) Comparison of KIWT gene expression with other wild type flies. No change in gene expression is observable for genes involved in lipid metabolism and insulin signalling. Normalized on *rp-49* expression levels in *w*^{1118}.Error bars indicate SEM.

5.2 *KINLS2* mutant: cell size and nuclear localization in fat body cells

Representative images for *KIWT* and *KINLS2* fat body cells (Sociale et al., 2018).

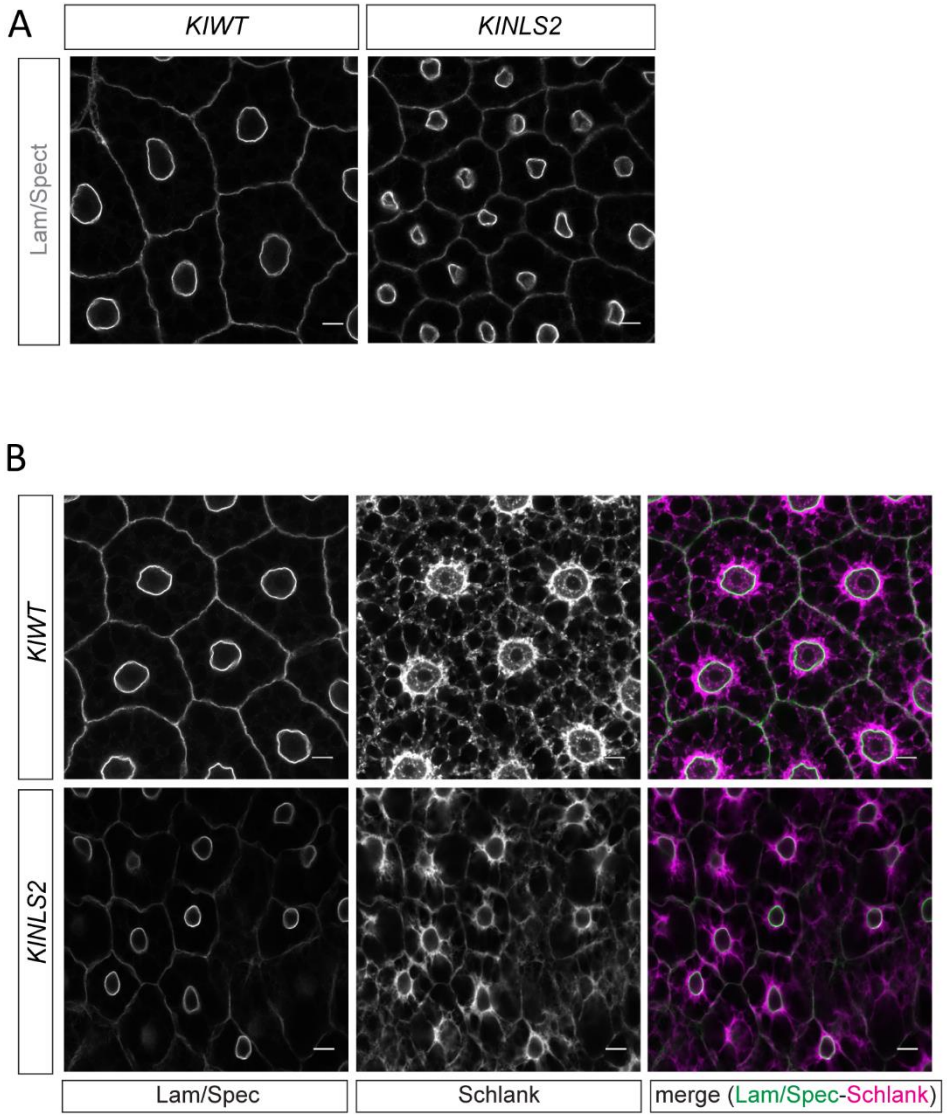

Figure A5.2. Fat body cells of *KINLS2* and *KIWT* (L3) larvae. **A**) Cells were stained for Lamin Dm0 to mark the nuclear membrane, Spectrin to mark cell membrane. **B**) Schlank nuclear localization in fat body cells. Cells were stained with an α -Schlank antibody recognising the C-Terminal of the protein (α-Schlank CT, magenta), with Lamin and Spectrin to mark the nuclear membrane and the cell membrane (green), respectively.

5.3 Sphingolipidomic analysis of *KINLS2*

To have a complete picture of *KINLS2* sphingolipidome, several samples of different larvae stages and one day old flies were sent for Mass Spec analysis, performed by Johanna Von Gerichten (AG R Sandhoff, DFKZ Heidelberg). At the early larval stage, the overall ceramide levels are similar to control larvae, accordingly with the *de novo* ceramide

generation. However, during the prolonged larval stage total ceramide levels decrease up to 50 %. Different TLC using several sphingolipid marker were performed, showing the enrichment of an atypical band that, to date, could not be yet identified. A possible explanation for the reduced ceramide levels in development might be found in an altered regulation of the sphingolipid signalling pathway. For this reason, gene expression of several enzymes involved in sphingolipid metabolism was tested. All of the tested genes no matter if up- or downstream Schlank resulted to be upregulated in comparison with *KIWT* control (Figure A5.3, A) meaning that the difference in ceramide metabolism might be due to a deregulation of gene expression resulting in a changed ceramide homeostasis e.g. by metabolizing it into complex sphingolipids or altered degradation.

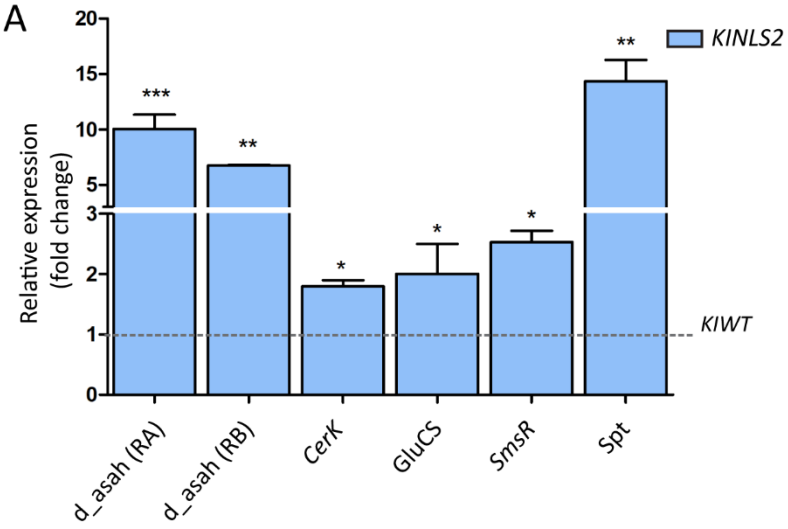

Figure A5.3. Analysis of transcript levels of genes of enzyme involved in sphingolipid biosynthesis. A) Gene expression levels in L3 *KINLS2* mutant larvae. Acronyms: d_asah, ceramidase (two isoforms RA and RB). CerK, Ceramide Kinase. GluCS, Glucosylceramide Synthase. SmsR, sphingomielynase related. Spt, Serine-palmitoyl-transferase. Transcript levels normalized on *KIWT* transcripts levels (spotted line) were determined using qRT-PCR (n = 3). Normalized on *rp-49* transcript levels Error bars indicate SEM, *** p<0.05, ** p<0.01, *p<0.001.

5.4 Nuclear localization and *in vivo* starvation

Changes in nuclear localization upon nutrients availability are confirmed *in vivo in* W^{1118} fat body cells (Sociale et al., 2018). Ectopic expression of homeodomain (aa 64-138) (localizing exclusively nuclear in cell culture experiments, Voelzmann et al., 2016) in hemizygous *schlank*^{G0061} mutants, which strongly upregulated *lip3*, as *KINLS2* mutants. The construct was expressed using pumpless-Gal4-driver lines (pplGal4). *Lip3* expression remained unchanged (Figure A5.4, B). In contrast the expression of a construct containing the N-Terminal of the protein (first TM domain) and the homeodomain (localizing mainly nuclear in cell culture experiments), rescued *lip3* upregulation in *schlank*^{G0061} (Voelzmann

et al., 2016). Supposing that in order to exert its function Schlank homeodomain needs to be anchored to the membrane.

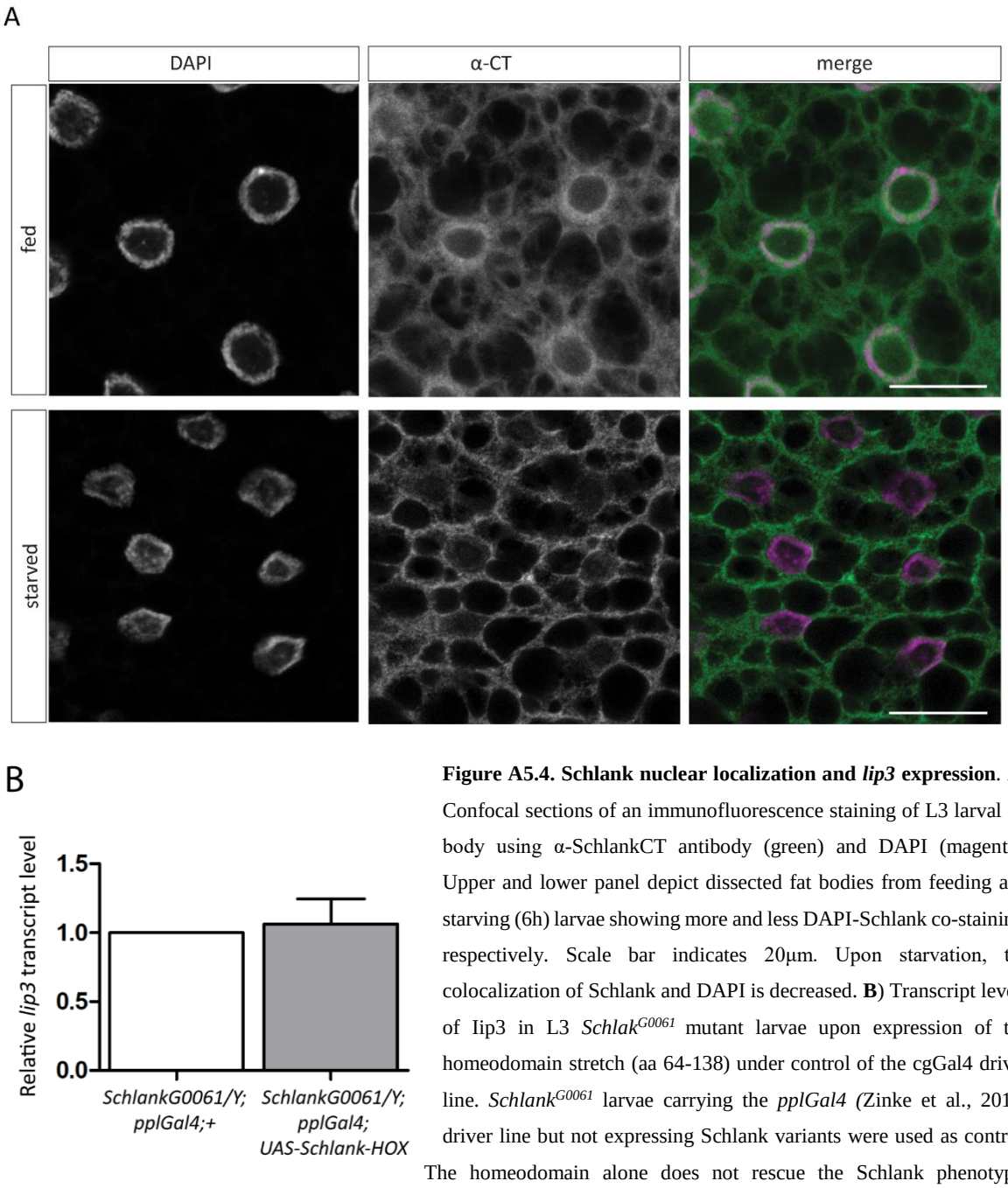

Figure A5.4. Schlank nuclear localization and *lip3* expression. **A**) Confocal sections of an immunofluorescence staining of L3 larval fat body using α-SchlankCT antibody (green) and DAPI (magenta). Upper and lower panel depict dissected fat bodies from feeding and starving (6h) larvae showing more and less DAPI-Schlank co-staining, respectively. Scale bar indicates 20µm. Upon starvation, the colocalization of Schlank and DAPI is decreased. **B**) Transcript levels of Iip3 in L3 *Schlak*^{G0061} mutant larvae upon expression of the homeodomain stretch (aa 64-138) under control of the cgGal4 driver line. *Schlank*^{G0061} larvae carrying the *pplGal4 (*Zinke et al., 2011*)* driver line but not expressing Schlank variants were used as control. The homeodomain alone does not rescue the Schlank phenotype. Normalized on *rp-49* transcript levels Error bars indicate SEM.

5.5 Generation of *Allele-Switch* lines

The Allele switch lines represent a tool of great value to study Schlank function in different organs and tissues during development. Since Hox- proteins are usually necessary during development, these lines are useful to understand in which stage and tissue Schlank transcriptional regulation (*AllSwitch*^{KINLS2}) or enzymatic activity (*AllSwitch*^{KIH215D}) are necessary to produce fly lacking any pathological phenotypes. In the scheme below is

represented the schematic of the reintegration and of the locus prior or after Flippase recombination event.

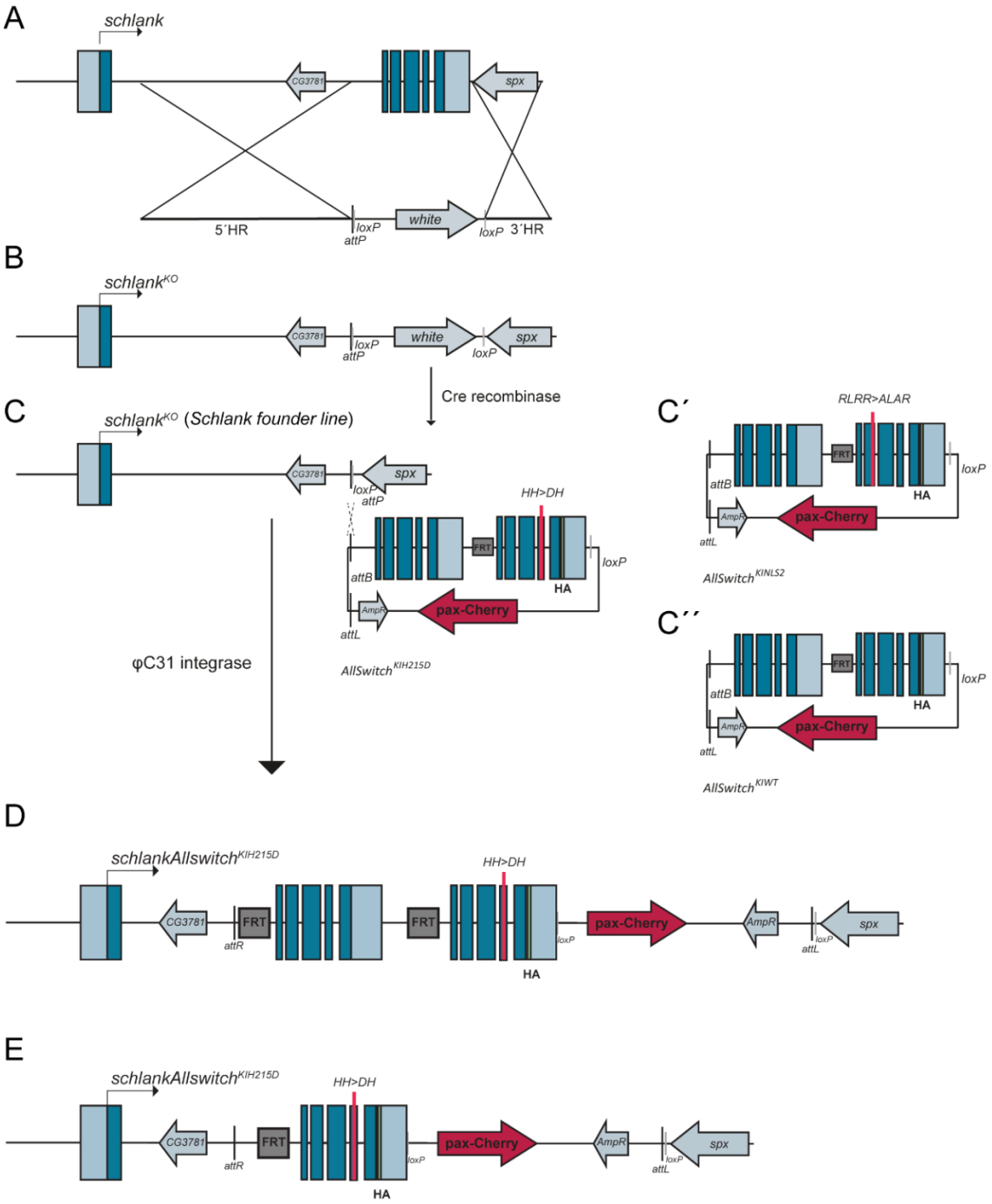

Figure A5.5. Reintegration scheme for Allele Switch lines. A) A 2.4 kb gDNA that encompassing exons 2-6 plus the 3' UTR sequence of Schlank was deleted and attP sites were inserted. **B)** The w^+, *Schlank*^{KO} lines is referred to as Schlank knockout line. **C)** After recombination events, the w^-, *Schlank*^{KO} line, the founder line, was used to reintegrate target constructs into the attP site. gDNA containing the deleted genomic DNA WT and a mutant H215D-HA (or C´ *Schlank*$^{NLS2\text{-}HA}$ or C´´*Schlank*^{WTHA,} as control lines) in a pGE-attB-RIV plasmid used for reintegration at the Schlank target locus of the Schlank founder line to generate the schlank-AlleleSwitch $^{KIWT\text{-}KIH215DHA}$ allele **D)**. **E)** Schematic of Schlank locus after Flipping out WT locus. Pax-Cherry marker is expressed during larval stage in the nervous system and during adult in the eyes (modified from Sociale et al., 2018).

5.6 Bioinformatics analysis for low complexity regions and phosphorylation sites within Schlank protein sequence

Low-complexity regions (LCRs) are amino acid sequences that contain repeats of single amino acids or short amino acid motifs (Green and Wang, 1994). While many LCRs are of unknown function, there are examples of LCRs playing various functional roles, including the modulation of protein– protein interactions (Xiao and Jeang, 1998), protein–nucleic acid interactions (Shen et al., 2004), and protein subcellular localization (Salichs et al., 2009). Expansion or contraction of LCRs can therefore potentially impact protein function (Toll-Riera et al., 2012). The analysis with the scanning tool DisEMBL 1.5 a predictor of intrinsic protein disorder revealed that beside the un-surprised homeodomain region (aa 50 to 125) a LCR is present at the CT-portion of Schlank present LCR (Figure A5.6, A, A´). LCRs are common in DNA-binding proteins and play a crucial role by increasing the affinity and specificity of DNA binding facilitating the helices loops. Intrinsically unstructured regions assist protein-DNA interactions in various mechanisms, and are usually responsible for co-factor binding and interactions. In the context of Schlank-Foxo interaction, would be interesting to study the role of the CT tail. DisEMBL analyses three different parameters to identify LCRs (Linding et al., 2003):

Loops/coils as defined by Kabsch and Sander, 1983. Loops/coils are not necessarily disordered; however, protein disorder is only found within loops. Representing a necessary but not sufficient requirement for disorder.

Hot loops constitute a refined subset of the above, namely those loops with a high degree of mobility as determined from Cα temperature factors (B factors). It follows that highly dynamic loops should be considered protein disorder. Several attempts have been made to try to use B factors for disorder prediction (Zoete et al., 2002).

Missing coordinates in X-Ray structure (remark465 entries in PDB) in fact, most often reflect intrinsic disorder, and have been used early on in disorder prediction (Li et al., 2000).

On the other hand, phosphorylation of cargos trafficking between the cytoplasm and nucleus is an important step to regulate nuclear availability, which directly affects gene expression (Nardozzi et al., 2010). For this reason a study for phosphorylation sites was carried on using two different bioinformatics tools NetPhos 2.0 and GPS 2.0 (Xue et al., 2008) (Figure A5.6, B, B´, B´´). NetPhos is a neural network-based method for predicting potential phosphorylation sites at serine, threonine or tyrosine residues in protein sequences (Blom et al., 1999), while GPS 2.0 is a tool to predict kinase-specific phosphorylation sites

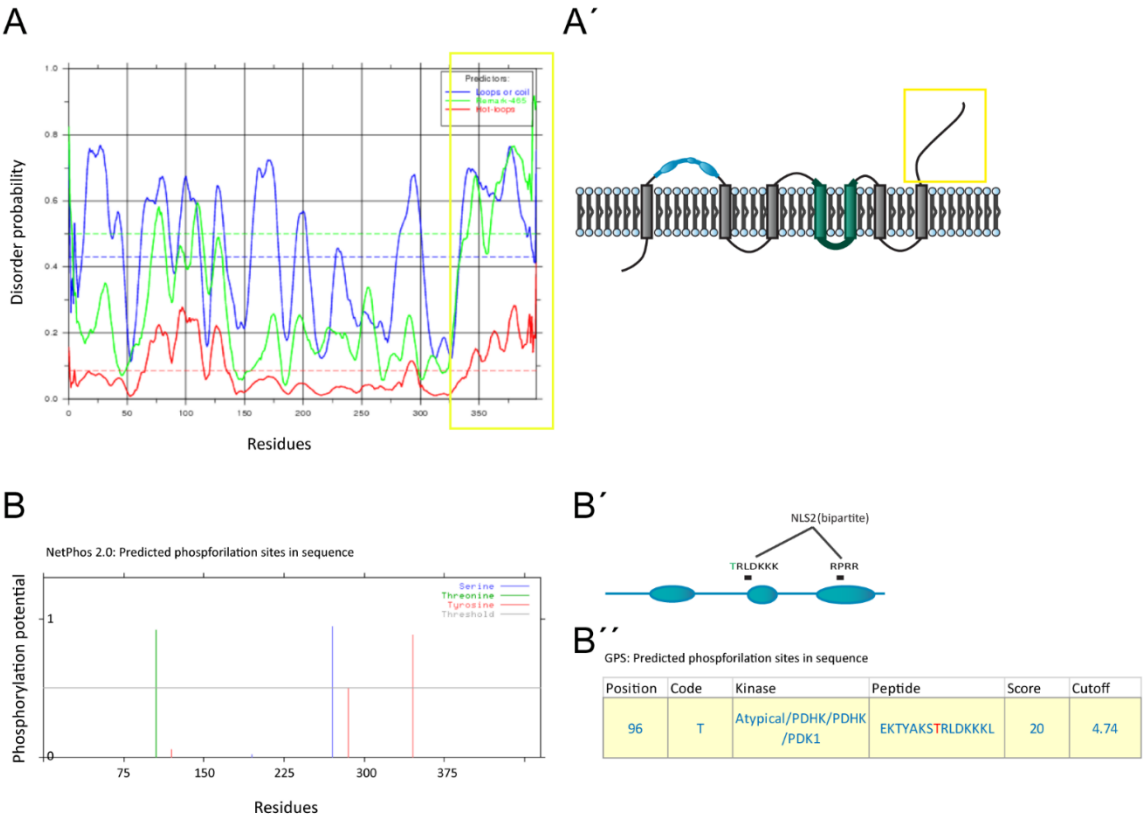

Figure A5.6. Output of bioinformatics analysis for LCR and phosphorylation. A) Output graph for disorder prediction where the aa sequence is plotted versus the disorder probability. The program recognises as LCR the regions that exceed the threshold (red, blue, green horizontal cut lines) for the three criteria previously described. Only the homeodomain region and the CT region meet the criteria. The yellow box highlight the region with the highest probability, and in **A´**) is shown the same region in protein structure. The output in **B**) show the possible phosphorylation sites one of which within the homeodomain, flanking the bipartite NLS2 site (T in green, **B´**) comes out also from the GPS 2.0 analysis, with one of the highest scores (T in re, **B´´**)

5.7 Protein alignment for NLS2 site

The mutation in the NLS2 site affected two arginine within the homeodomain (position 50-52 of the homeodomain or position 122-124 of protein sequence). The NLS2 site is conserved in all the mammalian CerSs (mCerSs) except CerS3, which nevertheless still contains the two Arginines (R) that are mutated in the NLS2 mutants, one of which in position 50 (**R**LRR to **A**LAR), is described to be crucial for DNA binding for homeodomain proteins (Bürglin and Affolter, 2015). Experimental evidences showed that the transcriptional regulation of CerS2b in zebrafish is dependent on the intact RRRR region (Mendelson et al., 2017).

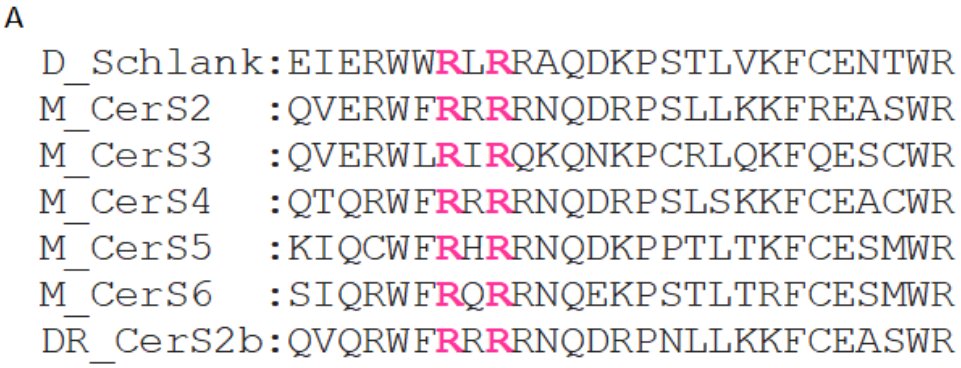

Figure A5.7. Partial protein alignment for homeodomains. The alignment is for the area of the homeodomain affected by the DNA-binding abolishing mutation NLS2. The first R in magenta is described as critical residue for DNA binding in Homeodomain TF. The two R are conserved among different species. In the *Drosophila* (D) Schlank, in the mammalian (M) CerSs (2-6), in (e.g.) the CerS2b (e.g.) of Zebrafish (DR, *Danio Rerio*).

5.8 Verification of ectopic human Elovl4 expression in S2 cells

Elovl4 is a member of the Elongases family, ER multi-transmembrane proteins that catalyse the first and limiting reaction of the long-chain fatty acids elongation cycle. In mammals elongases are essential in the biosynthesis of fatty acids longer than C12. For instance, elovl1 is responsible of specifically elongating C24:0 and C26:0 acyl-CoAs, participating in the production of saturated and monounsaturated VLCFA of different chain lengths that are involved in multiple biological processes as precursors of membrane lipids and lipid mediators. It has been shown, to play a critical role in early brain and skin development (Ohno et al., 2010). In collaboration with Roger Sandhoff (DFKZ, Heidelberg) the human elovl4-HA was cloned in a pUAST vector and tested for expression in S2 cells before embryo injection. S2 cells derive from a primary culture of late stage Drosophila melanogaster embryos (20-24h old), likely from a macrophage-like lineage. S2 cells start to differentiate in culture around passage 15th. For this reason every experiment in this thesis was performed with freshly thaw S2 cells. Even though, when S2 cell were transfected with pAc*Gal4* and *pUASTElovl4-HA*, to express the human elovl4, it was serendipitously noticed that S2 cells would differentiate (Figure A5.8, A). It is known that Elovl proteins are involved in *Drosophila* sperm development but only few of them have been studied so far (Jung et al., 2007).

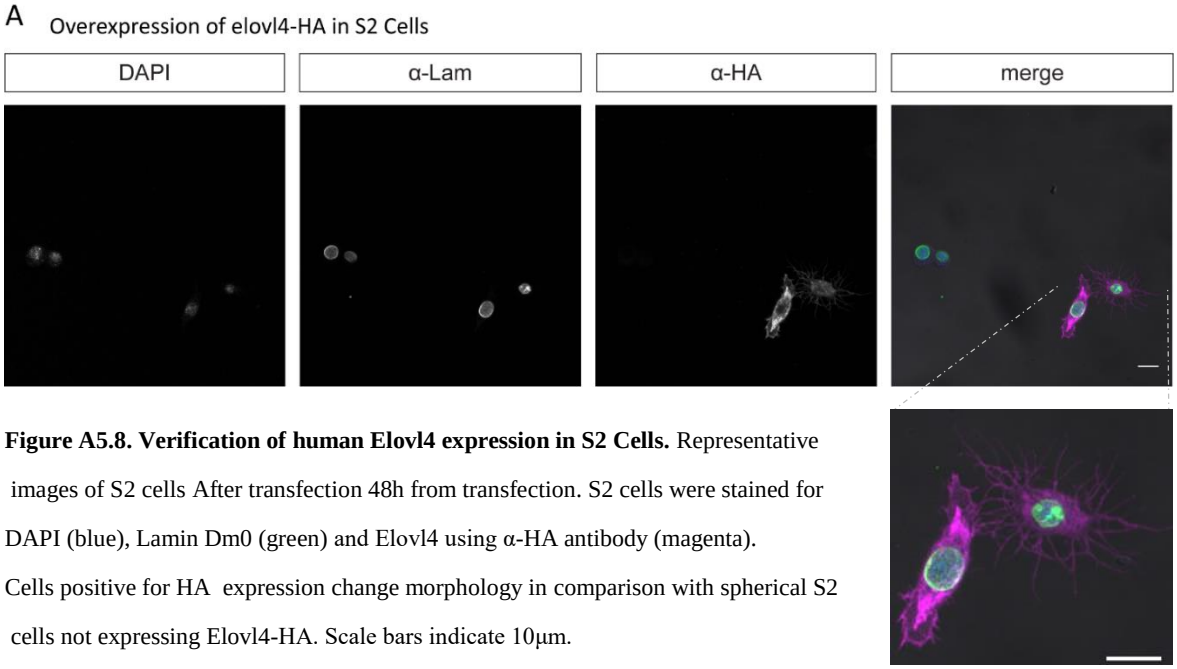

Figure A5.8. Verification of human Elovl4 expression in S2 Cells. Representative images of S2 cells After transfection 48h from transfection. S2 cells were stained for DAPI (blue), Lamin Dm0 (green) and Elovl4 using α-HA antibody (magenta). Cells positive for HA expression change morphology in comparison with spherical S2 cells not expressing Elovl4-HA. Scale bars indicate 10µm.

5.9 Verification of overexpression constructs and IP

Verification of newly generated UAS-constructs and pull down, IP.

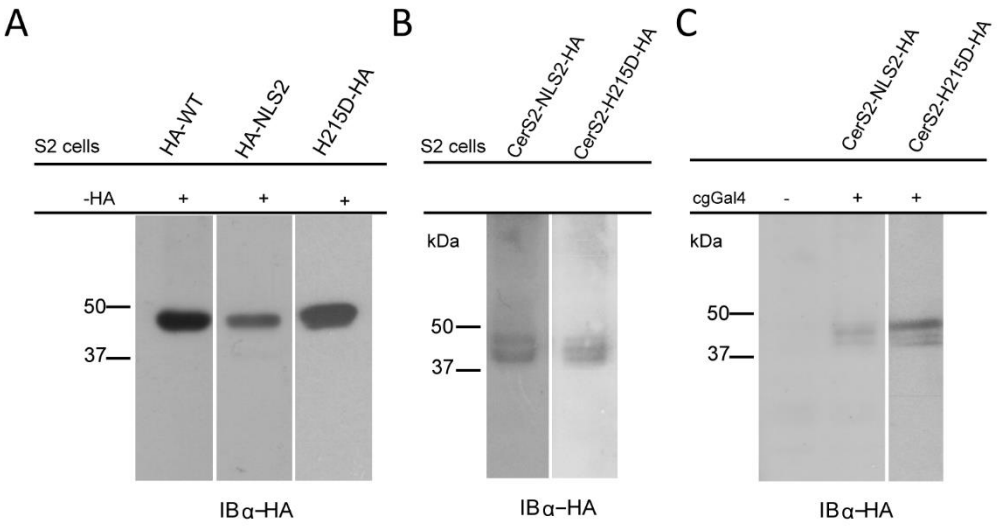

Figure A5.9. Verification of pUAST lines. A) Verification of the expression of HA-WT, HA-NLS2, H215D-HA protein in S2 cell extracts used for immunoprecipitation applying an α-HA antibody for immunoblotting. **B)** Verification of CerS2-NLS2-HA, CerS2-H215D-HA protein after overexpression in S2 cells. Immunoblot using an α-HA antibody shows a specific band corresponding to the predicted size for the CerS2 protein around 46 kDa. **C)** Verification of the CerS2-NLS2-HA and CerS2-H215D-HA fusion protein upon expression in the fat body using the cgGal4 fat body driver.

Acronyms

4E-BP Eukaryotic Initiation Factor 4E Binding Protein, *Thor*

A Alanine

aa amino acids

Acyl-CoA Fatty Acyl Coenzyme A,

AEL After Egg Laying

Akt or PKB

AMPK Activated Protein Kinase

AmpR Ampicillin Resistance

ASAH1 Acid Ceramidase

ATAC seq Assay for Transposase-Accessible Chromatin using sequencing

ATP Adenosine Triphosphate

Bmm Brummer

BSA Bovine Serum Albumin

C12- carbon chain lenght- Fatty Acyl Coenzyme A (Lauric Acid)

C14- carbon chain lenght- Fatty Acyl Coenzyme A (Myristic Acid)

C16- carbon chain lenght- Fatty Acyl Coenzyme A (Palmitic Acid)

C1PP Ceramide-1-Phosphate Phosphatase,

CerS Ceramide Synthase

CERT Ceramide Transfer Protein

CHARGE Consortium found an association between high levels of OCSFA

ChIP Chromatin Immunoprecipitation

coIP coimmunoprecipitation

cpt1 Carnitine palmitoyltransferase

D Aspartic Acid

d days

DEGS Dihydroceramide desaturase

Df31 Decondensation factor 31

DHR96 *Drosophila* Hormone Receptor 96

DILP Drosophila Insulin Like Peptide

E Glutamic Acid

Elovl4 Elongase Protein 4

ER Endoplasmic Reticulum

FA Fatty acids

FAIRE seq Formaldehyde-Assisted Isolation of Regulatory Elements sequencing

FAS Fatty Acid Synthase

FBS Fetal Bovine Serum

FFA Free Fatty Acids

Flp Flippase

FRT Flippase Recognition Target

gDNA genomic DNA

GFP Green Fluorescence Protein

GO Gene Onthology

h hours

H Hystidine

H3 Histone Protein

HA Hemmaglutinin tag

HAT Acetylase Transferases

HDAC Histone Deacetylases

HNF4 Hepatocyte Nuclear Factor

Hox Hox-Domain, Homeodomain

ILS Insulin Signaling Pathway

INM Inner Nuclear Membrane

InR Insulin Receptor

IP Immunoprecipitation

K Lysine

KD Knock Down

KDSR 3-keto-dehydrosphinganine reductase

KI Knock In

KO Knock Out

L1 First Instar Larva Stage

L2 Second Instar Larva Stage

L3 Third Instar Larva Stage

LAG1 Longevity Assurance Gene

LD Lipid droplet

Lip3 Lipase 3

LCR Low Complexity Regions

M Methionine

MAG Monoacylglycerols

MAGIC Meta-Analyses of Glucose and Insulin-related traits Consortium

MCFA Medium Chain Fatty acids

MFI Relative mean fluorescence intensities

NADPH Nicotinamide Adenine Dinucleotide Phosphate

NE Nuclear Envelope

NEFA Non-esterified fatty acids

neGFP nuclear GFP

NHR nuclear hormone receptor

NLS Nuclear Localization Site

NPC Nuclear Pore Complexes

OCSFA Odd-Numbered Chain Saturated Fatty Acids

ONM Outer Nuclear Membrane

P Proline

PBD Peroxisomal Biogenesis Disorders

PBS Phosphate Buffer Saline

PBST Phosphate Buffer Saline Tween

PCR Polymerase Chain Reaction

PEX Peroxine

PKB protein kinase B

PLB Passive Lysis Buffer

PPAR Peroxisome proliferator-activated receptors

PUFA Poly-unsaturated fatty acids ()

qRT-PCR quantitative Real Time Polymerase Chain Reaction

R Arginine

RNAi RNA interference

RP-49 Ribosomal Protein

S2 *Drosophila* Schneider cells

SCFA Short Chain Fatty Acids

SEM Standard Error of the Mean

Seq sequencing

SNP Single Nucleotide Polymorphism

SPT Serine Palmitoyltransferase

Spx Spliceosomal Complex Protein

SREBP Sterol Regulatory Element Binding Protein

sty *Sprouty*

T Threonine

TAG Triacylglycerols

TALE Transcription Activator-Like Effectors

TF Transcription Factor

TLC Thin Layer Chromatography

TLC Tram-Lag-CLN8

TM Transmembrane

UAS Upstream Activation Sequence

VDRC Vienna *Drosophila* Resource Center

VLCFA Very Long Chain Fatty Acids

ZF Zinc Finger

α-CT anti- C-Terminal antibody

α-Hox anti-homeodomain antibody

Bibliography

Accili D, and Arden KC. FoxOs at the crossroads of cellular metabolism, differentiation, and transformation. (2004) *Cell* 117, 421–426.

Adkins Y; Kelley DS. Mechanisms underlying the cardioprotective effects of omega-3 polyunsaturated fatty acids. *J. Nutr. Biochem*. 2010, 21, 781–792.

Agelopoulos M, McKay DJ, Mann RS. Developmental regulation of chromatin conformation by Hox proteins in Drosophila. *Cell Rep*. 2012 Apr 19;1(4):350-9

Aoun M, Feillet-Coudray C, Fouret G, Chabi B, Crouzier D, Ferreri C, Chatgilialoglu C, Wrutniak-Cabello C, Cristol JP, Carbonneau MA, et al. Rat liver mitochondrial membrane characteristics and mitochondrial functions are more profoundly altered by dietary lipid quantity than by dietary lipid quality: Effect of different nutritional lipid patterns. *Br. J. Nutr*. 2012, 107, 647–659.

Baena-Lopez LA, Alexandre C, Mitchell A, Pasakarnis L, Vincent JP. Accelerated homologous recombination and subsequent genome modification in Drosophila. *Development*.2013;140:4818–4825.

Bauer R, Voelzmann A, Breiden B, Schepers U, Farwanah H, Hahn I, Eckardt F, Sandhoff K, and Hoch M. (2009). Schlank, a member of the ceramide synthase family controls growth and body fat in Drosophila. *EMBO J*. 28, 3706–3716.

Baumbach J, Hummel P, Bickmeyer I, Kowalczyk KM, Frank M, Knorr K, Hildebrandt A, Riedel D, Jäckle H, and Kühnlein RP. (2014).A Drosophila in vivo screen identifies store-operated calcium entry as a key regulator of adiposity. *Cell Metab*. 19, 331–343.

Beh CY, El-Sharnouby S, Chatzipli A, Russell S, Choo SW, White R. Roles of cofactors and chromatin accessibility in Hox protein target specificity. *Epigenetics Chromatin*. 2016 Jan 8;9:1.

Bickert A, Kern P, van Uelft M, Herresthal S, Ulas T, Gutbrod K, Breiden B, Degen J, Sandhoff K, Schultze JL, Dörmann P, Hartmann D, Bauer R, Willecke K. Inactivation of ceramide synthase 2 catalytic activity in mice affects transcription of genes involved in lipid metabolism and cell division. *Biochim Biophys Acta*. 2018 Jul;1863(7):734-749.

Blom N, Gammeltoft S, Brunak S. Sequence- and structure-based prediction of eukaryotic protein phosphorylation sites. *Journal of Molecular Biology*: 294(5): 1351-1362, 1999.

Bobola N, Merabet S. Homeodomain proteins in action: similar DNA binding preferences, highly variable connectivity *Curr Opin Genet Dev*. 2017 Apr; 43:1-8.

Britton JS, and Edgar BA. (1998). Environmental control of the cell cycle in Drosophila: nutrition activates mitotic and endoreplicative cells by distinct mechanisms. *Development* 125, 2149–2158.

Bülow MH, Wingen C, Senyilmaz D, Gosejacob D, Sociale M, Bauer R, Schulze H, Sandhoff K, Teleman AA., Hoch M., and Sellin J. (2017). Unbalanced lipolysis results in lipotoxicity and mitochondrial damage in peroxisome-deficient Pex19 mutants. *Mol. Biol. Cell*.

Burgering BM, and Kops GJ. Cell cycle and death control: long live Forkheads. (2002) *Trends Biochem* Sci. 27, 352–360.

Bürglin TR and Affolter M. Homeodomain proteins: an update. *Chromosoma* (2015)

C. Zheng, F.Q. Jin, M. Chalfie. Hox proteins act as transcriptional guarantors to ensure terminal differentiation. *Cell Rep*, 13 (2015), pp. 1343-1352

Davidowitz G., D'Amico L.J., Nijhout H.F. Critical weight in the development of insect body size. *Evolut. and Develop*., 5 (2003), pp. 188-197

De Oliveira Otto MC, Lemaitre RN, Sun Q, King IB, Wu JHY, Manichaikul A, Rich SS, Tsai MY, Chen YD, Fornage M, Weihua G, Aslibekyan S, Irvin MR, Kabagambe EK, Arnett DK, Jensen MK, McKnight B, Psaty BM, Steffen LM, Smith EC, Riseärus U, Lind L, Hu FB, Rimm EB, Siscovick DS, Mozaffaria D. Genome-wide association meta-analysis of circulating odd-numbered chain saturated fatty acids: Results from the CHARGE Consortium. *PLoS ONE* 2018 13(5): e0196951.

D'Mello NP, Childress AM, Franklin DS, Kale SP, Pinswasdi C, Jazwinski SM. Cloning and characterization of LAG1, a longevity-assurance gene in yeast. *J. Biol. Chem.* 1994; 269:15451–15459.

Dunwell TL and Holland PWH. Diversity of human and mouse homeobox gene expression in development and adult tissues. *BMC Dev Biol*. 2016; 16: 40.

Dyson HJ and Wright PE. Intrinsically unstructured proteins and their functions *Nature Reviews Molecular Cell Biology* 2005 volume 6, pages 197–208.

Edgar BA. How flies get their size: genetics meets physiology Nat. Rev. Genet., 7 (2006), pp. 907-916

Fan W, Yanase T, Morinaga H, Okabe T, Nomura M, Daitoku H et al. (2007). Insulin-like growth factor 1/insulin signaling activates androgen signaling through direct interactions of Foxo1 with androgen receptor. *J Biol Chem* 282: 7329–7338.

Farooqui AA, Ong WY & Farooqui T (2010) Lipid mediators in the nucleus: Their potential contribution to Alzheimer's disease. *Biochimica et biophysica acta* 1801: 906–916

Field, C.J.; Clandinin, M.T. Modulation of adipose tissue fat composition by diet: A review. *Nutr. Res*. 1984, 4, 743–755.

Fox TE, Houck KL, O'Neill SM, Nagarajan M, Stover TC, Pomianowski PT, Unal O, Yun JK, Naides SJ & Kester M (2007) Ceramide recruits and activates protein kinase C zeta (PKC zeta) within structured membrane microdomains. *J. Biol. Chem* 282: 12450–12457

Fuller M (2010) Sphingolipids: the nexus between Gaucher disease and insulin resistance. *Lipids Health Dis* 9: 113

Futerman AH and Hannun YA. The complex life of simple sphingolipids. (2004) *EMBO Rep.* 5,8,777-782.

Gavin AG, Aloy P, Grandi P, Krause R, Boesche M, Marzioch M, Rau C, Jensen LJ; Bastuck S, Dümpelfeld B, Edelmann A. Proteome survey reveals modularity of the yeast cell machinery. *Nature Study*, Vol. 440, No. 7084, 2006, p. 631-6.

Gebelein B, McKay DJ, Mann RS. Direct integration of Hox and segmentation gene inputs during Drosophila development. *Nature.* 2004 Oct 7;431(7009):653-9.

Glaros EN, Kim A, Rye KA, Shayman JA, Garner B. Reduction of plasma glycosphingolipid levels has no impact on atherosclerosis in apolipoprotein E-null mice. (2008) *J. Lipid Res.* 49, 1677–1681

Goldberg, E.L. and Dixit, V.D.)Drivers of age-related inflammation and strategies for healthspan extension. (2015) *Immunol. Rev.* 265, 63–74

Goldberg, IJ, Trent CM, Schulze CP. Lipid metabolism and toxicity in the heart. (2012) *Cell Metab.* 15, 805–812

Gosejacob D, Jäger PS, vom Dorp K, Frejno M, Carstensen AC, Köhnke M, Degen J, Dörmann P, and Hoch M. Ceramide synthase 5 is essential to maintain C16:0-ceramide pools and contributes to the development of diet-induced obesity. *J Biol Chem* 2016, 291, 6989-7003.

Green H, Wang N. 1994. Codon reiteration and the evolution of proteins. *Proc Natl Acad Sci* USA. 91:4298–4302.

Greer E, and Brunet A. FOXO transcription factors at the interface between longevity and tumor suppression. (2005) *Oncogene* 24, 7410–7425.

Grönke S, Müller G, Hirsch J, Fellert S, Andreou A, Haase T, Jäckle H and Kühnlein RP. Dual Lipolytic Control of Body Fat Storage and Mobilization in Drosophila. *PLoS Biol*. 2007 Jun; 5(6): e137.

Grösch S, Schiffmann S, and Geisslinger G. (2012) Chain length-specific properties of ceramides. *Prog. Lipid Res.* 51, 50–62

Hannun YA, Obeid LM. Sphingolipids and their metabolism in physiology and disease. *Nat Rev Mol Cell Biol*. 2018 Mar;19(3):175-191

Hannun, Y.A. and Obeid, L.M. (2008). Principles of bioactive lipid signalling: lessons from sphingolipids. *Nat. Rev. Mol. Cell. Biol*. 9, 139–150.

Huang J, Zhou W, Watson AM, Jan Y-N, Hong Y. Efficient ends-out gene targeting in Drosophila. (2008) *Genetics* 180, 703–707.

Jackson Kim, G.; Jackson, K.G.; Maitin, V.; Leake, D.S.; Yaqoob, P.; Williams, Ch.M. Saturated fat-induced changes in Sf 60–400 particle composition reduces uptake of LDL by HepG2 cells. *J. Lipid Res.* 2006, *47*, 393–403.

Jones HE, Harwood JL, Bowen ID, Griffiths G. Lipid composition of subcellular membranes from larvae and prepupae of Drosophila melanogaster. *Lipids*. 1992 Dec;27(12):984-7.

Jump, D.B. The biochemistry of n-3 polyunsaturated fatty acids. *J. Biol. Chem*. 2002, 277, 8755–8758.

Jump, D.B.; Botolin, D.; Wang, Y.; Xu, J.; Christian, B.; Demeure, O. Fatty acid regulation of hepatic gene transcription. *J. Nutr*. 2005, *135*, 2503–2506.

Jump, D.B.; Tripathy, S.; Depner, C.M. Fatty acid-regulated transcription factors in the liver. Annu. Rev. Nutr. 2013, 33, 249–269. *Int. J. Mol. Sci*. 2015, 16 3847

Jung A, Hollmann M, Schäfer MA. The fatty acid elongase NOA is necessary for viability and has a somatic role in *Drosophila* sperm development. *Journal of Cell Science* 2007 120: 2924-2934

Kabsch W and Sander C. Dictionary of protein secondary structure (pattern recognition of hydrogen-bonded and geometrical features). *Biopolymers*. 1983;22:2577–2637

Kang, H.W.; Niepel, M.W.; Han, S.; Kawano, Y.; Cohen, D.E. Thioesterase superfamily member 2/acyl-CoA thioesterase 13 (Them2/Acot13) regulates hepatic lipid and glucose metabolism. *FASEB J.* 2012, *26*, 2209–2221.

Kaplan T, Biggin M.D. Quantitative models of the mechanisms that control genome-wide patterns of animal transcription factor binding. *Methods Cell Biol*, 110 (2012), pp. 263-283 13

Kaplan T, Li XY, Sabo PJ, Thomas S, Stamatoyannopoulos JA, Biggin MD, Eisen MB. Quantitative models of the mechanisms that control genome-wide patterns of transcription factor binding during early Drosophila development *PLoS Genet*, 7 (2011), p. e1001290

Karpac J, and Jasper H. (2009). Insulin and JNK: optimizing metabolic homeostasis and lifespan. *Trends in endocrinology and metabolism: TEM* 20, 100-106.

Kenyon C. The plasticity of aging: insights from long-lived mutants. (2005) *Cell* 120, 449–460.

Kolesnick RN, Goñi FM, Alonso A. Compartmentalization of ceramide signaling: physical foundations and biological effects. *J Cell Physiol.* 2000 Sep;184(3):285-300.

Kulaevaa OI, Nizovtsevaa EV, Polikanova YS, Ulianovb SV, Studitskya VM. Distant Activation of Transcription: Mechanisms of Enhancer Action. *Mol. Cell. Biol. December 2012 vol. 32 no. 24 4892-4897*

Lagarde M, Sicard B, Guichardant M. Fatty acid composition in native and cultured human endothelial cells. *In Vitro*, 1984, Volume 20-1 pp.33

Laviad EL, Albee L, Pankova-Kholmyansky I, Epstein S, Park H, Merrill AH Jr, and Futerman AH. Characterization of ceramide synthase 2: Tissue distribution, substrate specificity, and inhibition by sphingosine 1-phosphate. *J. Biol. Chem.* 2008 283, 5677–5684

Laviad EL, Kelly S, Merrill AH Jr, Futerman AH. Modulation of ceramide synthase activity via dimerization. *J Biol Chem*. 2012 Jun 15;287(25):21025-33.

Lemaitre RN, King IB, Kabagambe EK, Wu JH, McKnight B, Manichaikul A, et al. Genetic loci associated with circulating levels of very long-chain saturated fatty acids. *J Lipid Res.* 2015; 56(1):176±84.

Levy M & Futerman AH Mammalian Ceramide Synthases. *IUBMB Life* 2010 62: 347–356

Li P, Lee H, Guo S, Unterman TG, Jenster G, Bai W. (2003). AKTindependent protection of prostate cancer cells from apoptosis mediated through complex formation between the androgen receptor and FKHR. *Mol Cell Biol* 23: 104–118.

Li P, Nicosia SV, Bai W. (2001). Antagonism between PTEN/MMAC1/TEP-1 and androgen receptor in growth and apoptosis of prostatic cancer cells. *J Biol Chem* 276: 20444–20450.

Li X-Y, Thomas S, Sabo P, Eisen M, Stamatoyannopoulos J, Biggin M. The role of chromatin accessibility in directing the widespread, overlapping patterns of Drosophila transcription factor binding. *Genome Biol*. 2011;12(4):R34.

Lin, J.; Yang, R.; Tarr, P.T.; Wu, P.H.; Handschin, C.; Li, S.; Yang, W.; Pei, L.; Uldry, M.; Tontonoz, P.; *et al.* Hyperlipidemic effects of dietary saturated fats mediated through PGC-1b coactivation of SREBP. *Cell* 2005, *120*, 261–273.

Linding R, Jensen LJ, Diella F, Bork P, Gibson TJ, Russell RB. Protein Disorder Prediction Implications for Structural Proteomics. *Structure* 11-11 p1453–1459, November 2003.

Linding R, Jensen LJ, Diella F, Bork P, Gibson TJ, Russell RB. Protein disorder prediction: implications for structural proteomics. *Structure* 2003 Nov;11(11):1453-9

Ma, D.W.; Seo, J.; Davidson, L.A.; Callaway, E.S.; Fan, Y.Y.; Lupton, J.R.; Chapkin, R.S. n-3 PUFA alter caveolae lipid composition and resident protein localization in mouse colon. *FASEB J*. 2004, 18, 1040–1042.

Ma, D.W.; Seo, J.; Switzer, K.C.; Fan, Y.Y.; McMurray, D.N.; Lupton, J.R.; Chapkin, R.S. n-3 PUFA and membrane microdomains: A new frontier in bioactive lipid research. *J. Nutr. Biochem*. 2004, 15, 700–706.

Malhas A, Goulbourne C and Vaux DJ. The nucleoplasmic reticulum: form and function. *Trends Cell Biol* 2011, 21, 362–373.

Mann RS, Abu-Shaar M. Nuclear import of the homeodomain protein extradenticle in response to Wg and Dpp signalling. *Nature*, 1996;383:630–633.

Mann RS, Affolter M. Hox proteins meet more partners. *Curr. Opin. Genet. Dev*. 1998;8:423–429.

Mann RS, Lelli KM, Joshi R. Hox specificity unique roles for cofactors and collaborators. *Curr Top Dev Biol*. 2009;88:63-101

Mann RS. The specificity of homeotic gene function. *Bioessays*, 1995;17:855–863.

Marchesini N, Hannun YA. Acid and neutral sphingomyelinases: roles and mechanisms of regulation. *Biochem Cell Biol*. 2004 Feb;82(1):27-44.

Mekhail K and Moazed D. The nuclear envelope in genome organization, expression and stability. *Nature Reviews Molecular Cell Biology* (2010) volume 11, pages 317–328

Mendelson, K., Pandey, S., Hisano, Y., Carellini, F., Das, B.C., Hla, T., and Evans, T. (2017). The ceramide synthase 2b gene mediates genomic sensing and regulation of sphingosine levels during zebrafish embryogenesis. *eLife* 6, 6.

Mesika A, Ben-Dor S, Laviad EL, and Futerman AH. A New Functional Motif in Hox Domain-containing Ceramide Synthases: identification of a novel region flanking the Hox and TLC domains essential for activity. *J. Biol. Che*. 2007, 282, 27366–27373

Mesika, A., Ben-Dor, S., Laviad, E.L., and Futerman, A.H. (2007). A new functional motif in Hox domain-containing ceramide synthases: identification of a novel region flanking the Hox and TLC domains essential for activity. *J. Biol. Chem.* 282, 27366–27373.

Mizutani Y, Kihara A, and Igarashi Y. (2005) Mammalian Lass6 and its related family members regulate synthesis of specific ceramides. *Biochem. J.* 390, 263–271

Mizutani Y, Kihara A, and Igarashi Y. LASS3 (longevity assurance homologue 3) is a mainly testis-specific (dihydro)ceramide synthase with relatively broad substrate specificity. *Biochem. J.* 2006, 398, 531–538

Mullen TD, Spassieva S, Jenkins RW, Kitatani K, Bielawski J, Hannun YA, Obeid LM.Selective knockdown of ceramide synthases reveals complex interregulation of sphingolipid metabolism. *J Lipid Res*. 2011 Jan;52(1):68-77.

Nakamura, M.T.; Yudell, B.E.; Loor, J.J. Regulation of energy metabolism by long-chain fatty acids. *Prog. Lipid Res*. 2014, 53, 124–144.

Nardozzi JD, Lott K, Cingolani G. Phosphorylation meets nuclear import: a review. *Cell Commun Signal*. 2010; 8: 32.

Nijhout H.F. The control of body size in insects., *Dev. Biol*., 261 (2003), pp. 1-9

Noyes MB, Christensen RG, Wakabayashi A, Stormo GD, Brodsky MH, Wolfe SA. Analysis of Homeodomain Specificities Allows the Family-wide Prediction of Preferred Recognition Sites. (2016) *Cell* 133, 1277–1289

Noyes, M.B., Christensen, R.G., Wakabayashi, A., Stormo, G.D., Brodsky, M.H., and Wolfe, S.A. (2008). Analysis of homeodomain specificities allows the family-wide prediction of preferred recognition sites. *Cell* 133, 1277–1289.

Obeid LM, Linardic CM, Karolak LA, Hannun YA. Programmed cell death induced by ceramide. *Science* 1993, Mar 19;259(5102):1769-71

Ohno Y, Suto S, Yamanaka M, Mizutani Y, Mitsutake S, Igarashi Y, Sassa T, Kihara A. ELOVL1 production of C24 acyl-CoAs is linked to C24 sphingolipid synthesis. *PNAS* Oct 2010, 107 (43) 18439-18444

Pancsa R and Fuxreiter M. Interactions via Intrinsically Disordered Regions: What Kind of Motifs? *IUBMB Life*, June 2012 64(6): 513–520,

Papackova Z and Cahova M. Fatty Acid Signaling: The New Function of Intracellular Lipases. *Int. J. Mol. Sci*. 2015, 16, 3831-3855.

Park JW, Park WJ, Futerman AH. Ceramide synthases as potential targets for therapeutic intervention in human diseases. *Biochim. Biophys. Acta*, 1841 (2014), pp. 671-681

Park JW, Pewzner-Jung Y. Ceramide synthases: reexamining longevity. *Handb Exp Pharmacol*. 2013;(215):89-107.

Pastor-Pareja, JC, and Xu T. Shaping cells and organs in Drosophila by opposing roles of fat body-secreted collagen IV and perlecan. (2011). *Dev. Cell* 21, 245–256.

Pewzner-Jung Y, Brenner O, Braun S, Laviad E, Ben-Dor S, Feldmesser E, Horn-Saban S, Amann-Zalcenstein D, Raanan C, Berkutzki T, Erez-Roman R, Ben-David O, Levy M, Holzman D, Park H, Nyska A, Merrill AH Jr. Futerman AH. A Critical Role for Ceramide Synthase 2 in Liver Homeostasis II. INSIGHTS INTO MOLECULAR CHANGES LEADING TO HEPATOPATHY. (2010) *J. Biol. Chem* 285, 10911-10923.

Pewzner-Jung Y, Park H, Laviad EL, Silva LC, Lahiri S, Stiban J, Erez-Roman R, Brugger B, Sachsenheimer T, Wieland FT, Prieto M, Merrill AH, and Futerman AH. A Critical Role for

Ceramide Synthase 2 in Liver Homeostasis. I ALTERATIONS IN LIPID METABOLIC PATHWAYS (2010) *J. Biol. Chem*. 285, 10902–10910

Pistillo D, Manzi A, Tino A, Boyl PP, Graziani F, Malva C. The Drosophila melanogaster lipase homologs: a gene family with tissue and developmental specific expression. *J Mol Biol*. 1998 Mar 13;276(5):877-85.

Raclot, T; Oudart, H. Selectivity of fatty acids on lipid metabolism and gene expression. *Proc. Nutr. Soc*. 1999, 58, 633–646.

Raichur, S., Wang, S.T., Chan, P.W., Li, Y., Ching, J., Chaurasia, B., Dogra, S.,Öhman, M.K., Takeda, K., Sugii, S., et al. (2014). CerS2 haploinsufficiency inhibits b-oxidation and confers susceptibility to diet-induced steatohepatitis and insulin resistance. *Cell Metab.* 20, 687–695.

Reali F, Morine MJ, Kahramanoğullari O, Raichur S, Schneider HC, Crowther D, and Priami C. Mechanistic interplay between ceramide and insulin resistance. *Sci Rep* 2017, 7, 41231.

Riebeling C, Allegood JC, Wang E, Merrill AH Jr, and Futerman AH. Two mammalian longevity assurance gene (LAG1) family members, trh1 and trh4, regulate dihydroceramide synthesis using different fatty acyl-CoA donors. *J. Biol. Chem.* 2003, 278, 43452–43459

Ruiz-Sanz JI, Aldamiz-Echevarria L, Arrizabalaga J, Aquino L, Jimeno P, Pérez-Nanclares G, Sanjurjo P. Polyunsaturated fatty acid deficiency during dietary treatment of very long-chain acyl-CoA dehydrogenase deficiency. Rescue with soybean oil. *J Inherit Metab D*is. 2001 Aug;24(4):493-503

Russo, SB, Baicu CF, Van Laer A, Geng T, Kasiganesan H, Zile MR, Cowart LA.Ceramide synthase 5 mediates lipid-induced autophagy and hypertrophy in cardiomyocytes. (2012) *J. Clin. Invest.* 122, 3919–3930

Schiffmann S, Sandner J, Birod K, Wobst I, Angioni C, Ruckhäberle E, Kaufmann M, Ackermann, H., Lötsch J, Schmidt, H., et al. (2009). Ceramide synthases and ceramide levels are increased in breast cancer tissue. *Carcinogenesis* 30, 745-752.

Schulze H & Sandhoff K Lysosomal lipid storage diseases. *Cold Spring Harb Perspect Biol* 2011.

Schulze H & Sandhoff K. Sphingolipids and lysosomal pathologies. *Biochim. Biophys. Acta* 2013.

Schweitzer JK, Krivda JP & D'Souza-Schorey C. Neurodegeneration in Niemann-Pick Type C disease and Huntington's disease: impact of defects in membrane trafficking. (2009) *Curr Drug Targets*

Sellin J, Wingen C, Gosejacob D, Senyilmaz D, Hänschke L, Büttner S, Meyer K, Bano D, Nicotera P, Teleman AA, Bülow MH. Dietary rescue of lipotoxicity-induced mitochondrial damage in Peroxin19 mutants. *PLoS Biol.* 2018 Jun 19;16(6):e2004893.

Shimabukuro, M, Higa M, Zhou YT, Wang MY, Newgard CB, Unger RH. Lipoapoptosis in beta-cells of obese prediabetic fa/fa rats. Role of serine palmitoyltransferase overexpression. (1998) *J. Biol. Chem.* 273, 32487–32490

Shulman, G.I. Ectopic fat in insulin resistance, dyslipidemia, and cardiometabolic disease. (2014) *N. Engl. J. Med.* 371, 1131–1141

Sieber, M.H., and Thummel, C.S. (2009). The DHR96 nuclear receptor controls triacylglycerol homeostasis in Drosophila. *Cell Metab*. 10, 481–490.

Slack C, Giannakou ME, Foley A, Goss M, Partridge L. dFOXO-independent effects of reduced insulin-like signaling in Drosophila. *Aging Cell* 2011 Oct; 10(5): 735–748.

Spassieva, S., Seo, J.-G., Jiang, J.C., Bielawski, J., Alvarez-Vasquez, F., Jazwinski, S.M., Hannun, Y.A., and Obeid, L.M. (2006). Necessary role for the Lag1p motif in (dihydro)ceramide synthase activity. *J. Biol. Chem.* 281, 33931–33938.

Sridevi P, Alexander H, Laviad EL, Pewzner-Jung Y, Hannink M, Futerman AH, and Alexander S. Ceramide synthase 1 is regulated by proteasomal mediated turnover. *Biochim. Biophys. Acta* 2009, 1793, 1218–1227

Summers SA. Could Ceramides Become the New Cholesterol? *Cell Metab*. 2018 Feb 6;27(2):276-280.

Tennessen, J.M., Barry, W.E., Cox, J., and Thummel, C.S. (2014). Methods for studying metabolism in Drosophila. *Methods* 68, 105–115.

Tidhar R, Zelnik ID, Volpert G, Ben-Dor S, Kelly S, Merrill AH Jr., Futerman AH. Eleven residues determine the acyl chain specificity of ceramide synthases. *J. Biol. Chem*. RA118.001936.

Tidhar, R., Ben-Dor, S., Wang, E., Kelly, S., Merrill, A.H., Jr., and Futerman, A.H. (2012). Acyl chain specificity of ceramide synthases is determined within a region of 150 residues in the Tram-Lag-CLN8 (TLC) domain. *J. Biol. Chem.* 287, 3197–3206.

Tirodkar TS, Lu P, Bai A, Scheffel MJ, Gencer S, Garrett-Mayer E, Bielawska A, Ogretmen B and Voelkel-Johnson C. Expression of ceramide synthase 6 transcriptionally activates acid ceramidase in a c-Jun N-terminal Kinase (JNK)-dependent manner. *J Biol Chem*, 2015. 290, 13157–13167.

Toll-Riera M, Rado´-Trilla N, Martys F, Alba` MM. Role of Low-Complexity Sequences in the Formation of Novel Protein Coding Sequences. *Mol. Biol. Evol*. 29(3):883–886. 2012

Turpin S.M., Nicholls H.T., Willmes D.M., Mourier A., Brodesser S.,Wunderlich C.M., Mauer J., Xu E.,Hammerschmidt P., Brönneke H.S., et al. (2014). Obesity-induced CerS6-dependent C16:0 ceramide production promotes weight gain and glucose intolerance. *Cell Metab.* 20, 678–686.

Van Echten-Deckert G and Walter J (2012) Sphingolipids: critical players in Alzheimer's disease. *Prog. Lipid Res* 51: 378–393

Varga, T., Czimmerer, Z., and Nagy, L. (2011). PPARs are a unique set of fatty acid regulated transcription factors controlling both lipid metabolism and inflammation. *Biochim. Biophys. Acta* 1812, 1007–1022.

Vessby, B.; Gustafsson, I.B.; Tengblad, S.; Boberg, M.; Andersson, A. Desaturation and elongation of fatty acids and insulin action. *Ann. N. Y. Acad. Sci.* 2002, 967, 183–189.

Voelzmann A, Wulf AL, Eckardt F, Thielisch M, Brondolin M, Pesch YY, Sociale M, Bauer R, and Hoch M. (2016). Nuclear Drosophila CerS Schlank regulates lipid homeostasis via the homeodomain, independent of the lag1p motif. *FEBS Lett*. 590, 971–981.

Voelzmann, A., and Bauer, R. (2010). Ceramide synthases in mammalians, worms, and insects: emerging schemes. *Biomol. Concepts* 1, 411–422.

Voelzmann, A., and Bauer, R. (2011). Embryonic expression of Drosophila ceramide synthase schlank in developing gut, CNS and PNS. *Gene Expr. Patterns* 11, 501–510.

Wang ES, Norred WP, Bacon CW, Rileygll RT,Merrill AH Jr. Inhibition of Sphingolipid Biosynthesis by Fumonisins. Implications for diseases associated with Fusarium moniliforme. *J Biol Chem*. 1991 Aug 5;266(22):14486-90

Wang J, Zhuang J, Lyer S, Lin X, Whitfield TW, Greven MC, Pierce BG, Dong X, Kundaje A, Cheng Y. Sequence features and chromatin structure around the genomic regions bound by 119 human transcription factors *Genome Res*, 22 (2012), pp. 1798-1812

Wegner J, Loser K, Apsite G, Nischt R, Eckes B, Krieg T, Werner S, Sorokin L. Laminin α5 in the keratinocyte basement membrane is required for epidermal-dermal intercommunication. *Matrix Biol*. 2016 Dec;56:24-41.

Worgall, T.S.; Sturley, S.L.; Seo, T.; Osborne, T.F.; Deckelbaum, R.J. Polyunsaturated fatty acids decrease expression of promoters with sterol regulatory elements by decreasing levels of mature sterol regulatory element-binding protein. *J. Biol. Chem.* 1998, 273, 25537–25540.

Xia JY, Holland WL, Kusminski CM, Sun K, Sharma AX, Pearson MJ, Sifuentes AJ, McDonald JG, Gordillo R, Scherer PE. Targeted induction of ceramide degradation reveals roles for cermaides in non alcoholic fatty liver disease and glucose metabolism in mice. (2015) *Cell Metab.* 22, 266–278

Xu X, Gopalacharyulu P, Seppänen-Laakso T, Ruskeepää A-L, Aye CC, Carson BP, Mora S, Oresic M, Teleman AA. Insulin Signaling Regulates Fatty Acid Catabolism at the Level of CoA Activation. *PLoS Genet* 2012 8(1): e1002478.

Xu, J.; Nakamura, M.T.; Cho, H.P.; Clarke, S.D. Sterol regulatory element binding protein-1 expression is suppressed by dietary polyunsaturated fatty acids. A mechanism for the coordinate suppression of lipogenic genes by polyunsaturated fats. *J. Biol. Chem.* 1999, *274*, 23577–23583

Xue Y, Ren J, Gao X, Jin C, Wen L, Yao X. GPS 2.0, a Tool to Predict Kinase-specific Phosphorylation Sites in Hierarchy *Mol Cell Proteomics.* 2008; 7: 1598-1608

Youm, Y.H, Adijiang A, Vandanmagsar B, Burk D, Ravussin A, Dixit VD. Elimination of the NLRP3–ASC inflam-masome protects against chronic obesity-induced pancreatic damage. (2011) *Endocrinology* 152, 4039–4045

Zabielski P., Błachnio-Zabielska A.U., Wójcik B., Chabowski A., Górski J.Effect of plasma free fatty acid supply on the rate of ceramide synthesis in different muscle types in the rat. *PLoS One*. 2017 Nov 2;12(11):e0187136.

Zaret KS, Mango SE. Pioneer transcription factors, chromatin dynamics, and cell fate control *Curr Opin Genet Dev*, 37 (2016), pp. 76-81-12

Zinke I, Schütz CS, Katzenberger JD, Bauer M & Pankratz MJ. Nutrient control of gene expression in Drosophila: microarray analysis of starvation and sugar-dependent response. *EMBO J* 2002. 21: 6162–6173

Zoete V, Michielin O, Karplus M. Relation between sequence and structure of HIV-1 protease inhibitor complexes (a model system for the analysis of protein flexibility). *J. Mol. Biol.* 2002; 315: 21–52

Zuleger N, Kerr ARW, Schirmer EC. Many mechanisms, one entrance: membrane protein translocation into the nucleus. *Cell. Mol. Life Sci*. (2012) 69:2205–2216

Acknowledgments

“There is a purpose for everybody you meet on your way. Some are there to test you, some are there to use you, and some will bring out the best of you.

Everyone is there to change you.”

Unknown

I want to thank everyone who contributed to this work and helped me during the last years. Everyone who was there for listening when I was complaining. Every person who made me laugh when I just wanted to cry. And every person who let me feel at home.

Grazie per essere sempre al mio fianco e di avermi supportato in qualsiasi scelta io abbia mai fatto. Grazie per avere sopportato, e continuare a sopportare, la distanza che ho deciso di mettere tra noi.